

Sensor and Simulation Notes

Note 272

August 26, 1981

Quasi-Static Magnetic-Field EMP Simulator Design Study

Kenneth D. Granzow
Joe P. Martinez
Kendall F. Casey

The Dikewood Corporation
Albuquerque, New Mexico 87102

CLASSIFIED
FOR PUBLIC RELEASE

PL/PA 31 DEC 96

Abstract

The simulator studied consists of a pair of current loops (similar to a Helmholtz pair) and the generalization to two and three pairs. The loops are constrained to lie on the surface of a sphere. The loop positions and current ratios are found that minimize r.m.s. error functions defined in terms of integrals over the volume and surface of spherical test volumes. The functions are also minimized for various (easily realizable) integer ratios of currents for the two-pair case. Spatial error plots are included as well as mutual inductances needed to calculate the low-frequency driving-point impedance. Figures of merit and efficiency as defined by Chen and Baum are evaluated and discussed.

PL 96-1142

CONTENTS

<u>Section</u>		<u>Page</u>
I	INTRODUCTION	8
II	ANALYSIS	11
	1. Field Analysis	11
	2. Volume-Integral-Minimum Definition	14
	3. Surface-Integral-Minimum Definition	16
	4. The Minimization Procedure	18
III	RESULTS AND CONCLUSIONS	25
	1. Optimum Parameter Values	25
	2. Behavior of the Error Field	30
	3. Optimum Loop Positions for Fixed Current Ratios	44
	4. Sensitivity Analysis	65
	5. Driving Impedance Considerations	70
	6. Current Required to Achieve Peak Field	76
	7. Figure of Merit and Efficiency	77
	APPENDIX: DERIVATIVES FOR NEWTON-RAPHSON METHOD	83

ILLUSTRATIONS

<u>Figure</u>		<u>Page</u>
1	Geometry of current loops	9
2	B_{re} versus θ for one pair -- volume-integral method	31
3	B_{re} versus θ for two pairs -- volume-integral method	32
4	B_{re} versus θ for three pairs -- volume-integral method	33
5	B_{re} versus θ for one pair -- surface-integral method	34
6	B_{re} versus θ for two pairs -- surface-integral method	35
7	B_{re} versus θ for three pairs -- surface-integral method	36
8	Relative error versus radius, in the test volume, for either volume-integral or surface-integral method; $R = 0.1$ and $R = 0.2$ (two pairs of loops)	37
9	Relative error versus radius for volume-integral method; $R = 0.3$ and $R = 0.4$ (two pairs of loops)	38
10	Relative error versus radius for volume-integral method; $R = 0.5$ and $R = 0.6$ (two pairs of loops)	39
11	Relative error versus radius for volume-integral method; $R = 0.7$ and $R = 0.8$ (two pairs of loops)	40
12	Relative error versus radius for surface-integral method; $R = 0.3$ and $R = 0.4$ (two pairs of loops)	41

ILLUSTRATIONS (Continued)

<u>Figure</u>		<u>Page</u>
13	Relative error versus radius for surface-integral method; $R = 0.5$ and $R = 0.6$ (two pairs of loops)	42
14	Relative error versus radius for surface-integral method; $R = 0.7$ and $R = 0.8$ (two pairs of loops)	43
15	Contours of constant $(B_z - B_{z1})/B_{z1}$ (solid lines) and constant B_ρ/B_{z1} (dashed lines) for one pair of loops using the volume-integral method; $R = 0.1, 0.2, 0.3,$ and 0.4	45
16	Contours of constant $(B_z - B_{z1})/B_{z1}$ (solid lines) and constant B_ρ/B_{z1} (dashed lines) for one pair of loops using the volume-integral method; $R = 0.5, 0.6, 0.7,$ and 0.8	46
17	Contours of constant $(B_z - B_{z1})/B_{z1}$ (solid lines) and constant B_ρ/B_{z1} (dashed lines) for two pairs of loops using the volume-integral method; $R = 0.1, 0.2, 0.3,$ and 0.4	47
18	Contours of constant $(B_z - B_{z1})/B_{z1}$ (solid lines) and constant B_ρ/B_{z1} (dashed lines) for two pairs of loops using the volume-integral method; $R = 0.5, 0.6, 0.7,$ and 0.8	48
19	Contours of constant $(B_z - B_{z1})/B_{z1}$ (solid lines) and constant B_ρ/B_{z1} (dashed lines) for three pairs of loops using the volume-integral method; $R = 0.1, 0.2, 0.3,$ and 0.4	49
20	Contours of constant $(B_z - B_{z1})/B_{z1}$ (solid lines) and constant B_ρ/B_{z1} (dashed lines) for three pairs of loops using the volume-integral method; $R = 0.5, 0.6, 0.7,$ and 0.8	50

ILLUSTRATIONS (Continued)

<u>Figure</u>		<u>Page</u>
21	Contours of constant $(B_z - B_{z1})/B_{z1}$ (solid lines) and constant B_ρ/B_{z1} (dashed lines) for one pair of loops using the surface-integral method; $R = 0.1, 0.2, 0.3,$ and 0.4	51
22	Contours of constant $(B_z - B_{z1})/B_{z1}$ (solid lines) and constant B_ρ/B_{z1} (dashed lines) for one pair of loops using the surface-integral method; $R = 0.5, 0.6, 0.7,$ and 0.8	52
23	Contours of constant $(B_z - B_{z1})/B_{z1}$ (solid lines) and constant B_ρ/B_{z1} (dashed lines) for two pairs of loops using the surface-integral method; $R = 0.1, 0.2, 0.3,$ and 0.4	53
24	Contours of constant $(B_z - B_{z1})/B_{z1}$ (solid lines) and constant B_ρ/B_{z1} (dashed lines) for two pairs of loops using the surface-integral method; $R = 0.5, 0.6, 0.7,$ and 0.8	54
25	Contours of constant $(B_z - B_{z1})/B_{z1}$ (solid lines) and constant B_ρ/B_{z1} (dashed lines) for three pairs of loops using the surface-integral method; $R = 0.1, 0.2, 0.3,$ and 0.4	55
26	Contours of constant $(B_z - B_{z1})/B_{z1}$ (solid lines) and constant B_ρ/B_{z1} (dashed lines) for three pairs of loops using the surface-integral method; $R = 0.5, 0.6, 0.7,$ and 0.8	56
27	Current-loop labels for two-pair geometry	73
28	Figure of merit ξ_ρ vs. R for 1-, 2-, and 3-pair configurations for both volume-integral and surface integral methods without the turns factor (see text). Ticks indicate values of χ expressed as a percent of the central field	78

ILLUSTRATIONS (Concluded)

<u>Figure</u>		<u>Page</u>
29	Figure of merit ξ_g vs. R for 1-, 2-, and 3-pair configurations for both volume-integral and surface-integral methods including the turns factor (see text). Ticks indicate values of χ expressed as a percent of the central field	80
30	Efficiency parameter ξ_h vs. R for 1- and 2-pair configurations for both volume-integral and surface-integral methods. Ticks indicate values of χ expressed as a percent of the central field	82

TABLES

<u>Table</u>		<u>Page</u>
1	Optimum parameters--one pair of loops	26
2	Optimum parameters--two pairs of loops	27
3	Optimum parameters--three pairs of loops	28
4	Values of χ that differ due to parameter rounding	29
5	Optimum loop locations for fixed current ratios (two pairs of loops), $R = 0.1$	57
6	Optimum loop locations for fixed current ratios (two pairs of loops), $R = 0.2$	58
7	Optimum loop locations for fixed current ratios (two pairs of loops), $R = 0.3$	59
8	Optimum loop locations for fixed current ratios (two pairs of loops), $R = 0.4$	60
9	Optimum loop locations for fixed current ratios (two pairs of loops), $R = 0.5$	61
10	Optimum loop locations for fixed current ratios (two pairs of loops), $R = 0.6$	62
11	Optimum loop locations for fixed current ratios (two pairs of loops), $R = 0.7$	63
12	Optimum loop locations for fixed current ratios (two pairs of loops), $R = 0.8$	64
13	Values of C_{ij} for one pair of loops	67
14	Values of C_{ij} for two pairs of loops	68
15	Values of C_{ij} for three pairs of loops	69
16	Self and mutual inductance--one-pair case	71
17	Self and mutual inductance--two pairs, volume-integral-method parameters	74
18	Self and mutual inductance--two pairs, surface-integral-method parameters	75

I. INTRODUCTION

The study described in this report was motivated by the need for practical design information for a low-frequency, uniform magnetic-field EMP simulator using simple current loops. Such a simulator could be used to measure EMP magnetic field interaction with systems situated in the close-in region of a nuclear burst. (Knowledge of the magnetic field characteristics at the point of simulator application would be required.) The simulator could be used to measure field penetration through poor conductors such as earth, the induced currents on scattering objects of various shapes, or the field penetration through points of entry into highly-conducting shields.

The simulator loops are assumed to lie on the surface of a sphere and are in pairs; the loops of each pair are symmetrically placed on each side of the equator. This geometry is illustrated in Figure 1. Configurations with one, two, and three pairs were studied.

The approach toward optimizing the loop currents and positions for maximum field uniformity is a departure from the approach that began with Ampere's loop, the Helmholtz pair, and Maxwell's three-loop combination. This classical approach is described and generalized by Garrett (Ref. 1). Its basic principle is to attain uniformity by forcing to zero as many as possible of the lowest order derivatives of the field at the

-
1. Garrett, M.W., "Axially Symmetric Systems for Generating and Measuring Magnetic Fields," Part I, Journal of Applied Physics, Vol. 22, No. 9, pp. 1091-1107, September 1951.

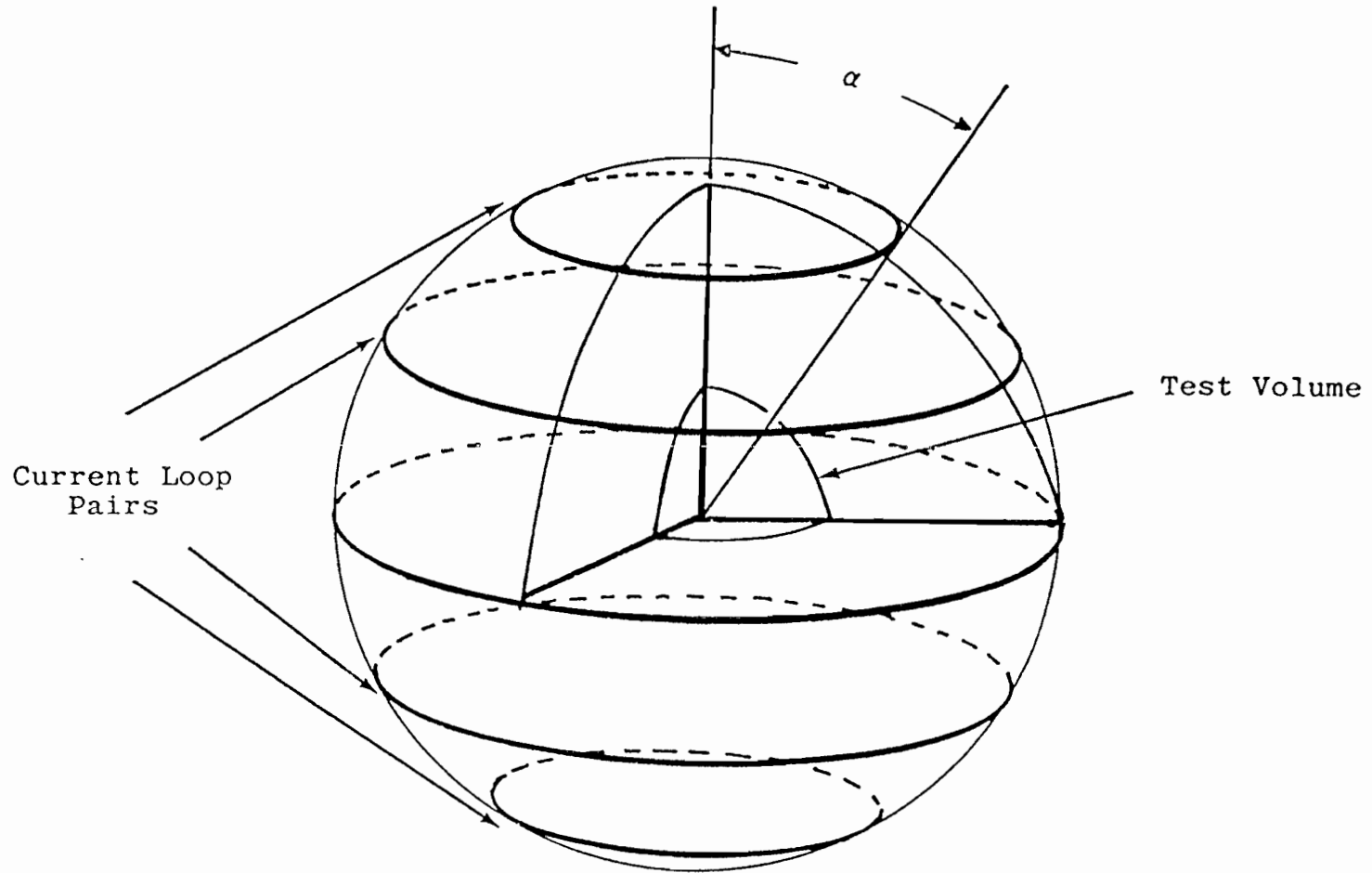


Figure 1. Geometry of current loops.

center of the geometry. This procedure is equivalent to forcing the low-order coefficients to zero in the Legendre-function expansion of the field potential.

In the present study, it was recognized that uniformity was desired in a finite-size "test volume." Or possibly it would be the effect of a uniform field, the induced currents in a test object, that should be optimized. Therefore, optimization was performed using two separate criteria, both defined as minimizations of relative errors calculated in an integral sense. The first was defined in the sense of a volume integral over a spherical test volume; the second was defined in the sense of a surface integral over a sphere. In both cases, as the radii of the spheres were allowed to become small, the optimum loop currents and positions approached those predicted by the classical theory. For test volumes of a realistic size, however, these parameters are significantly different.

After finding the optimum loop currents and positions for the two-pair case, physically realizable (fractions-of-small-integers) current ratios were defined close to the optimum values. New optimum positions were found while holding the current ratios constant to determine the effect on field uniformity of given realizable current ratios. It was found that little degradation occurred in the relative errors. This will be elaborated in the body of the report.

Finally, mutual inductances were calculated for the one-pair and two-pair cases. These can be combined with the self inductance of the current loops to obtain the driving point inductance for simulators under study.

II. ANALYSIS

In this section, the Legendre function expansions for the field components B_r and B_θ are derived from the expressions for a single loop given by Smythe (Ref. 2). The two optimization methods are then defined. That is, quantities χ_v (for the volume-integral method), and χ_s (for the surface-integral method) are defined, where these quantities are functions of the loop currents and positions (the "parameters"). The parameter values that minimize χ_v or χ_s represent a solution of the optimization problem. Since it is the relative currents that determine field uniformity (independent of their absolute magnitude), one current is set to unity and the other currents are allowed to vary to minimize χ_v or χ_s . Therefore, for L pairs of loops, there are $(L - 1)$ current parameters and L position (polar-angle) parameters for a total of $(2L - 1)$ parameters.

Concluding this section is a brief discussion of the numerical methods used to minimize χ_v and χ_s .

1. FIELD ANALYSIS

The magnetic field due to a circular current loop is given by Smythe (Ref. 2) as

$$B_r = \frac{\mu I \sin \alpha}{2a} \sum_{n=1}^{\infty} \left(\frac{r}{a}\right)^{n-1} P_n^1(\cos \alpha) P_n(\cos \theta) \quad (1a)$$

$$B_\theta = - \frac{\mu I \sin \alpha}{2a} \sum_{n=1}^{\infty} \frac{1}{n} \left(\frac{r}{a}\right)^{n-1} P_n^1(\cos \alpha) P_n^1(\cos \theta) \quad (1b)$$

2. Smythe, William R., Static and Dynamic Electricity, p. 275, McGraw-Hill Book Co., Inc., New York, 1950.

where the current loop lies on a sphere of radius a at angle α from the z axis (i.e., α is the spherical polar coordinate θ of the loop). Equations 1 yield the magnetic field at points (r, θ) such that $r < a$ (the field is independent of ϕ).

If a second current loop is present in the symmetrically opposite position (i.e., at $\theta = \pi - \alpha$) and carries the same current, the symmetry properties of the Legendre function result in the even terms canceling and the odd terms adding to yield

$$B_r = \frac{\mu I \sin \alpha}{a} \sum_{n=1(2)\infty} \left(\frac{r}{a}\right)^{n-1} P_n^1(\cos \alpha) P_n(\cos \theta) \quad (2a)$$

$$B_\theta = -\frac{\mu I \sin \alpha}{a} \sum_{n=1(2)\infty} \frac{1}{n} \left(\frac{r}{a}\right)^{n-1} P_n^1(\cos \alpha) P_n^1(\cos \theta) \quad (2b)$$

where the notation $n = n_1(n_2)n_3$ indicates that the summation is over $n_1, (n_1 + n_2), \dots, (n_1 + mn_2), \dots, n_3$. Finally, if L pairs of current loops are present with the pair at α_ℓ and $\pi - \alpha_\ell$ carrying current I_ℓ , the resulting magnetic field is given by

$$B_r = \frac{\mu}{a} \sum_{\ell=1}^L I_\ell \sin \alpha_\ell \sum_{n=1(2)\infty} \left(\frac{r}{a}\right)^{n-1} P_n^1(\cos \alpha_\ell) P_n(\cos \theta) \quad (3a)$$

$$B_\theta = -\frac{\mu}{a} \sum_{\ell=1}^L I_\ell \sin \alpha_\ell \sum_{n=1(2)\infty} \frac{1}{n} \left(\frac{r}{a}\right)^{n-1} P_n^1(\cos \alpha_\ell) P_n^1(\cos \theta) \quad (3b)$$

Note that the $n = 1$ term of Equations 3 represents a uniform magnetic field in the z direction. That is, the $n = 1$ term is

$$B_{r1} = \frac{\mu}{a} \sum_{\ell=1}^L I_{\ell} \sin^2 \alpha_{\ell} \cos \theta = B_{z1} \cos \theta \quad (4a)$$

$$B_{\theta 1} = -\frac{\mu}{a} \sum_{\ell=1}^L I_{\ell} \sin^2 \alpha_{\ell} \sin \theta = -B_{z1} \sin \theta \quad (4b)$$

and

$$B_{z1} = \frac{\mu}{a} \sum_{\ell=1}^L I_{\ell} \sin^2 \alpha_{\ell} \quad , \text{ a constant} \quad (5)$$

Next, the surface current density induced on a perfectly conducting sphere centered at the origin and immersed in the field given by Equation 3 will be determined. Using Smythe (Ref. 2, p. 273) Equations 2, 6, and 8, one finds that a current density i_{ϕ} on a spherical shell of radius \bar{a} given by

$$i_{\phi} = - \sum_n \frac{C_n}{\bar{a}} P_n^1(\cos \theta) \quad (6)$$

produces a magnetic field inside the shell given by

$$B_r = -\frac{\mu}{a} \sum_n \frac{n(n+1) C_n}{2n+1} \left(\frac{r}{a}\right)^{n-1} P_n(\cos \theta) \quad (7a)$$

$$B_{\theta} = \frac{\mu}{a} \sum_n \frac{(n+1) C_n}{2n+1} \left(\frac{r}{a}\right)^{n-1} P_n^1(\cos \theta) \quad (7b)$$

If the shell is immersed in the field of Equations 3, the induced current density must be such as to result in a total field inside the shell of zero; hence,

$$\frac{\mu}{\bar{a}^n} \frac{n(n+1)C_n}{2n+1} = \begin{cases} \frac{\mu}{\bar{a}^n} \sum_{\ell=1}^L I_{\ell} \sin \alpha_{\ell} P_n^1(\cos \alpha_{\ell}) & , n \text{ odd} \\ 0 & , n \text{ even} \end{cases}$$

$$C_n = \begin{cases} \frac{2n+1}{n(n+1)} \left(\frac{\bar{a}}{a}\right)^n \sum_{\ell=1}^L I_{\ell} \sin \alpha_{\ell} P_n^1(\cos \alpha_{\ell}) & , n \text{ odd} \\ 0 & , n \text{ even} \end{cases} \quad (8)$$

and

$$i_{\phi} = -\frac{1}{\bar{a}} \sum_{n=1}^{\infty} \frac{2n+1}{n(n+1)} \left[\left(\frac{\bar{a}}{a}\right)^n \sum_{\ell=1}^L I_{\ell} \sin \alpha_{\ell} P_n^1(\cos \alpha_{\ell}) \right] P_n^1(\cos \theta) \quad (9)$$

The first term ($n = 1$) of Equation 9 is the induced surface current due to the uniform part of the field given by Equations 4.

2. VOLUME-INTEGRAL-MINIMUM DEFINITION

It is desired to find the loop positions and currents that yield the most nearly uniform field over a spherical test volume. For purposes of this study, the most nearly uniform field is defined to be that with the least r.m.s. deviation from uniformity over the test volume, normalized to the uniform component of the field. The r.m.s. deviation is defined in terms of an integral over the spherical test volume. That is, χ_v^2 is minimized where

$$\chi_v^2 = \frac{\int_{T.V.} |\vec{B} - B_{z1} \hat{k}|^2 dV}{\int_{T.V.} B_{z1}^2 dV} \quad (10)$$

T.V. is the test volume

\vec{B} is given by Equations 3

B_{z1} is given by Equation 5

The quantity χ_V^2 is a function of the parameters I_ℓ and α_ℓ and the radius \bar{a} of the test volume.

The integrals of Equation 10 can be evaluated analytically.

Let

$$u = \int_{T.V.} |\vec{B} - B_{z1}\hat{k}|^2 dV \quad (11)$$

Since the first ($n = 1$) term of Equations 3 is exactly $B_{z1}\hat{k}$, one obtains

$$u = 2\pi \int_0^{\bar{a}} \int_0^\pi (\tilde{B}_r^2 + \tilde{B}_\theta^2) r^2 \sin\theta d\theta dr \quad (12)$$

where \tilde{B}_r and \tilde{B}_θ are given by Equations 3 with the $n = 1$ term omitted. The orthogonality of the sets of functions P_n and P_n^1 imply that only the squared terms of P_n and P_n^1 survive the θ integration in Equation 12; thus, u can be written

$$u = \frac{2\pi\mu^2}{a^2} \int_0^{\bar{a}} \sum_{n=3(2)\infty} \left\{ \left[\left(\frac{r}{a}\right)^{n-1} \sum_{\ell=1}^L I_\ell \sin\alpha_\ell P_n^1(\cos\alpha_\ell) \right]^2 \right. \\ \times \int_0^\pi [P_n(\cos\theta)]^2 \sin\theta d\theta + \left[\frac{1}{n} \left(\frac{r}{a}\right)^{n-1} \sum_{\ell=1}^L I_\ell \sin\alpha_\ell \right. \\ \left. \times P_n^1(\cos\alpha_\ell) \right]^2 \int_0^\pi [P_n^1(\cos\theta)]^2 \sin\theta d\theta \left. \right\} r^2 dr \quad (13)$$

From Abramowitz and Stegun (Ref. 3), one obtains

$$\int_0^\pi [P_n(\cos\theta)]^2 \sin\theta d\theta = \int_{-1}^{+1} [P_n(x)]^2 dx = \frac{2}{2n+1} \quad (14a)$$

3. Abramowitz, Milton, and Stegun, Irene A., Handbook of Mathematical Functions, AMS 55, p. 338, National Bureau of Standards, 1970.

and

$$\int_0^\pi \left[P_n^1(\cos\theta) \right]^2 \sin\theta \, d\theta = \int_{-1}^{+1} \left[P_n^1(x) \right]^2 dx = \frac{2n(n+1)}{2n+1} \quad (14b)$$

Substituting these values into Equation 13, performing the integration over r , and combining terms, one obtains

$$u = 4\pi\mu^2 \bar{a} \sum_{n=3(2)\infty} \frac{1}{n(2n+1)} \left[\left(\frac{\bar{a}}{a} \right)^n \sum_{\ell=1}^L I_\ell \sin\alpha_\ell P_n^1(\cos\alpha_\ell) \right]^2 \quad (15)$$

Let v be defined by

$$v = \int_{T.V.} B_{z1}^2 \, dv \quad (16)$$

Since B_{z1} is constant over the test volume, the integration is trivial; substituting from Equation 5 one obtains

$$v = \frac{4}{3} \frac{\pi \bar{a}^3 \mu^2}{a^2} \left[\sum_{\ell=1}^L I_\ell \sin^2 \alpha_\ell \right]^2 \quad (17)$$

and χ_v^2 (Eq. 10) can be written

$$\chi_v^2 = \frac{\sum_{n=3(2)\infty} \frac{3}{n(2n+1)} \left[\left(\frac{\bar{a}}{a} \right)^n \sum_{\ell=1}^L I_\ell \sin\alpha_\ell P_n^1(\cos\alpha_\ell) \right]^2}{\left[\left(\frac{\bar{a}}{a} \right) \sum_{\ell=1}^L I_\ell \sin^2 \alpha_\ell \right]^2} \quad (18)$$

3. SURFACE-INTEGRAL-MINIMUM DEFINITION

In this case, the purpose of the system of wire loops is to induce a surface current that approximates the surface current induced by a uniform field on a spherical, perfectly conducting scattering object. This ideal surface current is given by the first term ($n = 1$) of Equation 9. The method is similar to that

given in the preceding section. The r.m.s. deviation is defined in terms of a surface integral over the sphere rather than by a volume integral.

The quantity to be minimized is

$$\chi_S^2 = \frac{\int_S |i_\phi - i_{\phi 1}|^2 da}{\int_S i_{\phi 1}^2 da} \quad (19)$$

where i_ϕ is given by Equation 9, $i_{\phi 1}$ is the first term ($n = 1$) of Equation 9, and S is the surface of a sphere of radius \bar{a} centered at the origin. The integration can be performed analytically. Let

$$u = \int_S |i_\phi - i_{\phi 1}|^2 da$$

Again, using the orthogonality of P_n^1 , one obtains

$$\begin{aligned} u &= 2\pi \sum_{n=3(2)\infty} \left[\frac{2n+1}{n(n+1)} \left(\frac{\bar{a}}{a}\right)^n \sum_{\ell=1}^L I_\ell \sin \alpha_\ell P_n^1(\cos \theta) \right]^2 \\ &\quad \times \int_0^\pi [P_n^1(\cos \theta)]^2 \sin \theta d\theta \\ u &= 4\pi \sum_{n=3(2)\infty} \frac{2n+1}{n(n+1)} \left[\left(\frac{\bar{a}}{a}\right)^n \sum_{\ell=1}^L I_\ell \sin \alpha_\ell P_n^1(\cos \alpha_\ell) \right]^2 \end{aligned} \quad (20)$$

Let

$$\begin{aligned} v &= \int_S i_{\phi 1}^2 da \\ v &= 6\pi \left[\left(\frac{\bar{a}}{a}\right) \sum_{\ell=1}^L I_\ell \sin^2 \alpha_\ell \right]^2 \end{aligned} \quad (21)$$

Then χ_S^2 (Eq. 19) is given by

$$\chi_S^2 = \frac{\frac{2}{3} \sum_{n=3}^{\infty} \frac{2n+1}{n(n+1)} \left[\left(\frac{\bar{a}}{a}\right)^n \sum_{\ell=1}^L I_{\ell} \sin \alpha_{\ell} P_n^1(\cos \alpha_{\ell}) \right]^2}{\left[\left(\frac{\bar{a}}{a}\right) \sum_{\ell=1}^L I_{\ell} \sin^2 \alpha_{\ell} \right]^2} \quad (22)$$

Note that the form of χ_S^2 is identical to that of χ_V^2 ; only the values of the coefficients of the expansion in the numerator are different.

4. THE MINIMIZATION PROCEDURE

Several algorithms for finding the minima of χ_V and χ_S in parameter space were programmed and run on the AFWL computer system. None of the methods quickly found minima if the number of pairs was greater than two (three parameters); that is, for three pairs (five parameters), the procedure was tedious. No serious attempts were made to find optimum parameters for four or more pairs.

The reason for the difficulty is found in the nature of the functions χ_V and χ_S in parameter space. These functions have paths through parameter space along which they have (1) extremely small values, (2) a very large gradient perpendicular to the path axis, and (3) an extremely small gradient parallel to these axes. Most algorithms tend to converge to the axis of such a path with reasonable speed, but can make little progress along the axis.

Though this behavior causes difficulty in finding the minimum points, it can be both a help and a hindrance from the engineering standpoint. It is a help in that there are many sets of parameter values that yield small values of χ_V or χ_S . Hence, for

the two-pair case, realistic current ratios can be chosen close to, but not equal to, the ideal; then loop positions can be found such that either χ_v or χ_s is almost as small as the minimum value. Such a point is on, or close to, the path of small values. However, the property of having a large gradient perpendicular to the path axis can cause a fabrication tolerance problem. Small variations in the parameters such that their vector displacement is not parallel to a path axis can cause a large increase in χ_v or χ_s . This property requires careful consideration of the required tolerances when constructing such a simulator.

Four methods to locate the minima of $\chi(\chi_v \text{ or } \chi_s)$ were written into computer codes. Each method will be discussed. First, the method will be described including the derivation of required formula; then, comments will be given as to its usefulness.

a. Methods of steepest descent--The gradient of χ^2 was calculated in parameter space. Since $-\nabla\chi^2$ is a vector pointing in the direction of smaller χ^2 , small steps were taken along that direction until χ^2 increased; then the step size was decreased and the process continued. A modified version took 25 steps, stored the parameters, took 25 more steps and subtracted to find the vector displacement over the last 25 steps. It then extrapolated a distance determined by the analyst and used the new point to start the process over. The gradient expressions are given in the Appendix for the Modified Newton-Raphson method and are not repeated here. This was the least successful of any of the methods tried and was discarded early in the study. Many thousands of steps

often led to a very poor result. After the minima were found using other methods, it was discovered that some of the results, primarily for $\bar{a}/a > 0.6$, were fairly close.

b. Brute-force minimum seeking--In this method, a first guess of the parameters, say \vec{p}_0 , and a distance of δ is entered as input to the code. The value of χ^2 is evaluated for all the possible vector locations given by \vec{p}_0 with 0 or $\pm\delta$ added to its components. For N parameters, χ^2 is evaluated at 3^N such points (including $\vec{p}_0 + \vec{0}$), the location of the smallest value of χ^2 becomes the new \vec{p}_0 , and 0.9δ becomes the new δ . The procedure is then iterated. Tertiary numbers were generated to calculate the vectors. A DO loop for $M = 1, 3^N$ was entered, then the tertiary digits of $M-1$ were found; i.e.,

$$M - 1 = (n_1, n_2, \dots, n_N)_3 \quad (23)$$

where the $n_i = 0, 1, \text{ or } 2$. The vector of interest, then, has components

$$p_i = p_{0i} + (n_i - 1)\delta, \quad i = 1, \dots, N \quad (24)$$

This method appears to be very deliberate. It always finds a point with a smaller value of χ^2 . It does not converge to the smallest value of χ^2 , however, except when the first guess point is very close; i.e., accurate to 3 to 7 places (depending on the number of pairs and \bar{a}/a) and δ is appropriately small. This method was used extensively to find a "downhill" direction to extrapolate along as input to the Modified Newton-Raphson method described next. The minimum χ 's for three pairs were found primarily by alternating between this method and the Modified Newton-Raphson method.

c. Modified Newton-Raphson--To find the minimum of χ^2 in parameter space, one seeks the solution of the equations

$$\frac{\partial \chi^2}{\partial p_i} = 0, \quad i = 1, \dots, N \quad (24)$$

where the p_i are the parameters, i.e., the current ratios and positions (polar angles) of the current loops. Solving the Equations 24 using Newton-Raphson, one assumes a "first guess" for the parameters, say $\bar{p} = \bar{p}^0$; near \bar{p}^0 , $\partial \chi^2 / \partial p_i$ can be approximated by the first two terms of a Taylor expansion. That is,

$$\left. \frac{\partial \chi^2}{\partial p_i} \right|_{\bar{p}^0 + \delta \bar{p}} \approx \left. \frac{\partial \chi^2}{\partial p_i} \right|_{\bar{p}^0} + \sum_j \left. \frac{\partial^2 \chi^2}{\partial p_j \partial p_i} \right|_{\bar{p}^0} \delta p_j \quad (25)$$

For matrix notation, define the matrices

$$\bar{A} = \left\| \left\| \left. \frac{\partial^2 \chi^2}{\partial p_j \partial p_i} \right|_{\bar{p}^0} \right\| \right\|, \quad \text{an } N \times N \text{ matrix} \quad (26a)$$

$$\bar{y} = \left\| \left\| \left. \frac{\partial \chi^2}{\partial p_i} \right|_{\bar{p}^0} \right\| \right\|, \quad \text{an } N \text{ column vector} \quad (26b)$$

$$\delta \bar{p} = \left\| \left\| \delta p_i \right\| \right\|, \quad \text{an } N \text{ column vector} \quad (26c)$$

In a neighborhood of \bar{p}^0 , Equation 24 becomes

$$\bar{y} + \bar{A} \delta \bar{p} \approx \bar{0} \quad (27)$$

$$\delta \bar{p} \approx -\bar{A}^{-1} \bar{y} \quad (28)$$

Hence, an improved value of \bar{p} is \bar{p}^+ , where

$$\begin{aligned}\bar{p}^+ &= \bar{p}^0 + \delta\bar{p} \\ \bar{p}^+ &= \bar{p}^0 - \bar{A}^{-1}\bar{y}\end{aligned}\tag{29}$$

the Newton-Raphson formula. The required derivatives (elements of \bar{A} and \bar{y}) are given in the Appendix.

Since Equation 24 holds at both maxima and minima of χ^2 , this algorithm may converge to either a maximum or a minimum. Therefore, the code was modified to test whether χ^2 increased or decreased over each step. If χ^2 increased, the correction term ($\bar{A}^{-1}\bar{y}$) was multiplied by a factor of (-0.9) to force downhill movement and avoid an unending oscillation if, indeed, the step was across a minimum. The (-0.9) factors were cumulative and the number of multiplications were counted. In the final version of the code, this was allowed to continue for 50 steps at which time the factor $(-0.9)^n$ was reinitialized to +1 and the procedure was repeated until the total number of steps were taken that had been chosen by the analyst. The number of multiplications by (-0.9) in each 50-step block provided an indication of the convergence properties of the run.

It was found that neither this method nor the Brute-Force method converged quickly unless very accurate initial guesses were provided. Each method would make a great deal of progress (in terms of reducing χ^2) when it began calculating, then it would seem to "converge" to a parameter value. This "convergence" was an illusion; giving the "final answer" to the Brute-Force code usually resulted in a lower χ^2 and parameters modified much more

than one would expect, making it very difficult to estimate the accuracy of any given result.

This problem led to further modification of the Newton-Raphson code. The final version accepts two parameter values \bar{p}^1 and \bar{p}^2 (such as the beginning and ending values of a Brute-Force run). These two values are used to define a straight line in parameter space. Another input parameter defines a number of increments between \bar{p}^1 and \bar{p}^2 along the line. Two index parameters are then used to define a set of points along the line chosen as first guesses for Newton-Raphson iteration. The points chosen can interpolate between, or extrapolate beyond, the points \bar{p}^1 and \bar{p}^2 . Using the points along the line as first guesses, Newton-Raphson was allowed to iterate typically 100 times from each starting point. By carefully choosing the points, one could find a region along the line where the Newton-Raphson results had a minimum value of χ^2 . The parameter vector at this point was then typically used as input to the Brute-Force method. When neither the Brute-Force method nor the Newton-Raphson method changed the results in the seventh or eighth place, it was assumed that the result was near a minimum.

d. Newton-Raphson shotgun method--A version of the Newton-Raphson code was written that used as first guesses the same array of points generated in the Brute-Force method (Eqs. 23 and 24). A limited number of Newton-Raphson iterations (typically 25), were performed from each point. The final value of \bar{p} yielding the smallest χ became the center point for the next calculation, δ was reduced by the factor 0.5 and the whole process repeated. This

scheme seems to combine the best features of the Brute-Force and Newton-Raphson schemes. However, it does not converge to the desired result any faster or more consistently than its predecessor schemes. It was developed late in the effort and not used extensively.

III. RESULTS AND CONCLUSIONS

1. OPTIMUM PARAMETER VALUES

For a single pair of loops (one parameter), the Newton-Raphson method converges in 3 to 5 iterations. The optimum parameters are given in Table 1. The parameter R is the ratio of the test-volume radius (\bar{a}) to the radius of the sphere containing the loops (a). (The radius of a loop is given by $a \cdot \sin \alpha$.) The position of the loops for the Helmholtz configuration is given at the bottom of Table 1. For the two-pair and three-pair cases the current ratios are also optimized. These results are given in Tables 2 and 3. The "generalized Helmholtz configurations" given at the bottom of Tables 2 and 3 are the classical solutions discussed in the Introduction and in Reference 1.

It should be pointed out that the values of χ given in Tables 1, 2 and 3 are the values of χ calculated with the full (double-precision) values of current (I) and position (α) in the computer. The values of χ are the minimum values to the three places given. The accuracy of the parameters yielding the small values of χ is unknown; hence, parameter values rounded to four places are given here. (We are highly confident that four places are correct.) Since χ is extremely sensitive to changes in the parameter values, the values rounded to four places yield much larger values of χ in some cases, namely, for two and three pairs and small values of R . The actual values of χ implied by the rounded values of the parameters that differ from those shown in Tables 2 and 3 are given in Table 4.

TABLE 1. OPTIMUM PARAMETERS--ONE PAIR OF LOOPS

<u>R</u>	<u>Volume Integral</u>		<u>Surface Integral</u>	
	<u>α (Deg)</u>	<u>Minimum χ</u>	<u>α (Deg)</u>	<u>Minimum χ</u>
0.1	63.44	4.20×10^{-5}	63.44	8.90×10^{-5}
0.2	63.45	6.73×10^{-4}	63.46	1.42×10^{-3}
0.3	63.51	3.41×10^{-3}	63.56	7.21×10^{-3}
0.4	63.67	1.08×10^{-2}	63.82	2.28×10^{-2}
0.5	64.01	2.65×10^{-2}	64.39	5.60×10^{-2}
0.6	64.63	5.55×10^{-2}	65.42	1.17×10^{-1}
0.7	65.65	1.05×10^{-1}	67.17	2.23×10^{-1}
0.8	67.28	1.88×10^{-1}	70.02	4.08×10^{-1}

Helmholtz Configuration: $\alpha = 63.4349^{\circ}$

TABLE 3. OPTIMUM PARAMETERS--THREE PAIRS OF LOOPS

R	Volume Integral			Surface Integral		
	α (Deg)	I	Minimum χ	α (Deg)	I	Minimum χ
0.1	77.92	1	2.43×10^{-13}	77.92	1	8.25×10^{-13}
	53.72	0.8270		53.72	0.8270	
	29.34	0.5108		29.34	0.5108	
0.2	77.92	1	9.95×10^{-10}	77.92	1	3.38×10^{-9}
	53.72	0.8270		53.72	0.8270	
	29.34	0.5108		29.34	0.5108	
0.3	77.95	1	1.29×10^{-7}	77.95	1	4.39×10^{-7}
	53.79	0.8289		53.80	0.8292	
	29.40	0.5135		29.41	0.5140	
0.4	78.01	1	4.07×10^{-6}	78.03	1	1.39×10^{-5}
	53.94	0.8328		53.98	0.8339	
	29.53	0.5195		29.57	0.5211	
0.5	78.14	1	5.94×10^{-5}	78.18	1	2.02×10^{-4}
	54.25	0.8409		54.36	0.8432	
	29.84	0.5326		29.94	0.5369	
0.6	78.38	1	5.31×10^{-4}	78.46	1	1.80×10^{-3}
	54.86	0.8546		55.09	0.8589	
	30.46	0.5583		30.73	0.5681	
0.7	78.78	1	3.41×10^{-3}	78.95	1	1.15×10^{-2}
	55.94	0.8753		56.45	0.8827	
	31.71	0.6059		32.39	0.6273	
0.8	79.45	1	1.73×10^{-2}	79.84	1	5.81×10^{-2}
	57.85	0.9053		59.01	0.9174	
	34.22	0.6922		36.08	0.7337	

Generalized Helmholtz Configuration:

α (Deg)	I
77.9187	1
53.7222	0.827047
29.3385	0.510849

TABLE 4. VALUES OF χ THAT DIFFER DUE TO PARAMETER ROUNDING

a. Two Pairs of Loops

R	Volume Integral		Surface Integral	
	Minimum χ	χ --Rounded Parameters	Minimum χ	χ --Rounded Parameters
0.1	2.99×10^{-9}	6.84×10^{-7}	8.46×10^{-9}	5.07×10^{-7}
0.2	7.65×10^{-7}	3.46×10^{-6}	2.16×10^{-6}	2.44×10^{-6}
0.3	1.96×10^{-5}	2.04×10^{-5}	5.55×10^{-5}	5.72×10^{-5}

b. Three Pairs of Loops

R	Volume Integral		Surface Integral	
	Minimum χ	χ --Rounded Parameters	Minimum χ	χ --Rounded Parameters
0.1	2.43×10^{-13}	4.05×10^{-8}	8.25×10^{-13}	6.70×10^{-8}
0.2	9.95×10^{-10}	1.75×10^{-7}	3.38×10^{-9}	3.02×10^{-7}
0.3	1.29×10^{-7}	4.62×10^{-6}	4.39×10^{-7}	5.88×10^{-6}
0.4	4.07×10^{-6}	1.35×10^{-5}	1.39×10^{-5}	3.34×10^{-5}
0.5	5.94×10^{-5}	6.22×10^{-5}	2.02×10^{-4}	2.03×10^{-4}
0.6	5.31×10^{-4}	5.32×10^{-4}		

2. BEHAVIOR OF THE ERROR FIELD

The variation of the field within the test volume is of interest to simulator designers. To gain insight into the behavior of this variation, several types of graphs were made.

The first quantity plotted was the relative error field

$$B_{re} = \frac{|\vec{B} - B_{z1}\hat{k}|}{B_{z1}} \quad (30)$$

where B_{z1} is the constant part of the field and \vec{B} is the total field. The quantity B_{re} yields an overall view of the variation of the field independent of the vector direction of that variation. In Figures 2 through 7, B_{re} is plotted versus θ on the surface of the test volume for $R = 0.1$ through 0.8 , for one, two, and three pairs and for both volume- and surface-integral methods. In Figures 8 through 14, the behavior of B_{re} as a function of r is shown for $\theta = 0, 45^\circ, \text{ and } 90^\circ$, where r is the radial distance in units of the loop-sphere radius a . The values of r shown are inside the test volume; hence, r takes on values from zero to R only. The plots indicate that B_{re} is a smooth function with no large spikes. Its value is largest on the surface of the test volume and decreases rapidly as the observer moves toward the center of the test volume. At about 0.8 of the radius of the test volume, half the volume is inside and half outside; at this point B_{re} approximates χ_v as one might expect.

To display the vector behavior of the error fields, contours of constant values of the two error-field components were plotted. That is, contours of constant B_ρ/B_{z1} (where B_ρ is the cylindrical,

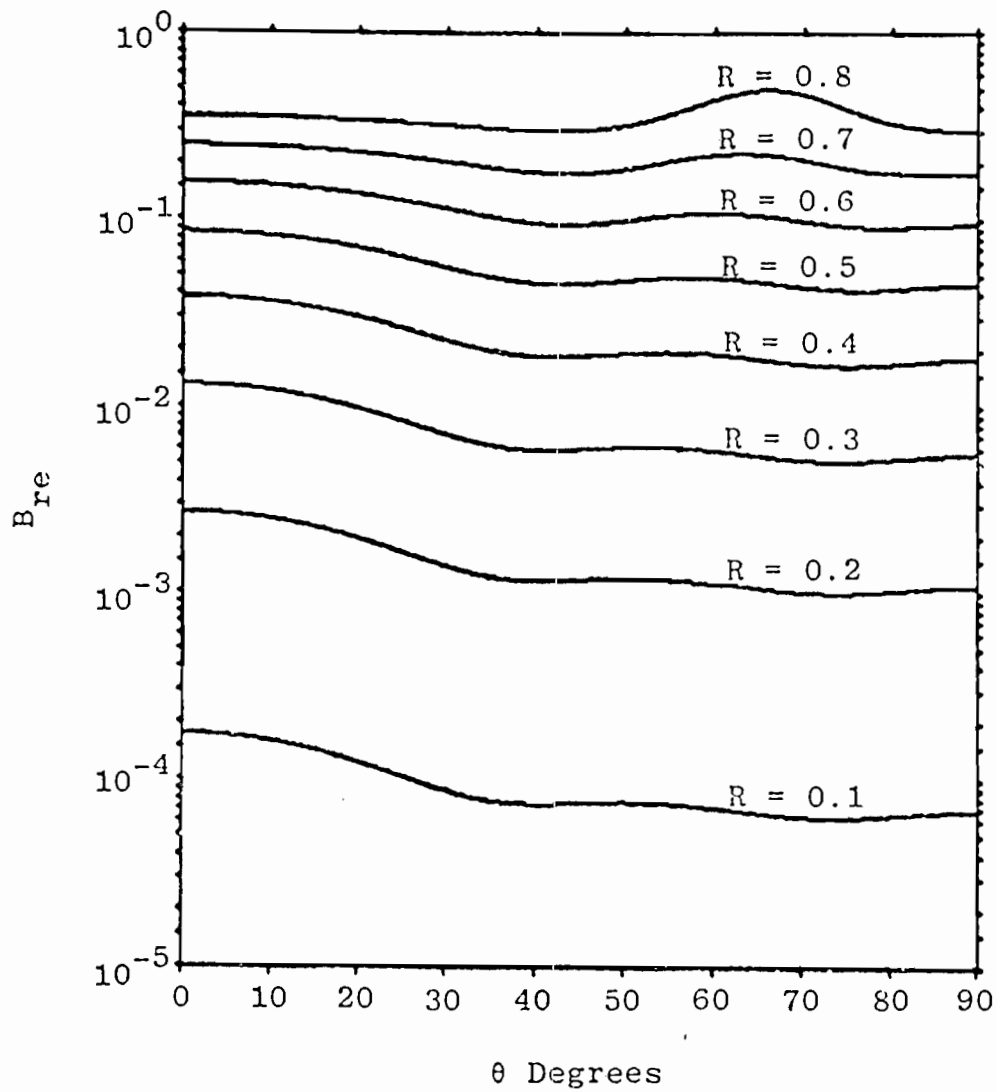


Figure 2. B_{re} versus θ for one pair --
volume-integral method.

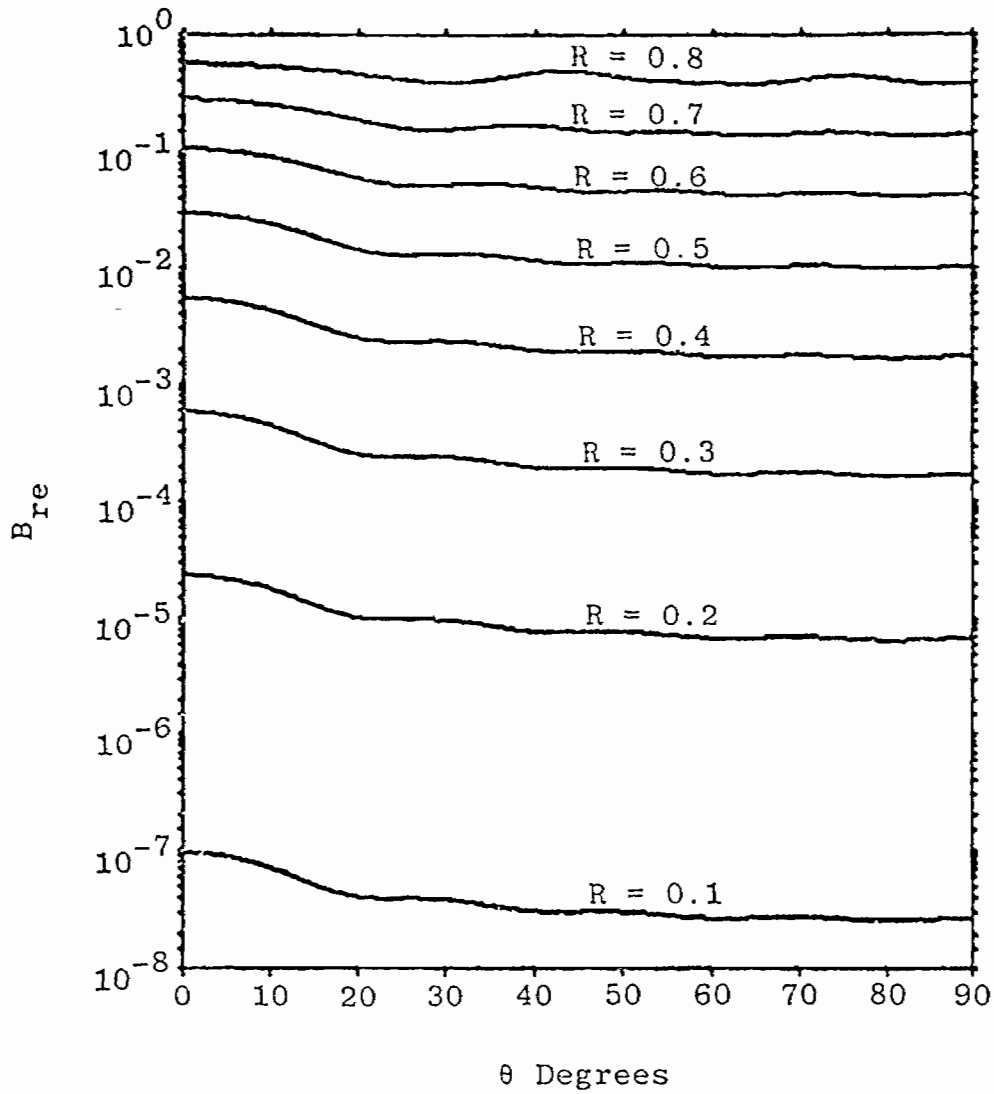


Figure 3. B_{re} versus θ for two pairs -- volume-integral method.

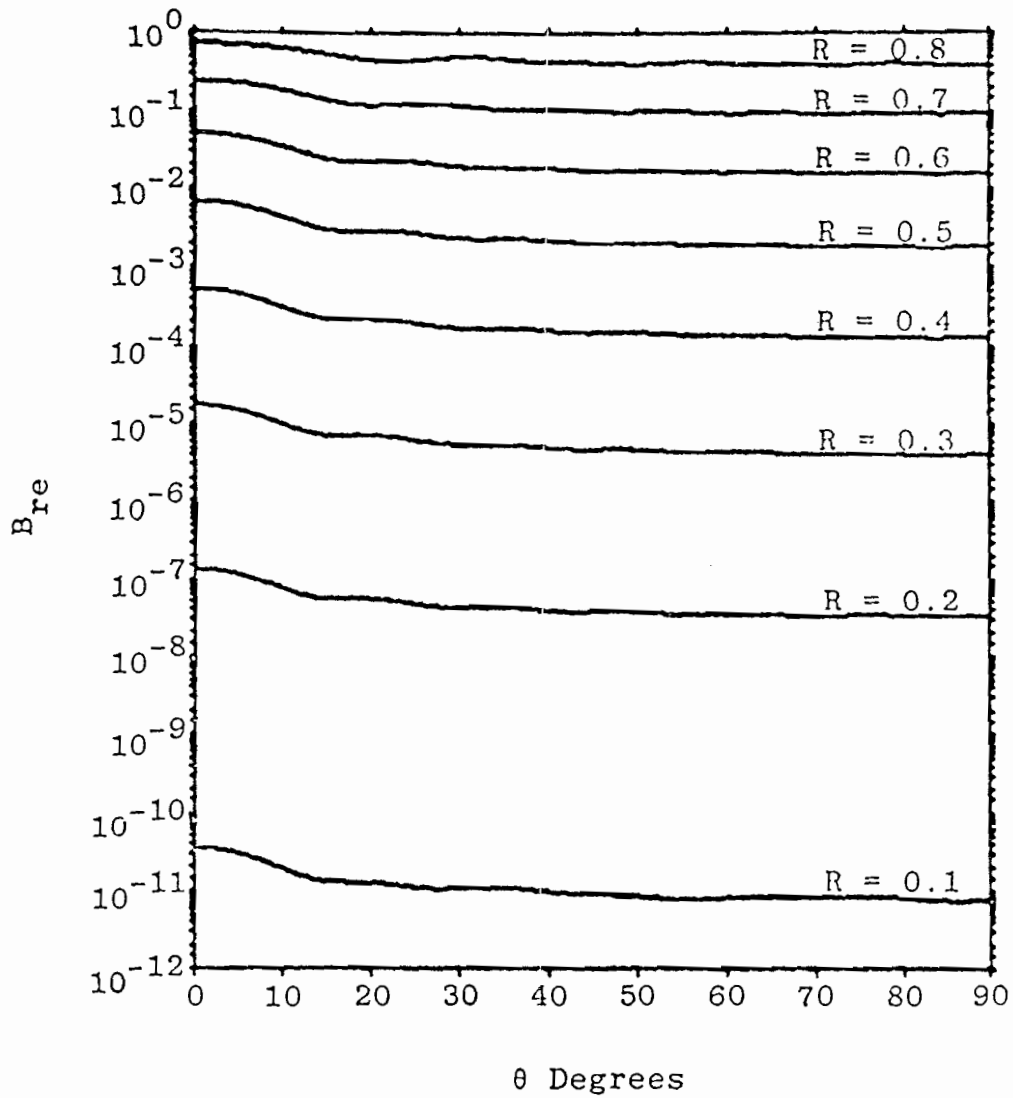


Figure 4. B_{re} versus θ for three pairs -- volume-integral method.

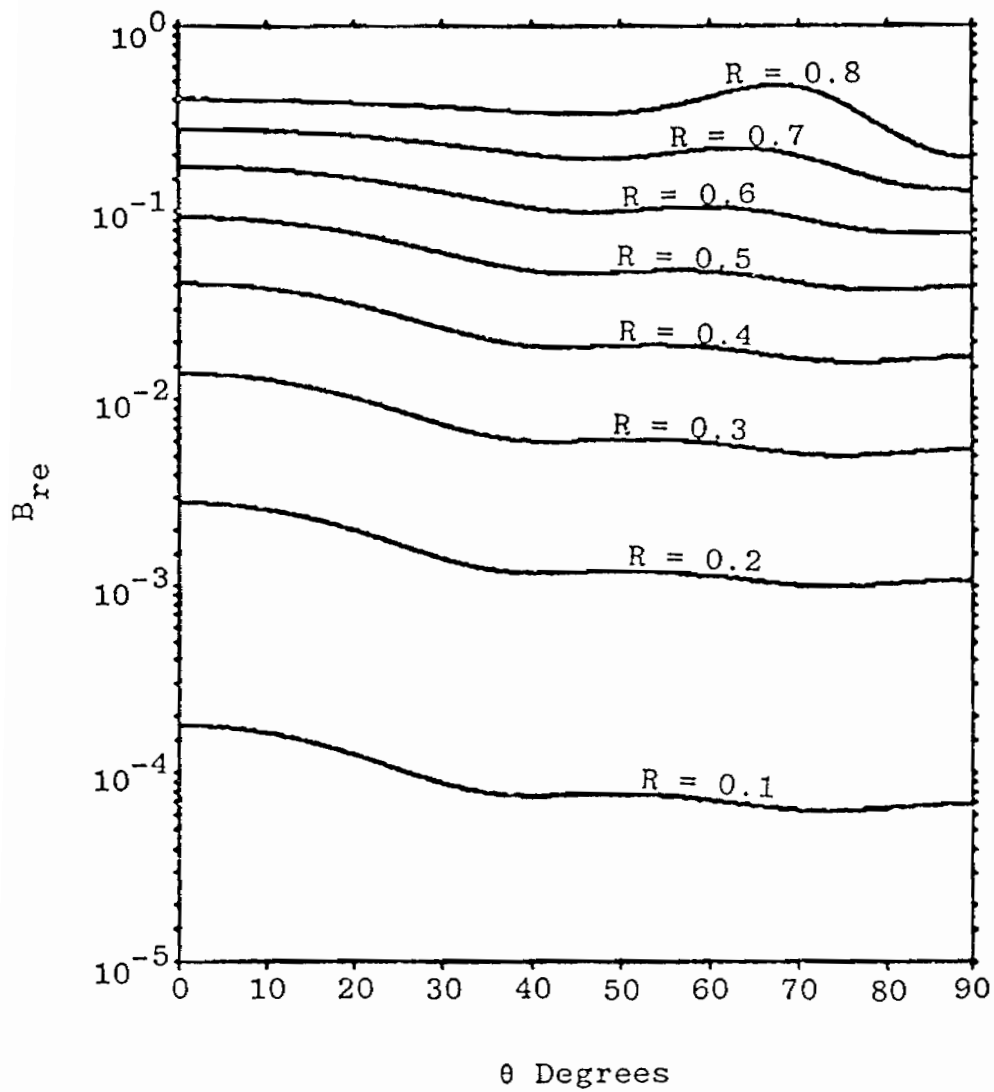


Figure 5. B_{re} versus θ for one pair -- surface-integral method.

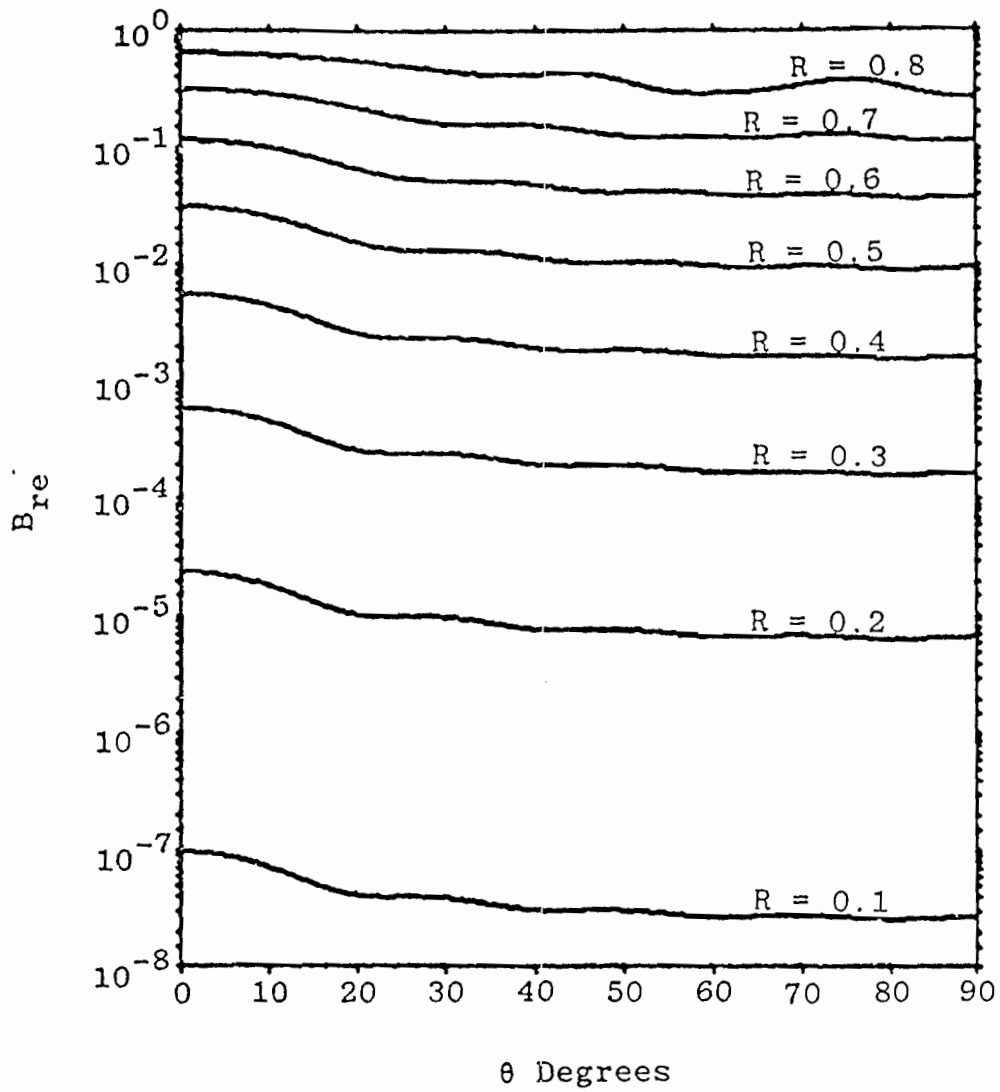


Figure 6. B_{re} versus θ for two pairs -- surface-integral method.

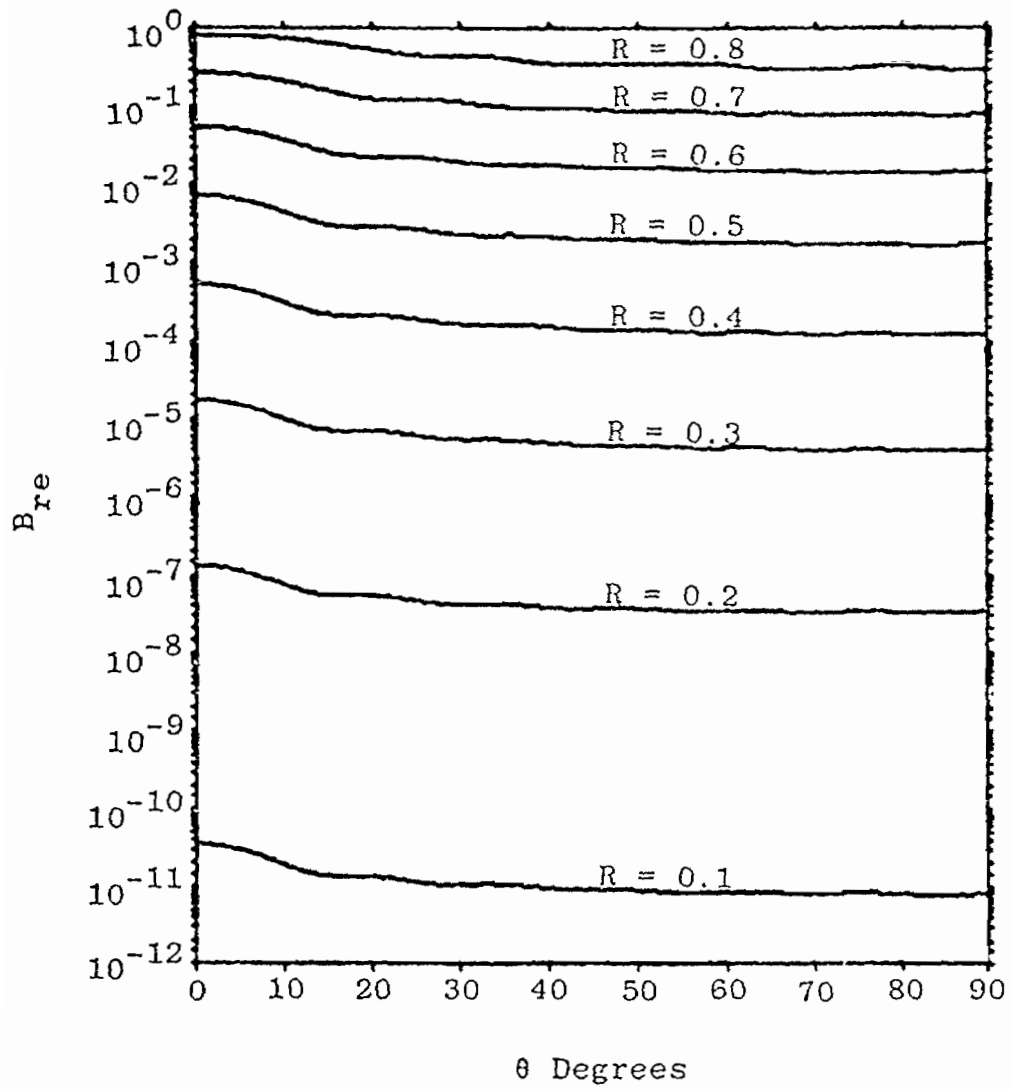


Figure 7. B_{re} versus θ for three pairs -- surface-integral method.

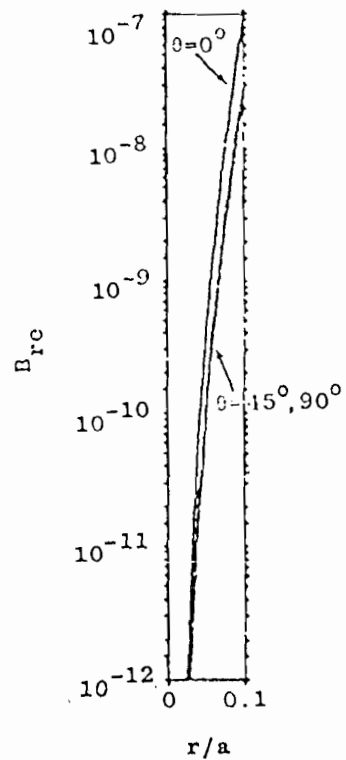
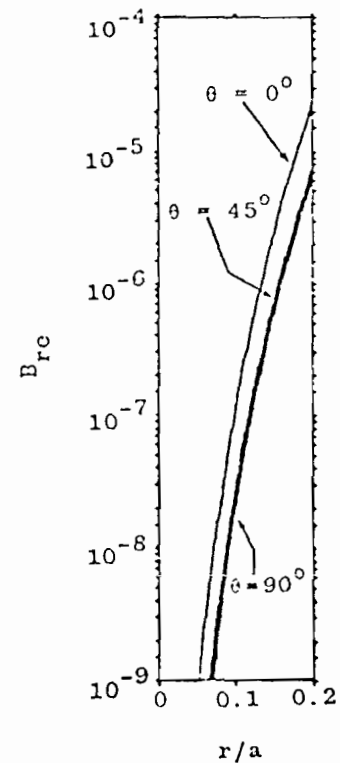
(a) $R = 0.1$ (b) $R = 0.2$

Figure 8. Relative error versus radius, in the test volume, for either volume-integral or surface-integral method; $R = 0.1$ and $R = 0.2$ (two pairs of loops).

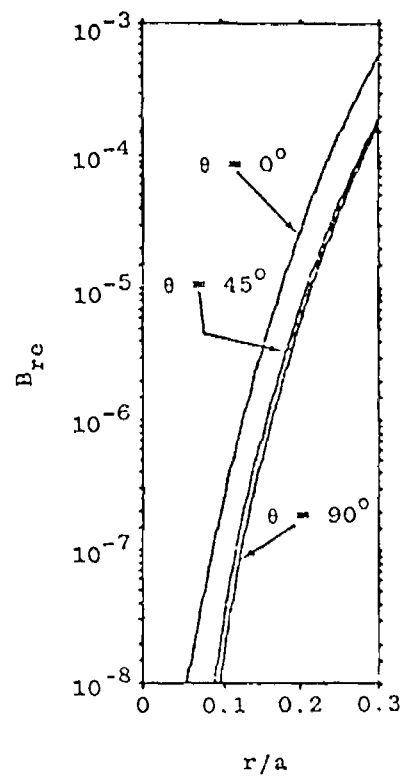
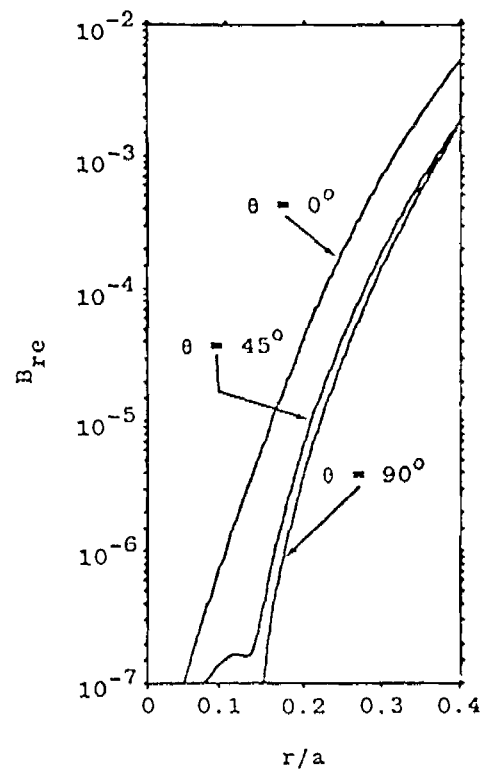
(a) $R = 0.3$ (b) $R = 0.4$

Figure 9. Relative error versus radius for volume-integral method; $R = 0.3$ and $R = 0.4$ (two pairs of loops).

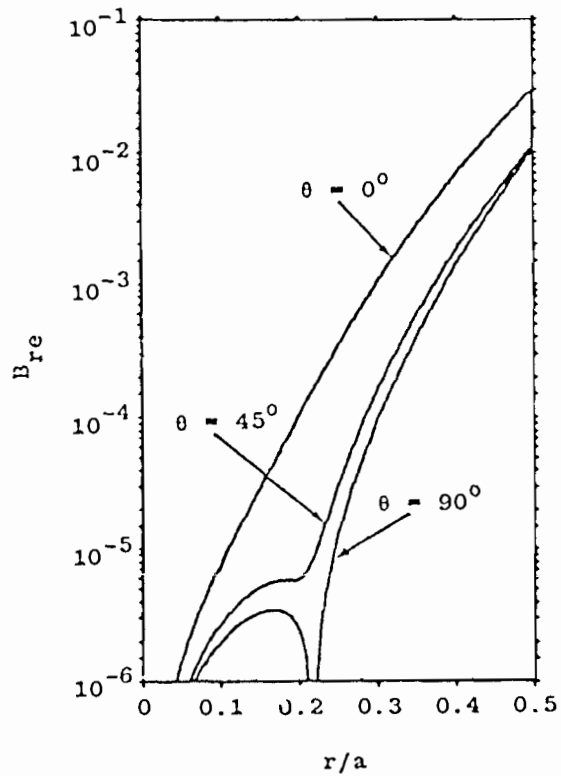
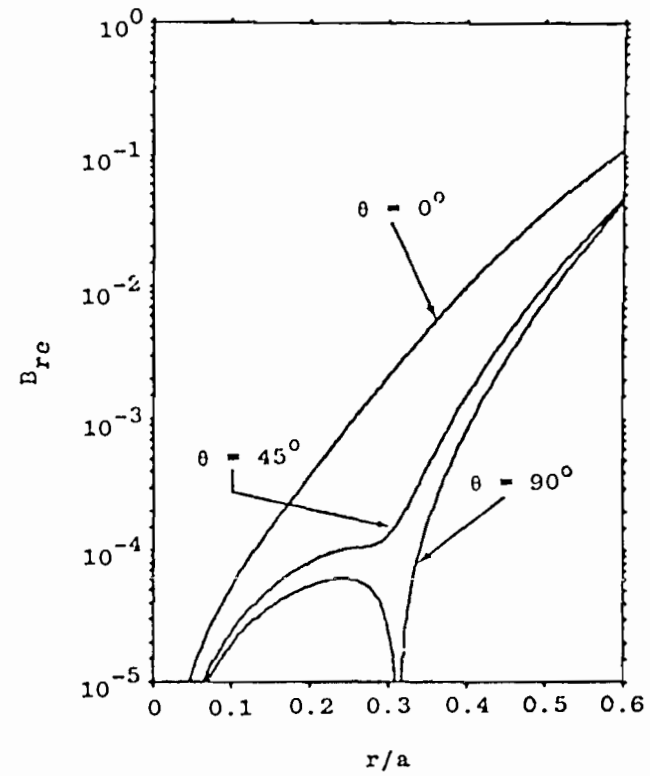
(a) $R = 0.5$ (b) $R = 0.6$

Figure 10. Relative error versus radius for volume-integral method; $R = 0.5$ and $R = 0.6$ (two pairs of loops).

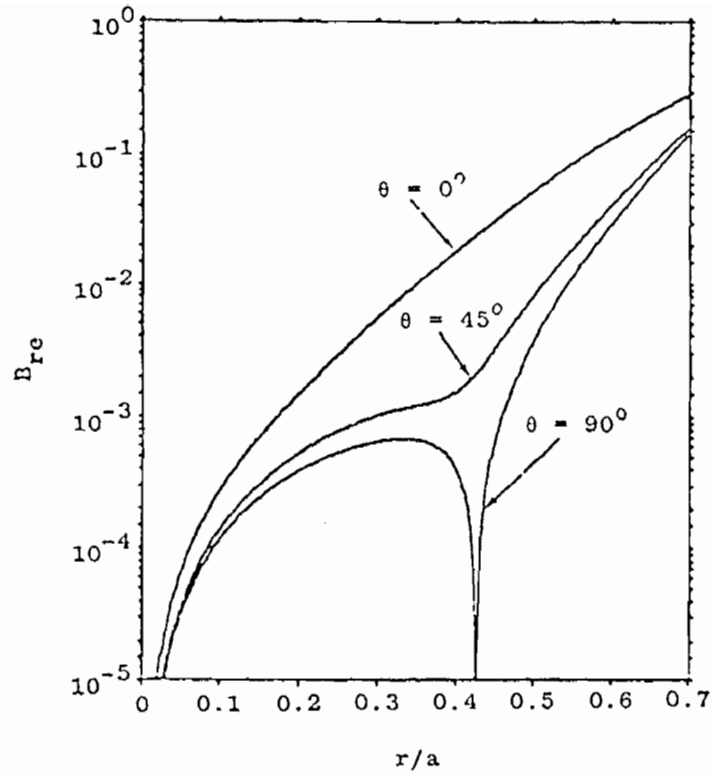
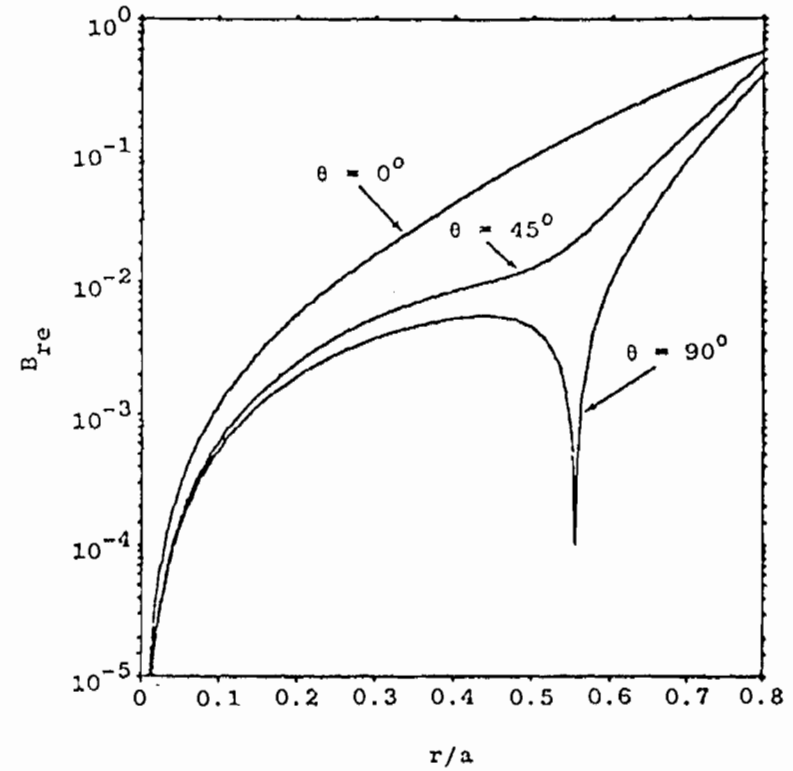
(a) $R = 0.7$ (b) $R = 0.8$

Figure 11. Relative error versus radius for volume-integral method; $R = 0.7$ and $R = 0.8$ (two pairs of loops).

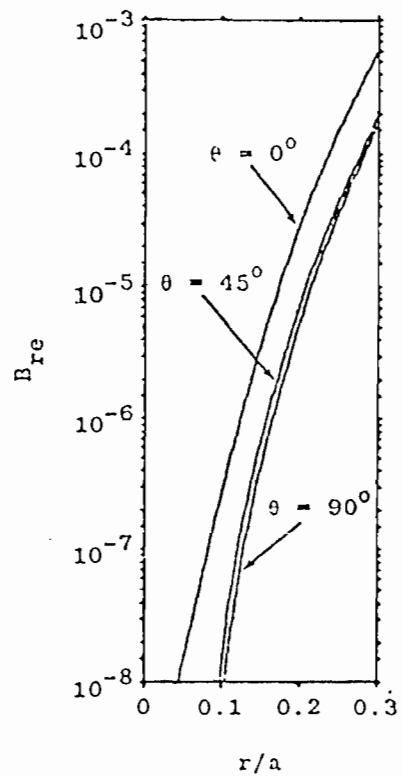
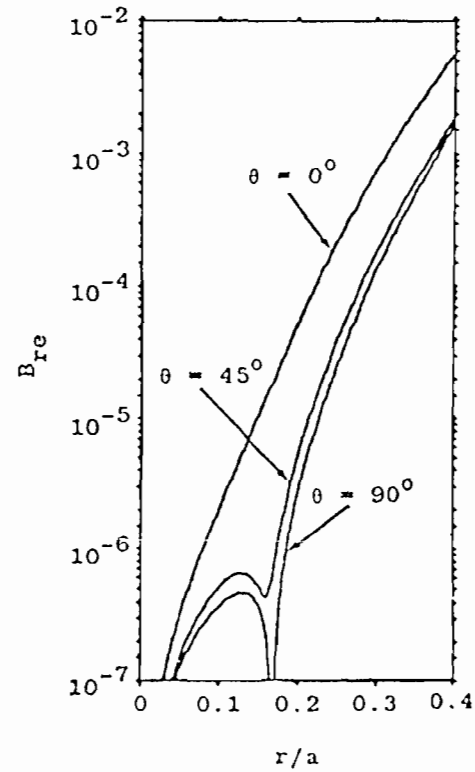
(a) $R = 0.3$ (b) $R = 0.4$

Figure 12. Relative error versus radius for surface-integral method; $R = 0.3$ and $R = 0.4$ (two pairs of loops).

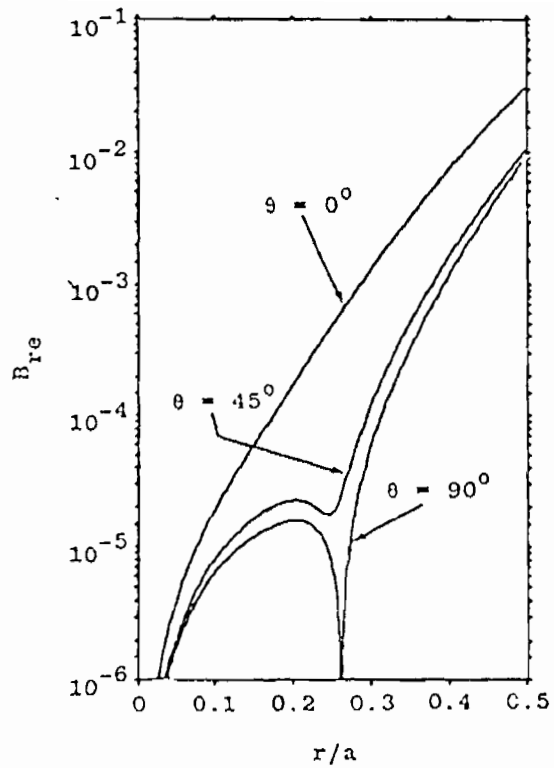
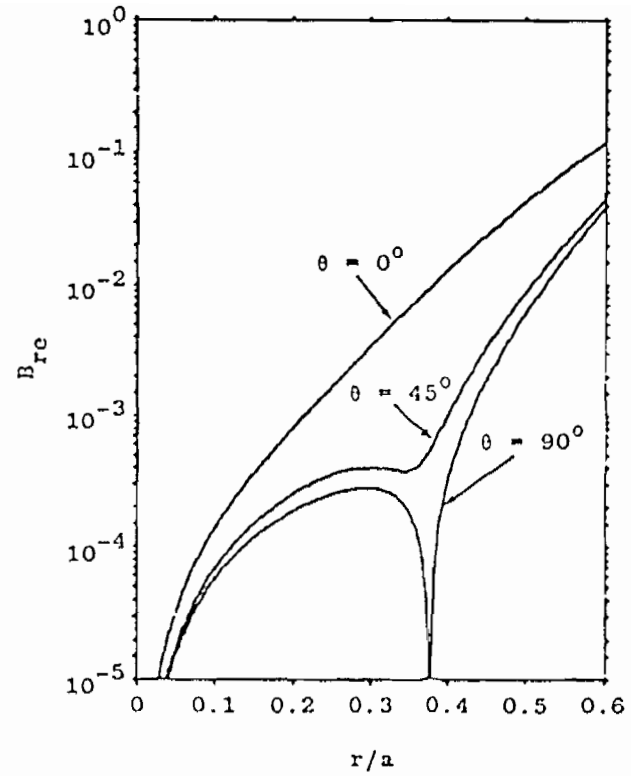
(a) $R = 0.5$ (b) $R = 0.6$

Figure 13. Relative error versus radius for surface-integral method; $R = 0.5$ and $R = 0.6$ (two pairs of loops).

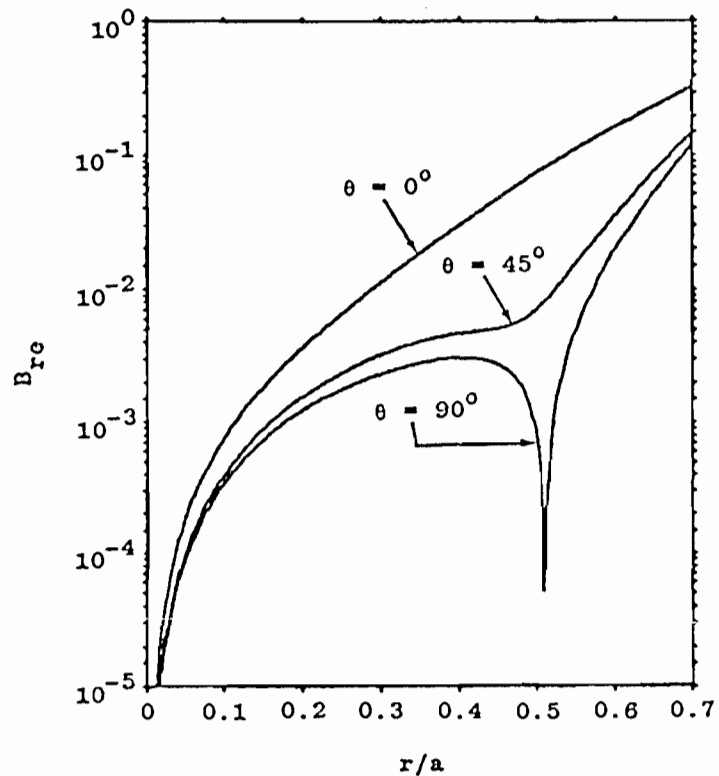
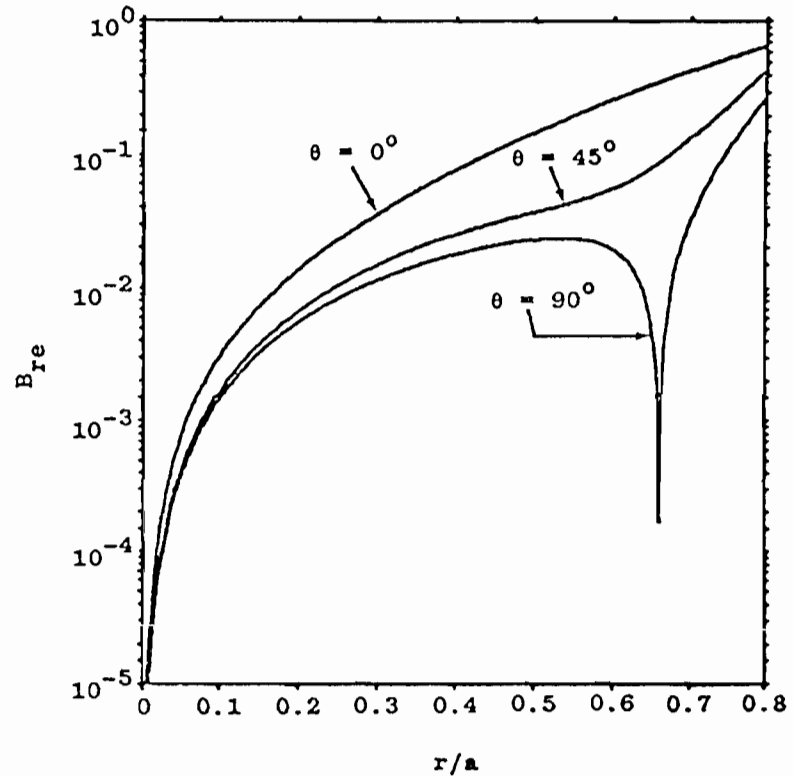
(a) $R = 0.7$ (b) $R = 0.8$

Figure 14. Relative error versus radius for surface-integral method; $R = 0.7$ and $R = 0.8$ (two pairs of loops).

radial component of \vec{B} orthogonal to B_z) were plotted and contours of constant $B_{ze} = (B_z - B_{z1})/B_{z1}$ were plotted. These are shown as overlays in Figures 15 through 26.

3. OPTIMUM LOOP POSITIONS FOR FIXED CURRENT RATIOS

It would be difficult to design a practical simulator with the ratio of currents in the various loops equal to or approximating an irrational number. The most reasonable approach would be to wire the loops (at least a symmetrical half of the loops) in series and adjust the number of turns in each loop to attain the appropriate ratios. For an accurate approximation to an irrational number, a large number of turns would generally be required. This would result in a large inductance and a difficulty in achieving sufficiently fast rise times. Therefore, a practical design will have a small number of turns in each loop. In this case, the ratio of currents can be represented by a fraction given by the turns ratio.

To explore the implications of fixing the current ratio to such fractions for the two-pair case, optimum loop positions were found for $I_2/I_1 = 1/2, 2/3, 3/4, 4/5, 5/6, 6/7, 7/8,$ and 1. These values bracket the optimum values given in Table 2. The results are given in Tables 5 through 12. It was found that, because of the peculiar behavior of χ as a function of the parameters, loop positions could be found for several of the current ratios that result in χ not much larger than its optimum value. This behavior gives the designer much more latitude than one might have originally expected.

KEY TO CONTOUR IDENTIFICATION	
CONTOUR I.D.	CONTOUR VALUE
0	0
±1	±5×10 ⁻¹³
±2	±1×10 ⁻¹²
±3	±2×10 ⁻¹²
±4	±5×10 ⁻¹²
±5	±1×10 ⁻¹¹
±6	±2×10 ⁻¹¹
±7	±5×10 ⁻¹¹
±8	±1×10 ⁻¹⁰
±9	±2×10 ⁻¹⁰
±10	±5×10 ⁻¹⁰
±11	±1×10 ⁻⁹
±12	±2×10 ⁻⁹
±13	±5×10 ⁻⁹
±14	±1×10 ⁻⁸
±15	±2×10 ⁻⁸
±16	±5×10 ⁻⁸
±17	±1×10 ⁻⁷
±18	±2×10 ⁻⁷
±19	±5×10 ⁻⁷
±20	±1×10 ⁻⁶
±21	±2×10 ⁻⁶
±22	±5×10 ⁻⁶
±23	±1×10 ⁻⁵
±24	±2×10 ⁻⁵
±25	±5×10 ⁻⁵
±26	±1×10 ⁻⁴
±27	±2×10 ⁻⁴
±28	±5×10 ⁻⁴
±29	±1×10 ⁻³
±30	±2×10 ⁻³
±31	±5×10 ⁻³
±32	±1×10 ⁻²
±33	±2×10 ⁻²
±34	±5×10 ⁻²
±35	±1×10 ⁻¹
±36	±2×10 ⁻¹
±37	±5×10 ⁻¹

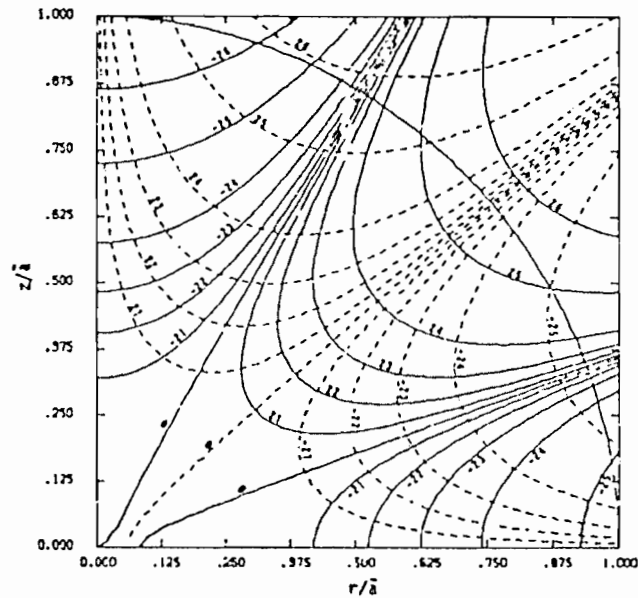
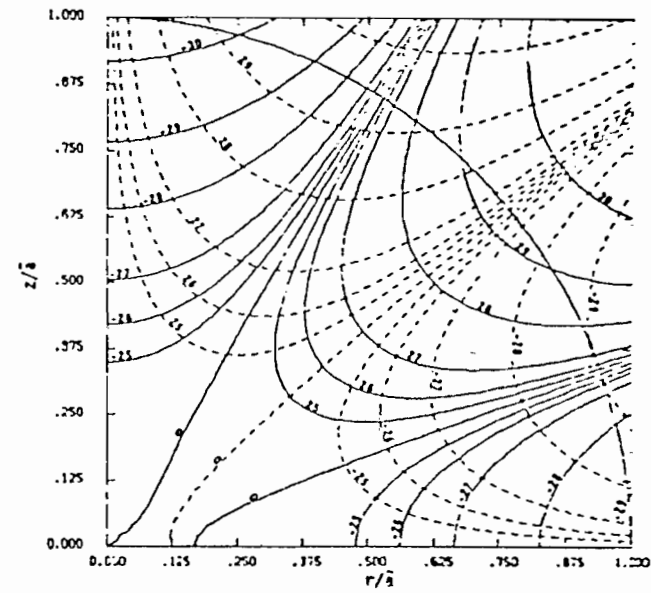
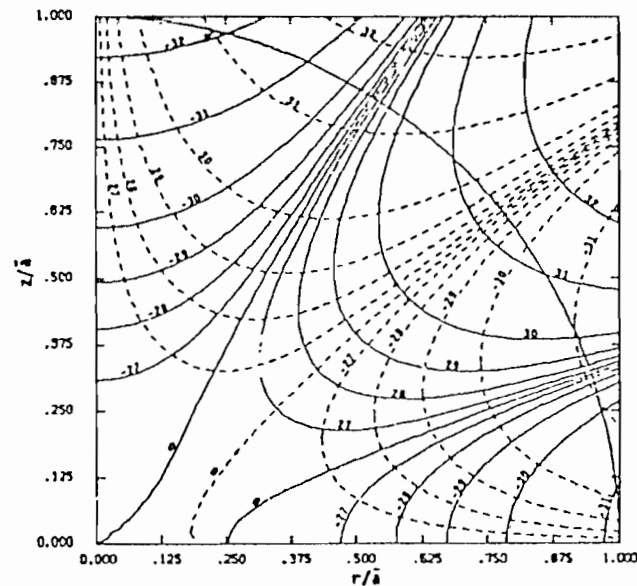
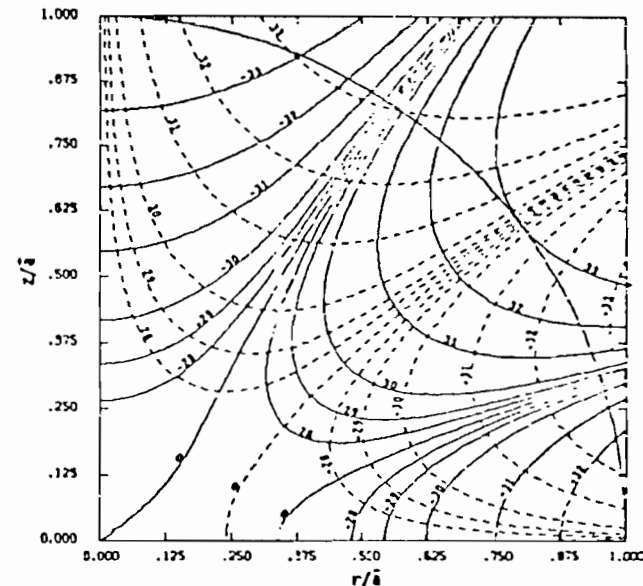
(a) $R = 0.1$ (b) $R = 0.2$ (c) $R = 0.3$ (d) $R = 0.4$

Figure 15. Contours of constant $(B_z - B_{z1})/B_{z1}$ (solid lines) and constant B_ρ/B_{z1} (dashed lines) for one pair of loops using the volume-integral method; $R = 0.1, 0.2, 0.3, \text{ and } 0.4$.

KEY TO CONTOUR IDENTIFICATION

CONTOUR I.D.	CONTOUR VALUE
0	0
±1	±5x10 ⁻¹³
±2	±1x10 ⁻¹²
±3	±2x10 ⁻¹²
±4	±5x10 ⁻¹²
±5	±1x10 ⁻¹¹
±6	±2x10 ⁻¹¹
±7	±5x10 ⁻¹¹
±8	±1x10 ⁻¹⁰
±9	±2x10 ⁻¹⁰
±10	±5x10 ⁻¹⁰
±11	±1x10 ⁻⁹
±12	±2x10 ⁻⁹
±13	±5x10 ⁻⁹
±14	±1x10 ⁻⁸
±15	±2x10 ⁻⁸
±16	±5x10 ⁻⁸
±17	±1x10 ⁻⁷
±18	±2x10 ⁻⁷
±19	±5x10 ⁻⁷
±20	±1x10 ⁻⁶
±21	±2x10 ⁻⁶
±22	±5x10 ⁻⁶
±23	±1x10 ⁻⁵
±24	±2x10 ⁻⁵
±25	±5x10 ⁻⁵
±26	±1x10 ⁻⁴
±27	±2x10 ⁻⁴
±28	±5x10 ⁻⁴
±29	±1x10 ⁻³
±30	±2x10 ⁻³
±31	±5x10 ⁻³
±32	±1x10 ⁻²
±33	±2x10 ⁻²
±34	±5x10 ⁻²
±35	±1x10 ⁻¹
±36	±2x10 ⁻¹
±37	±5x10 ⁻¹

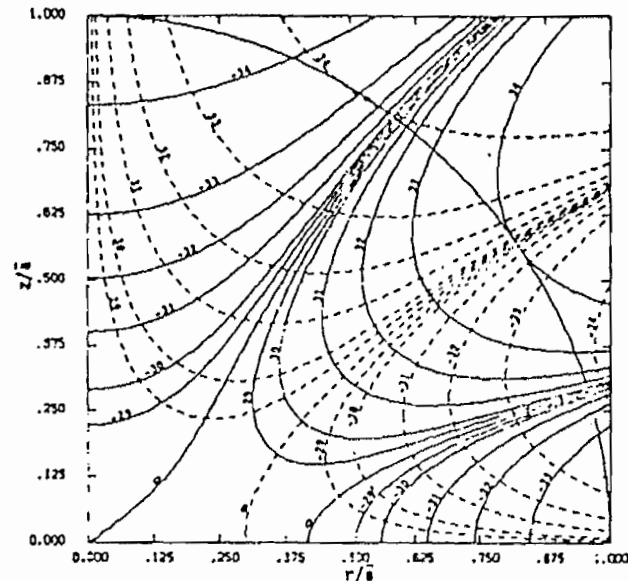
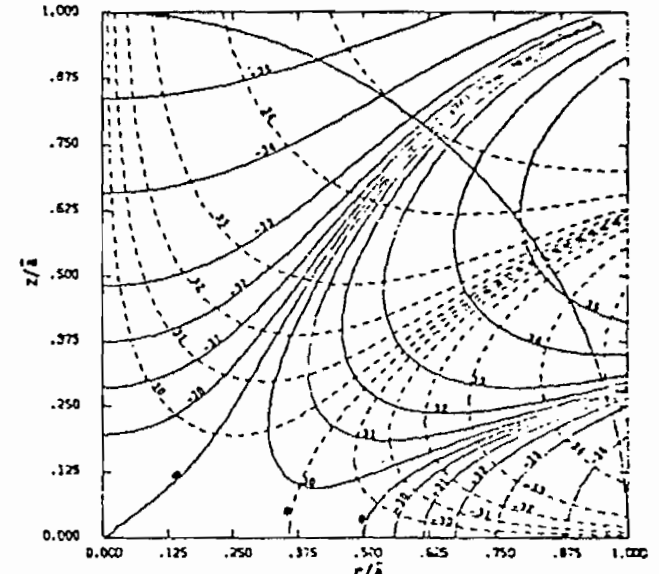
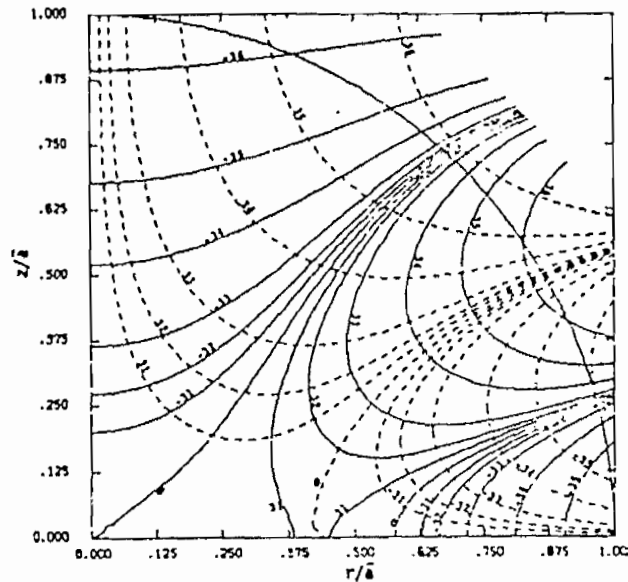
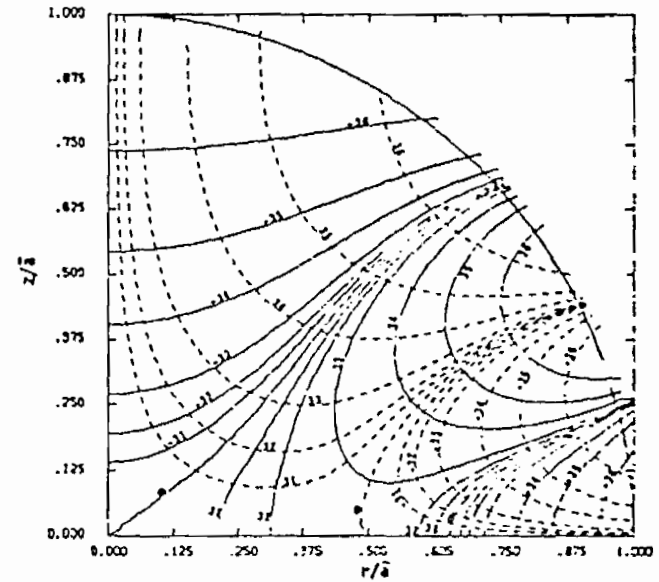
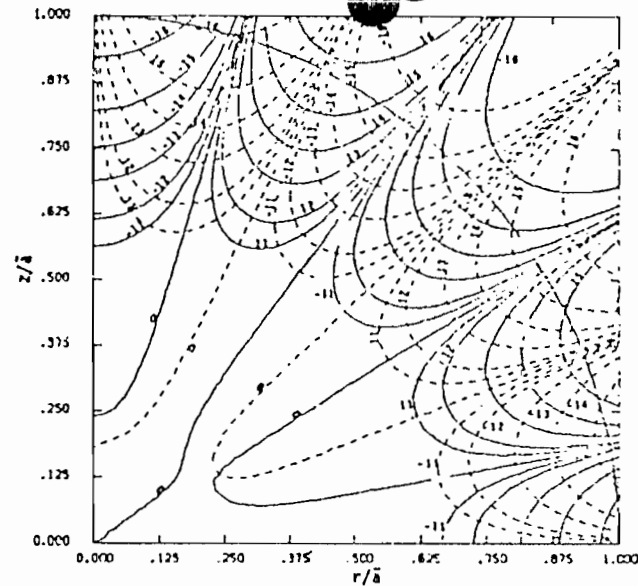
(a) $R = 0.5$ (b) $R = 0.6$ (c) $R = 0.7$ (d) $R = 0.8$

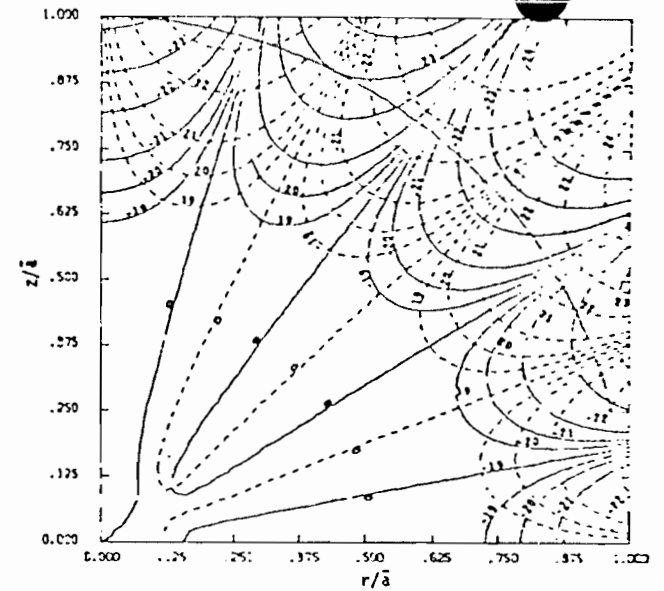
Figure 16. Contours of constant $(B_z - B_{z1})/B_{z1}$ (solid lines) and constant B_ρ/B_{z1} (dashed lines) for one pair of loops using the volume-integral method; $R = 0.5, 0.6, 0.7,$ and 0.8 .

KEY TO CONTOUR IDENTIFICATION

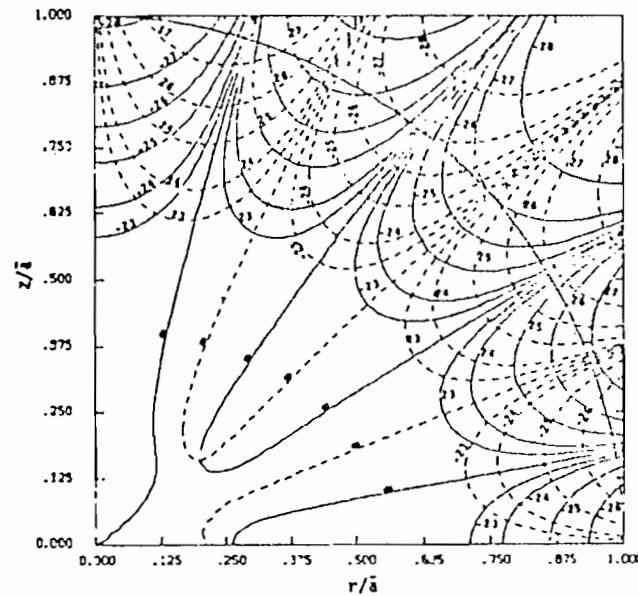
CONTOUR I.D.	CONTOUR VALUE
0	0
±1	±5x10 ⁻¹³
±2	±1x10 ⁻¹²
±3	±2x10 ⁻¹²
±4	±5x10 ⁻¹²
±5	±1x10 ⁻¹¹
±6	±2x10 ⁻¹¹
±7	±5x10 ⁻¹¹
±8	±1x10 ⁻¹⁰
±9	±2x10 ⁻¹⁰
±10	±5x10 ⁻¹⁰
±11	±1x10 ⁻⁹
±12	±2x10 ⁻⁹
±13	±5x10 ⁻⁹
±14	±1x10 ⁻⁸
±15	±2x10 ⁻⁸
±16	±5x10 ⁻⁸
±17	±1x10 ⁻⁷
±18	±2x10 ⁻⁷
±19	±5x10 ⁻⁷
±20	±1x10 ⁻⁶
±21	±2x10 ⁻⁶
±22	±5x10 ⁻⁶
±23	±1x10 ⁻⁵
±24	±2x10 ⁻⁵
±25	±5x10 ⁻⁵
±26	±1x10 ⁻⁴
±27	±2x10 ⁻⁴
±28	±5x10 ⁻⁴
±29	±1x10 ⁻³
±30	±2x10 ⁻³
±31	±5x10 ⁻³
±32	±1x10 ⁻²
±33	±2x10 ⁻²
±34	±5x10 ⁻²
±35	±1x10 ⁻¹
±36	±2x10 ⁻¹
±37	±5x10 ⁻¹



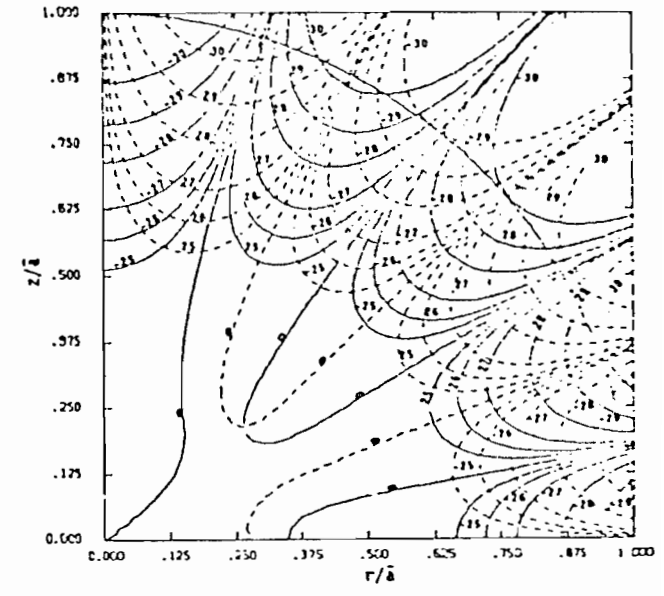
(a) R = 0.1



(b) R = 0.2



(c) R = 0.3



(d) R = 0.4

Figure 17. Contours of constant $(B_z - B_{z1})/B_{z1}$ (solid lines) and constant B_ρ/B_{z1} (dashed lines) for two pairs of loops using the volume-integral method; $R = 0.1, 0.2, 0.3,$ and 0.4 .

KEY TO CONTOUR IDENTIFICATION	
CONTOUR I.D.	CONTOUR VALUE
0	0
±1	±5x10 ⁻¹³
±2	±1x10 ⁻¹²
±3	±2x10 ⁻¹²
±4	±5x10 ⁻¹²
±5	±1x10 ⁻¹¹
±6	±2x10 ⁻¹¹
±7	±5x10 ⁻¹¹
±8	±1x10 ⁻¹⁰
±9	±2x10 ⁻¹⁰
±10	±5x10 ⁻¹⁰
±11	±1x10 ⁻⁹
±12	±2x10 ⁻⁹
±13	±5x10 ⁻⁹
±14	±1x10 ⁻⁸
±15	±2x10 ⁻⁸
±16	±5x10 ⁻⁸
±17	±1x10 ⁻⁷
±18	±2x10 ⁻⁷
±19	±5x10 ⁻⁷
±20	±1x10 ⁻⁶
±21	±2x10 ⁻⁶
±22	±5x10 ⁻⁶
±23	±1x10 ⁻⁵
±24	±2x10 ⁻⁵
±25	±5x10 ⁻⁵
±26	±1x10 ⁻⁴
±27	±2x10 ⁻⁴
±28	±5x10 ⁻⁴
±29	±1x10 ⁻³
±30	±2x10 ⁻³
±31	±5x10 ⁻³
±32	±1x10 ⁻²
±33	±2x10 ⁻²
±34	±5x10 ⁻²
±35	±1x10 ⁻¹
±36	±2x10 ⁻¹
±37	±5x10 ⁻¹

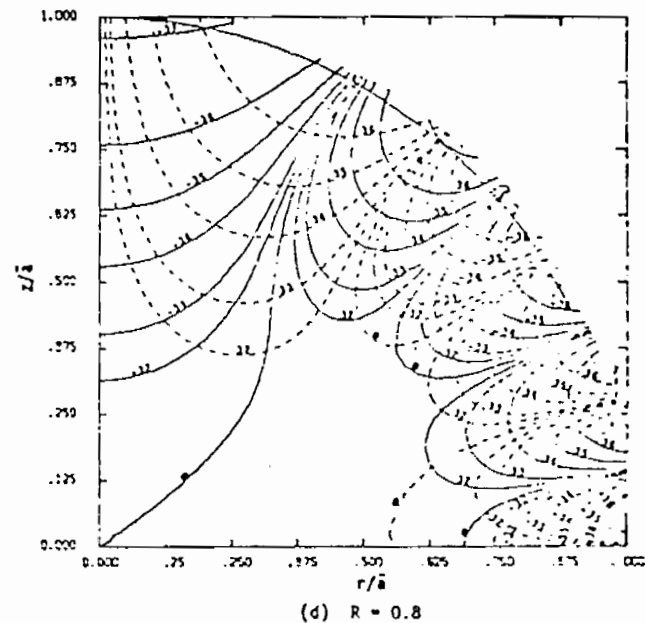
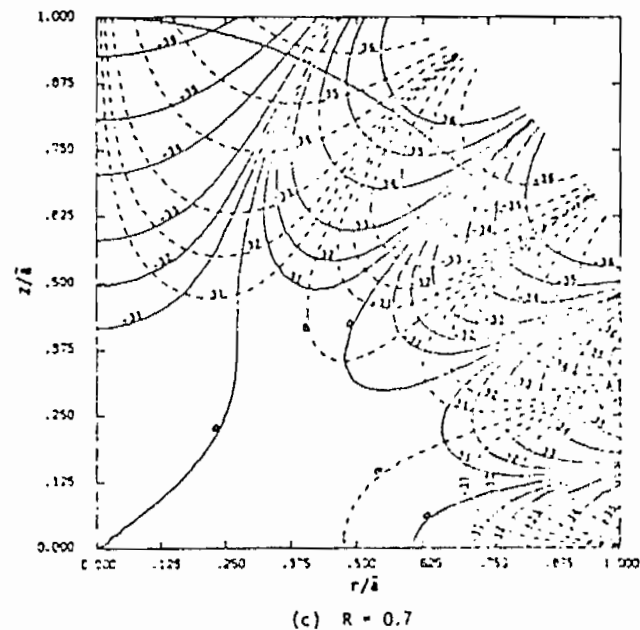
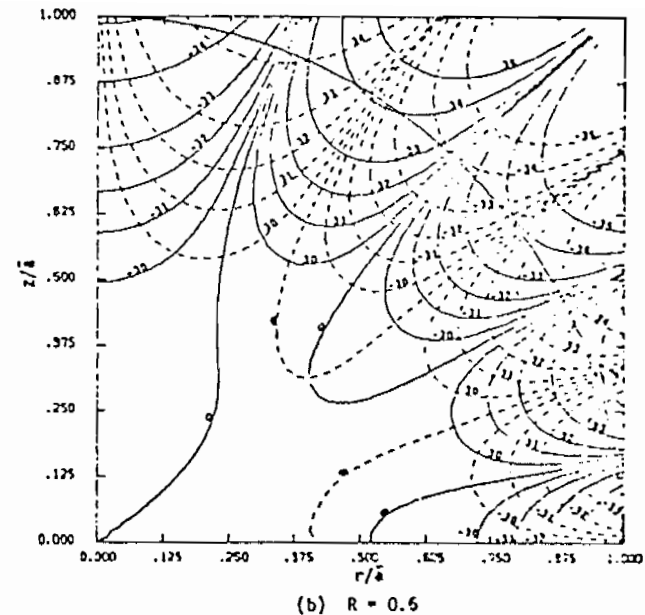
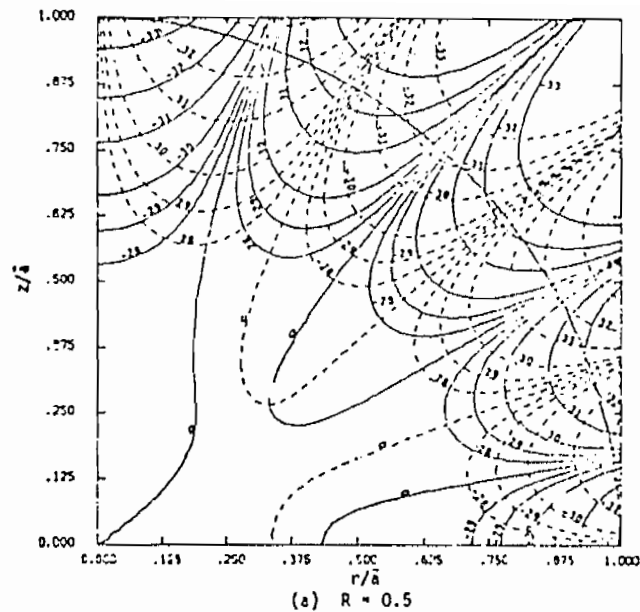


Figure 18. Contours of constant $(B_z - B_{z1})/B_{z1}$ (solid lines) and constant B_z/B_{z1} (dashed lines) for two pairs of loops using the volume-integral method; $R = 0.5, 0.6, 0.7, \text{ and } 0.8$

KEY TO CONTOUR IDENTIFICATION

CONTOUR I.D.	CONTOUR VALUE
0	0
±1	±5x10 ⁻¹³
±2	±1x10 ⁻¹²
±3	±2x10 ⁻¹²
±4	±5x10 ⁻¹²
±5	±1x10 ⁻¹¹
±6	±2x10 ⁻¹¹
±7	±5x10 ⁻¹¹
±8	±1x10 ⁻¹⁰
±9	±2x10 ⁻¹⁰
±10	±5x10 ⁻¹⁰
±11	±1x10 ⁻⁹
±12	±2x10 ⁻⁹
±13	±5x10 ⁻⁹
±14	±1x10 ⁻⁸
±15	±2x10 ⁻⁸
±16	±5x10 ⁻⁸
±17	±1x10 ⁻⁷
±18	±2x10 ⁻⁷
±19	±5x10 ⁻⁷
±20	±1x10 ⁻⁶
±21	±2x10 ⁻⁶
±22	±5x10 ⁻⁶
±23	±1x10 ⁻⁵
±24	±2x10 ⁻⁵
±25	±5x10 ⁻⁵
±26	±1x10 ⁻⁴
±27	±2x10 ⁻⁴
±28	±5x10 ⁻⁴
±29	±1x10 ⁻³
±30	±2x10 ⁻³
±31	±5x10 ⁻³
±32	±1x10 ⁻²
±33	±2x10 ⁻²
±34	±5x10 ⁻²
±35	±1x10 ⁻¹
±36	±2x10 ⁻¹
±37	±5x10 ⁻¹

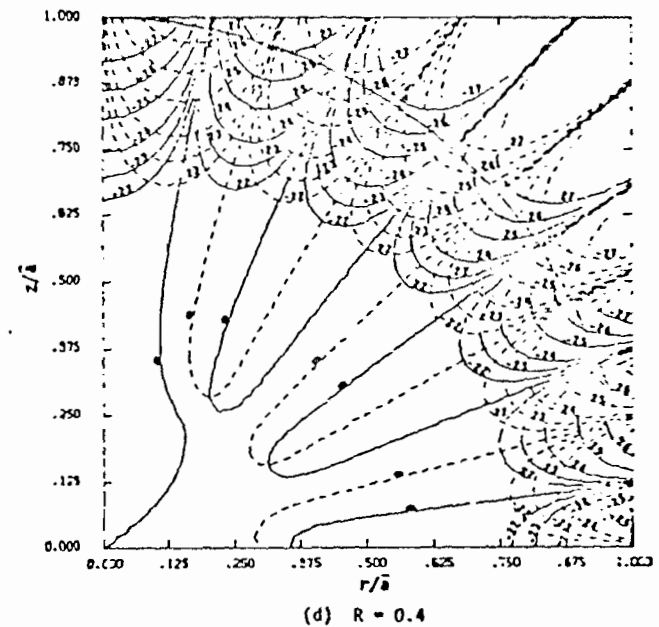
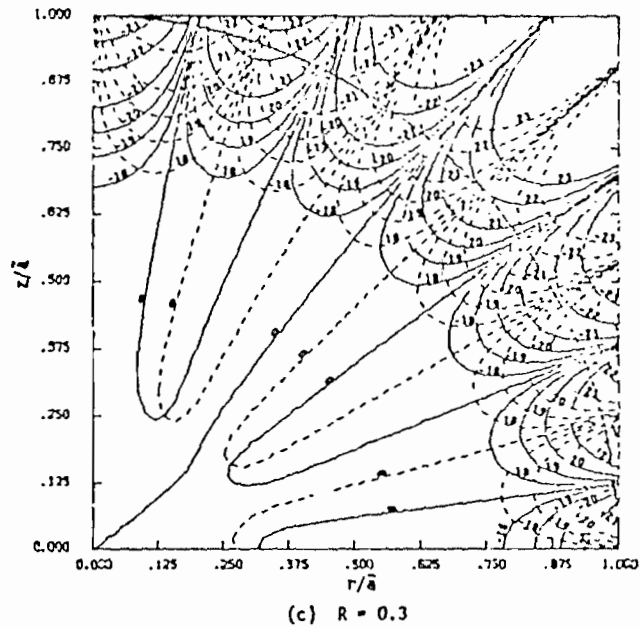
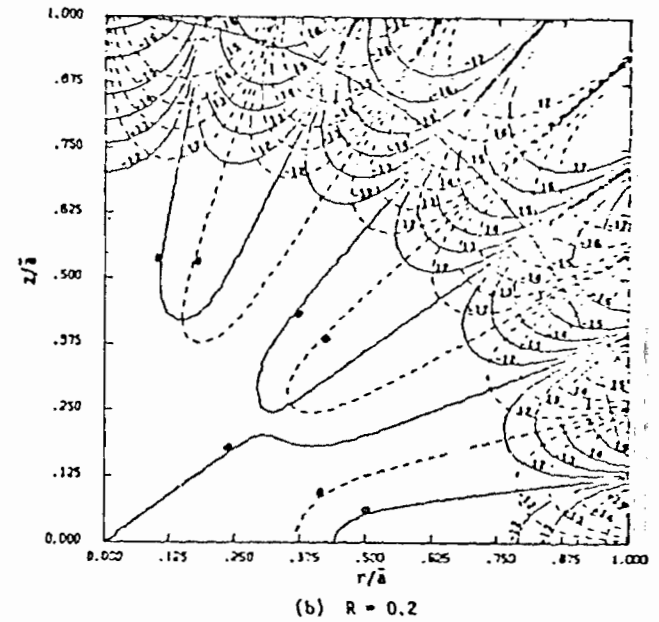
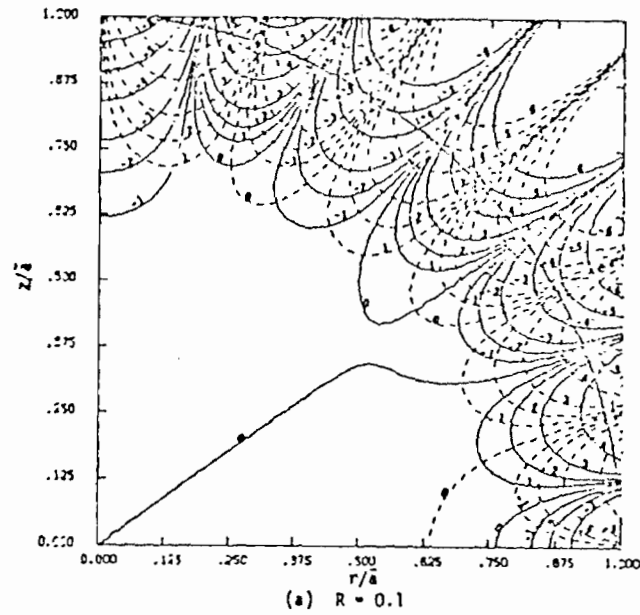


Figure 19. Contours of constant $(B_z - B_{z1})/B_{z1}$ (solid lines) and constant B_ρ/B_{z1} (dashed lines) for three pairs of loops using the volume-integral method; $R = 0.1, 0.2, 0.3,$ and 0.4 .

KEY TO CONTOUR IDENTIFICATION	
CONTOUR I.D.	CONTOUR VALUE
0	0
±1	±5x10 ⁻¹³
±2	±1x10 ⁻¹²
±3	±2x10 ⁻¹²
±4	±5x10 ⁻¹²
±5	±1x10 ⁻¹¹
±6	±2x10 ⁻¹¹
±7	±5x10 ⁻¹¹
±8	±1x10 ⁻¹⁰
±9	±2x10 ⁻¹⁰
±10	±5x10 ⁻¹⁰
±11	±1x10 ⁻⁹
±12	±2x10 ⁻⁹
±13	±5x10 ⁻⁹
±14	±1x10 ⁻⁸
±15	±2x10 ⁻⁸
±16	±5x10 ⁻⁸
±17	±1x10 ⁻⁷
±18	±2x10 ⁻⁷
±19	±5x10 ⁻⁷
±20	±1x10 ⁻⁶
±21	±2x10 ⁻⁶
±22	±5x10 ⁻⁶
±23	±1x10 ⁻⁵
±24	±2x10 ⁻⁵
±25	±5x10 ⁻⁵
±26	±1x10 ⁻⁴
±27	±2x10 ⁻⁴
±28	±5x10 ⁻⁴
±29	±1x10 ⁻³
±30	±2x10 ⁻³
±31	±5x10 ⁻³
±32	±1x10 ⁻²
±33	±2x10 ⁻²
±34	±5x10 ⁻²
±35	±1x10 ⁻¹
±36	±2x10 ⁻¹
±37	±5x10 ⁻¹

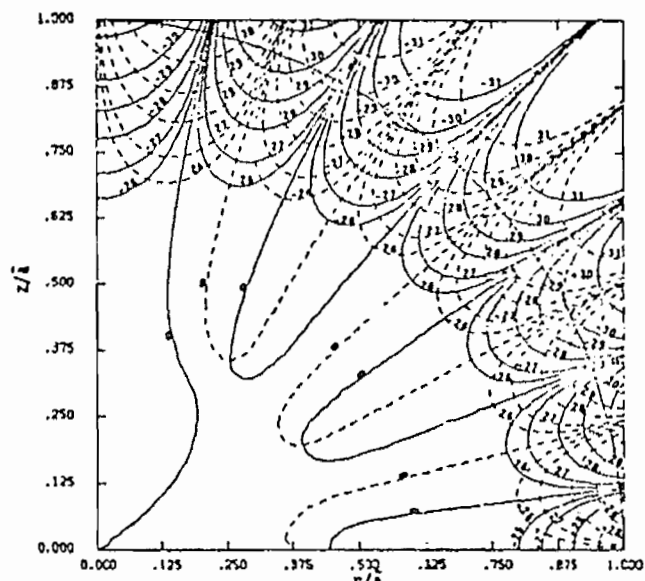
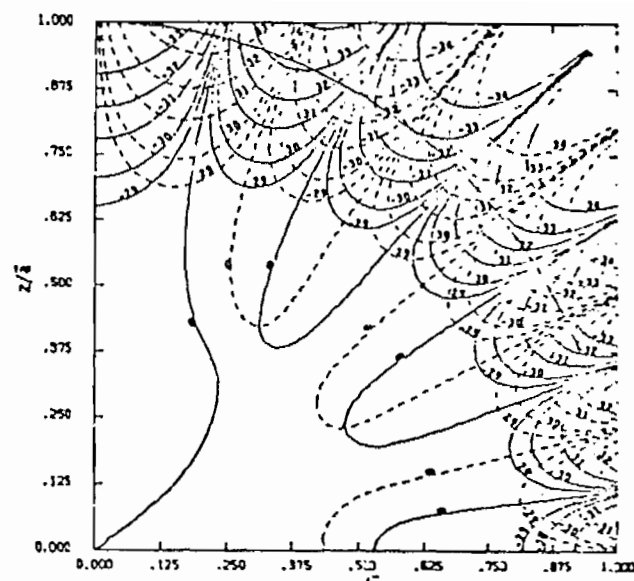
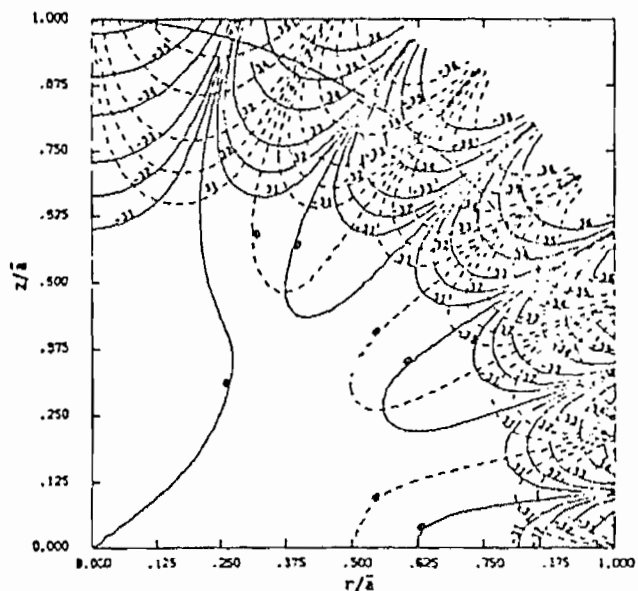
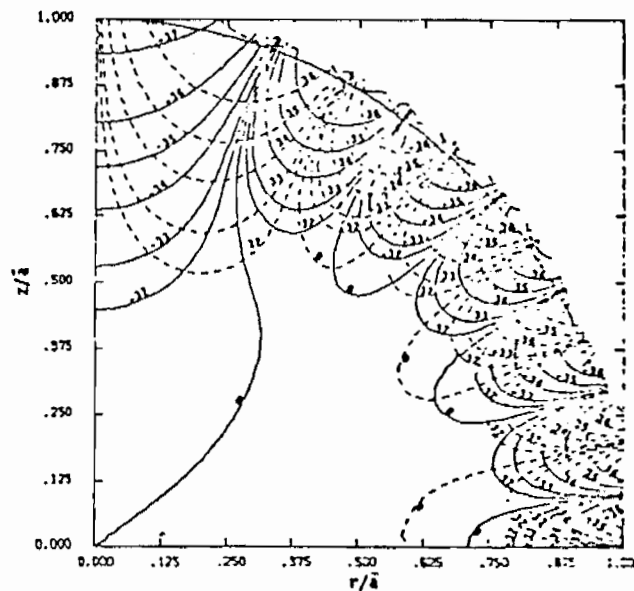
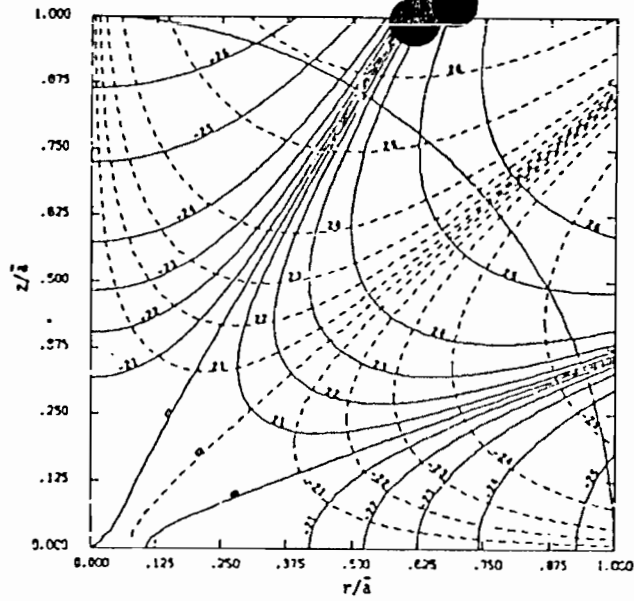
(a) $R = 0.5$ (b) $R = 0.6$ (c) $R = 0.7$ (d) $R = 0.8$

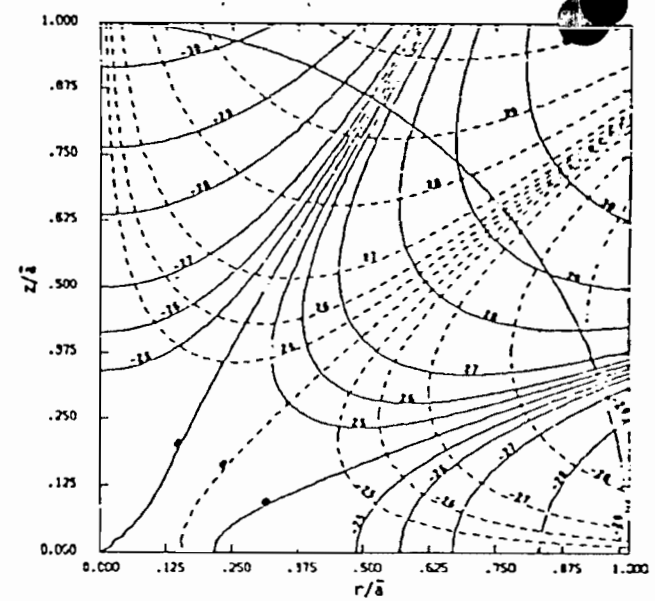
Figure 20. Contours of constant $(B_z - B_{z1})/B_{z1}$ (solid lines) and constant B_0/B_{z1} (dashed lines) for three pairs of loops using the volume-integral method; $R = 0.5, 0.6, 0.7, \text{ and } 0.8$.

TO CONTOUR IDENTIFICATION
 CONTOUR I.D. CONTOUR VALUE

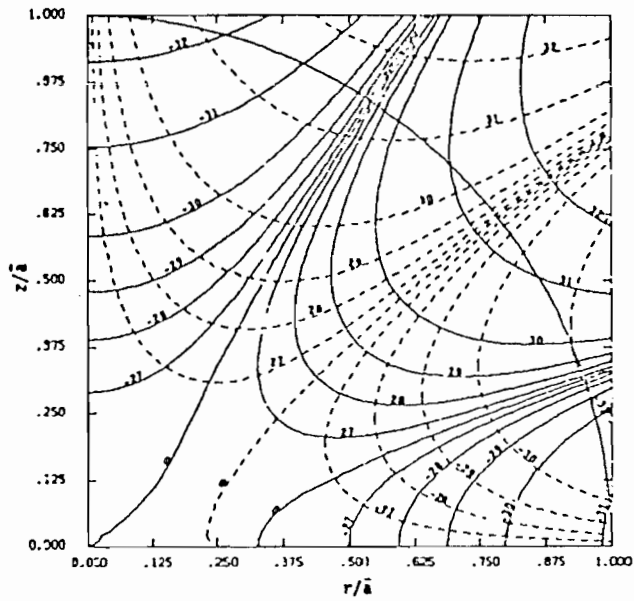
0	0
±1	±5x10 ⁻¹³
±2	±1x10 ⁻¹²
±3	±2x10 ⁻¹²
±4	±5x10 ⁻¹²
±5	±1x10 ⁻¹¹
±6	±2x10 ⁻¹¹
±7	±5x10 ⁻¹¹
±8	±1x10 ⁻¹⁰
±9	±2x10 ⁻¹⁰
±10	±5x10 ⁻¹⁰
±11	±1x10 ⁻⁹
±12	±2x10 ⁻⁹
±13	±5x10 ⁻⁹
±14	±1x10 ⁻⁸
±15	±2x10 ⁻⁸
±16	±5x10 ⁻⁸
±17	±1x10 ⁻⁷
±18	±2x10 ⁻⁷
±19	±5x10 ⁻⁷
±20	±1x10 ⁻⁶
±21	±2x10 ⁻⁶
±22	±5x10 ⁻⁶
±23	±1x10 ⁻⁵
±24	±2x10 ⁻⁵
±25	±5x10 ⁻⁵
±26	±1x10 ⁻⁴
±27	±2x10 ⁻⁴
±28	±5x10 ⁻⁴
±29	±1x10 ⁻³
±30	±2x10 ⁻³
±31	±5x10 ⁻³
±32	±1x10 ⁻²
±33	±2x10 ⁻²
±34	±5x10 ⁻²
±35	±1x10 ⁻¹
±36	±2x10 ⁻¹
±37	±5x10 ⁻¹



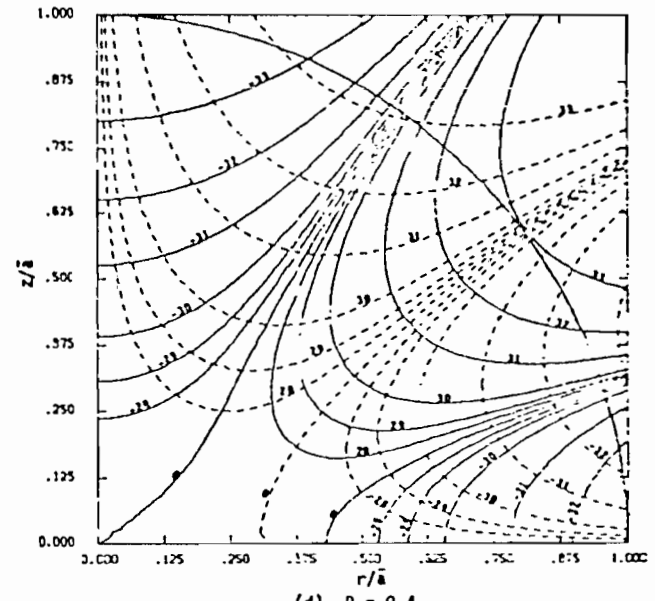
(a) R = 0.1



(b) R = 0.2



(c) R = 0.3



(d) R = 0.4

Figure 21. Contours of constant $(B_z - B_{z1})/B_{z1}$ (solid lines) and constant B_ρ/B_{z1} (dashed lines) for one pair of loops using the surface-integral method; $R = 0.1, 0.2, 0.3, \text{ and } 0.4$.

KEY TO CONTOUR IDENTIFICATION

CONTOUR I.D.	CONTOUR VALUE
0	0
±1	±5×10 ⁻¹³
±2	±1×10 ⁻¹²
±3	±2×10 ⁻¹²
±4	±5×10 ⁻¹²
±5	±1×10 ⁻¹¹
±6	±2×10 ⁻¹¹
±7	±5×10 ⁻¹¹
±8	±1×10 ⁻¹⁰
±9	±2×10 ⁻¹⁰
±10	±5×10 ⁻¹⁰
±11	±1×10 ⁻⁹
±12	±2×10 ⁻⁹
±13	±5×10 ⁻⁹
±14	±1×10 ⁻⁸
±15	±2×10 ⁻⁸
±16	±5×10 ⁻⁸
±17	±1×10 ⁻⁷
±18	±2×10 ⁻⁷
±19	±5×10 ⁻⁷
±20	±1×10 ⁻⁶
±21	±2×10 ⁻⁶
±22	±5×10 ⁻⁶
±23	±1×10 ⁻⁵
±24	±2×10 ⁻⁵
±25	±5×10 ⁻⁵
±26	±1×10 ⁻⁴
±27	±2×10 ⁻⁴
±28	±5×10 ⁻⁴
±29	±1×10 ⁻³
±30	±2×10 ⁻³
±31	±5×10 ⁻³
±32	±1×10 ⁻²
±33	±2×10 ⁻²
±34	±5×10 ⁻²
±35	±1×10 ⁻¹
±36	±2×10 ⁻¹
±37	±5×10 ⁻¹

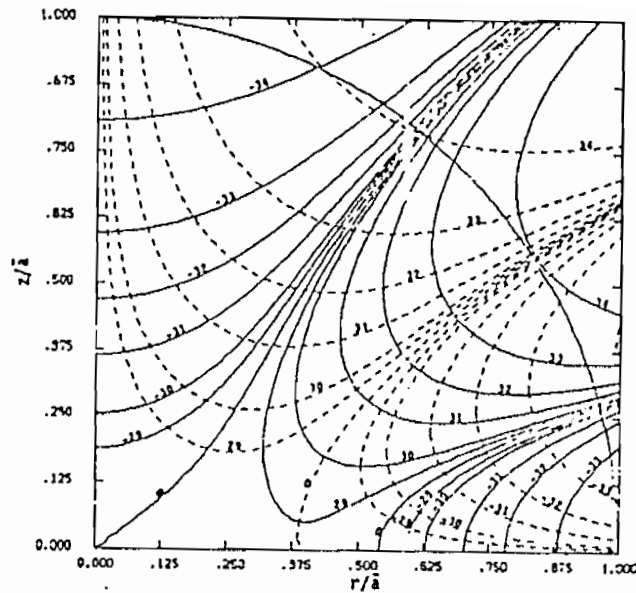
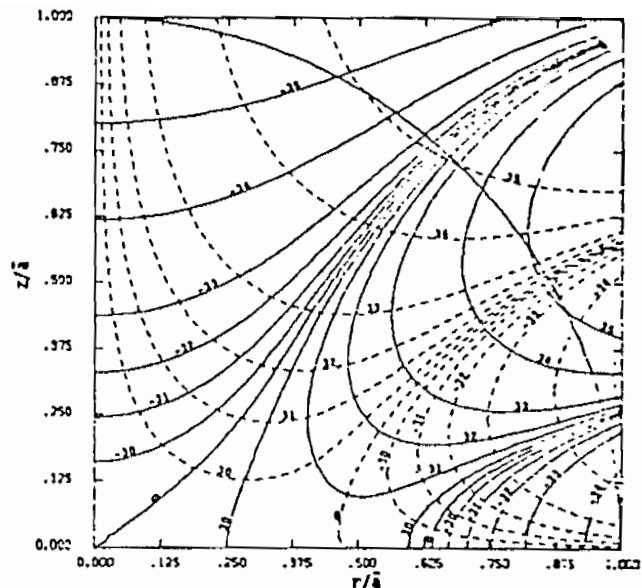
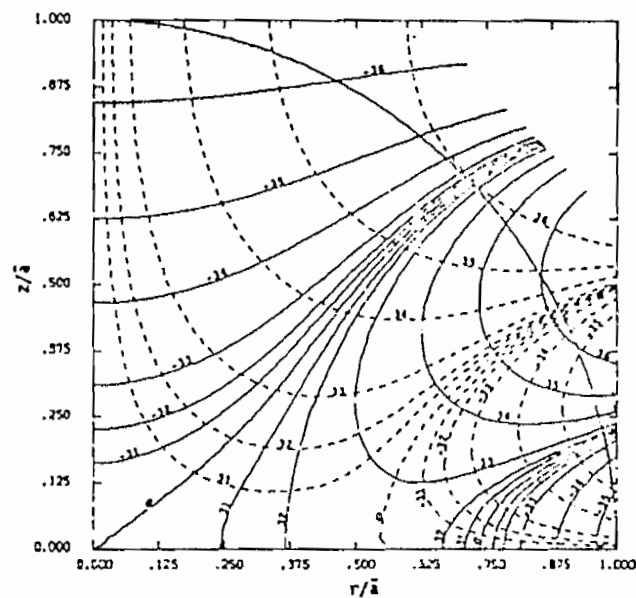
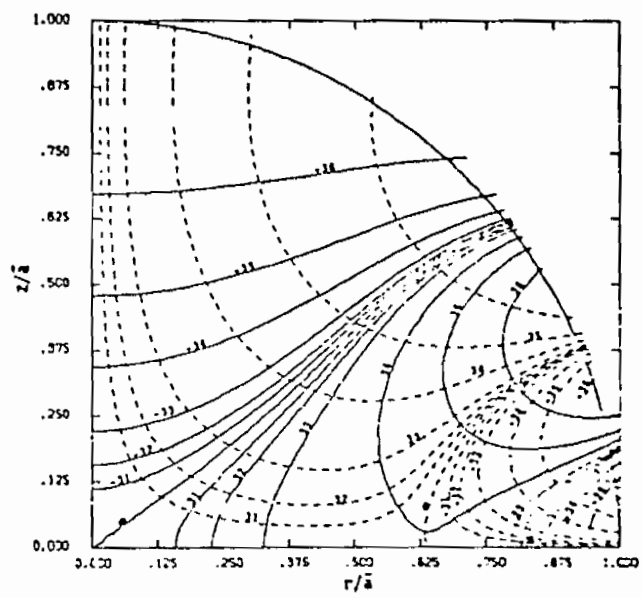
(a) $R = 0.5$ (b) $R = 0.6$ (c) $R = 0.7$ (d) $R = 0.8$

Figure 22. Contours of constant $(B_z - B_{z1})/B_{z1}$ (solid lines) and constant B_ρ/B_{z1} (dashed lines) for one pair of loops using the surface-integral method; $R = 0.5, 0.6, 0.7,$ and 0.8 .

KEY TO CONTOUR IDENTIFICATION	
CONTOUR I.D.	CONTOUR VALUE
0	0
±1	±5×10 ⁻¹³
±2	±1×10 ⁻¹²
±3	±2×10 ⁻¹²
±4	±5×10 ⁻¹²
±5	±1×10 ⁻¹¹
±6	±2×10 ⁻¹¹
±7	±5×10 ⁻¹¹
±8	±1×10 ⁻¹⁰
±9	±2×10 ⁻¹⁰
±10	±5×10 ⁻¹⁰
±11	±1×10 ⁻⁹
±12	±2×10 ⁻⁹
±13	±5×10 ⁻⁹
±14	±1×10 ⁻⁸
±15	±2×10 ⁻⁸
±16	±5×10 ⁻⁸
±17	±1×10 ⁻⁷
±18	±2×10 ⁻⁷
±19	±5×10 ⁻⁷
±20	±1×10 ⁻⁶
±21	±2×10 ⁻⁶
±22	±5×10 ⁻⁶
±23	±1×10 ⁻⁵
±24	±2×10 ⁻⁵
±25	±5×10 ⁻⁵
±26	±1×10 ⁻⁴
±27	±2×10 ⁻⁴
±28	±5×10 ⁻⁴
±29	±1×10 ⁻³
±30	±2×10 ⁻³
±31	±5×10 ⁻³
±32	±1×10 ⁻²
±33	±2×10 ⁻²
±34	±5×10 ⁻²
±35	±1×10 ⁻¹
±36	±2×10 ⁻¹
±37	±5×10 ⁻¹

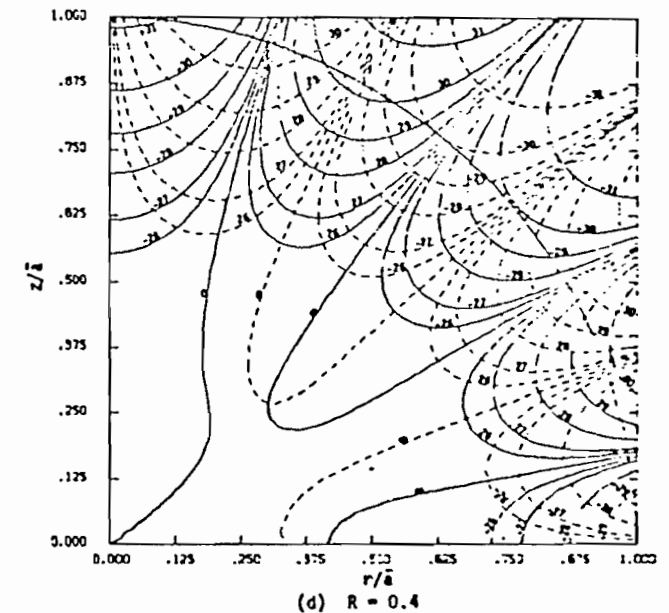
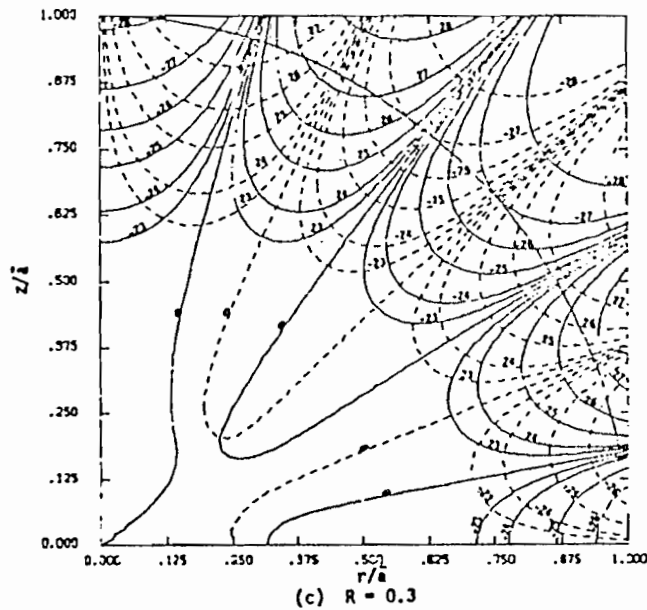
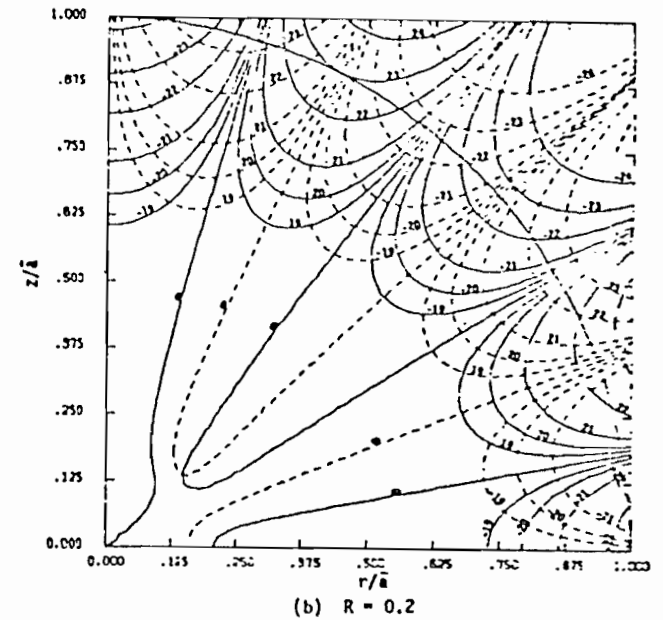
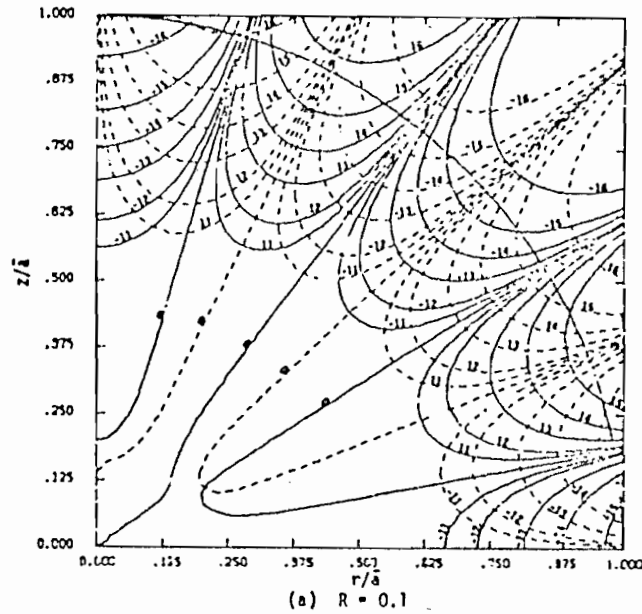


Figure 23. Contours of constant $(B_z - B_{z1})/B_{z1}$ (solid lines) and constant B_ρ/B_{z1} (dashed lines) for two pairs of loops using the surface-integral method; $R = 0.1, 0.2, 0.3,$ and 0.4 .

KEY TO CONTOUR IDENTIFICATION	
CONTOUR I.D.	CONTOUR VALUE
0	0
±1	±5×10 ⁻¹³
±2	±1×10 ⁻¹²
±3	±2×10 ⁻¹²
±4	±5×10 ⁻¹²
±5	±1×10 ⁻¹¹
±6	±2×10 ⁻¹¹
±7	±5×10 ⁻¹¹
±8	±1×10 ⁻¹⁰
±9	±2×10 ⁻¹⁰
±10	±5×10 ⁻¹⁰
±11	±1×10 ⁻⁹
±12	±2×10 ⁻⁹
±13	±5×10 ⁻⁹
±14	±1×10 ⁻⁸
±15	±2×10 ⁻⁸
±16	±5×10 ⁻⁸
±17	±1×10 ⁻⁷
±18	±2×10 ⁻⁷
±19	±5×10 ⁻⁷
±20	±1×10 ⁻⁶
±21	±2×10 ⁻⁶
±22	±5×10 ⁻⁶
±23	±1×10 ⁻⁵
±24	±2×10 ⁻⁵
±25	±5×10 ⁻⁵
±26	±1×10 ⁻⁴
±27	±2×10 ⁻⁴
±28	±5×10 ⁻⁴
±29	±1×10 ⁻³
±30	±2×10 ⁻³
±31	±5×10 ⁻³
±32	±1×10 ⁻²
±33	±2×10 ⁻²
±34	±5×10 ⁻²
±35	±1×10 ⁻¹
±36	±2×10 ⁻¹
±37	±5×10 ⁻¹

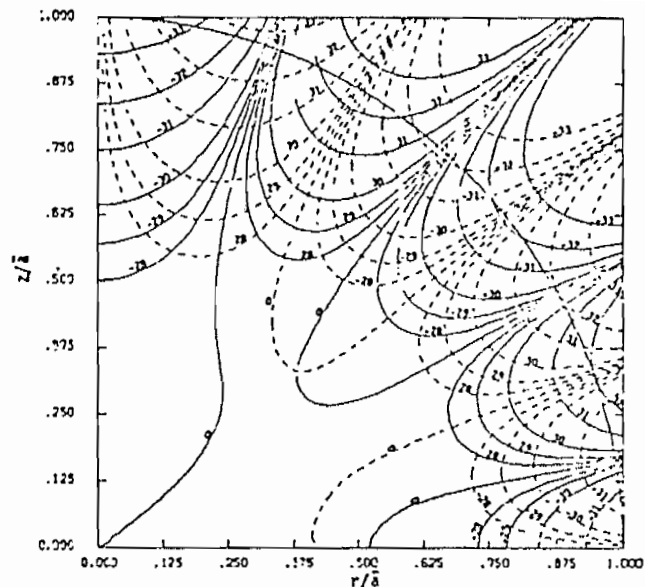
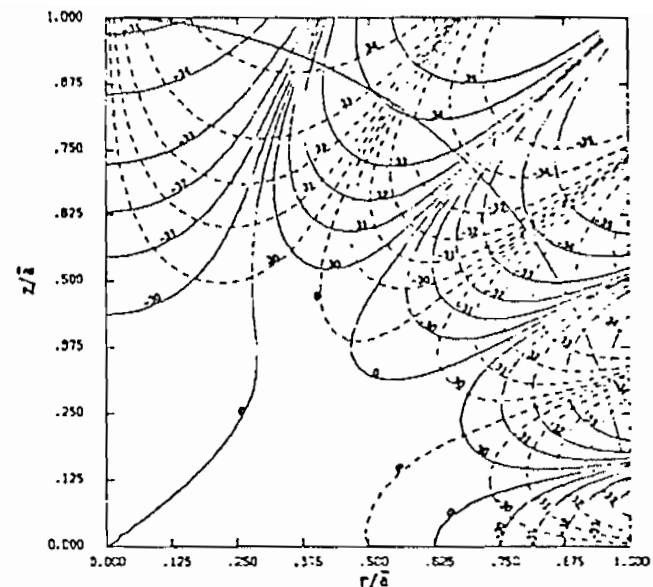
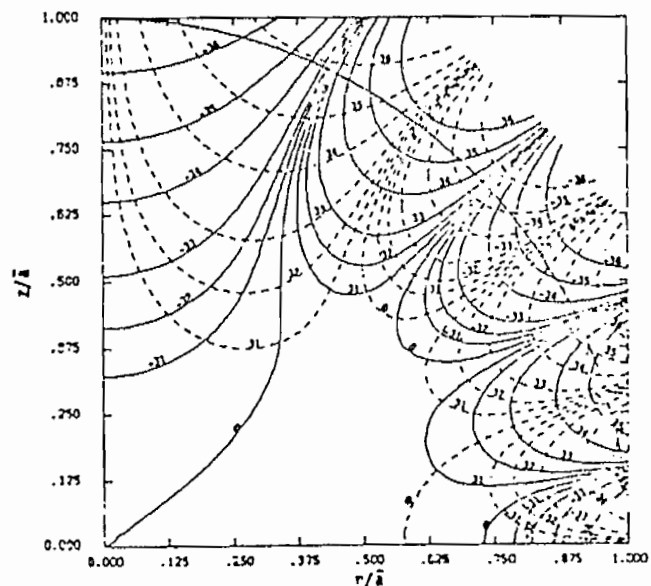
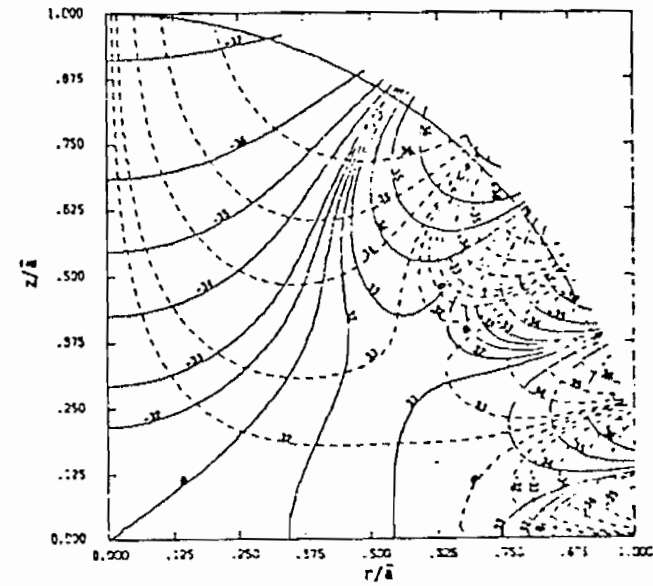
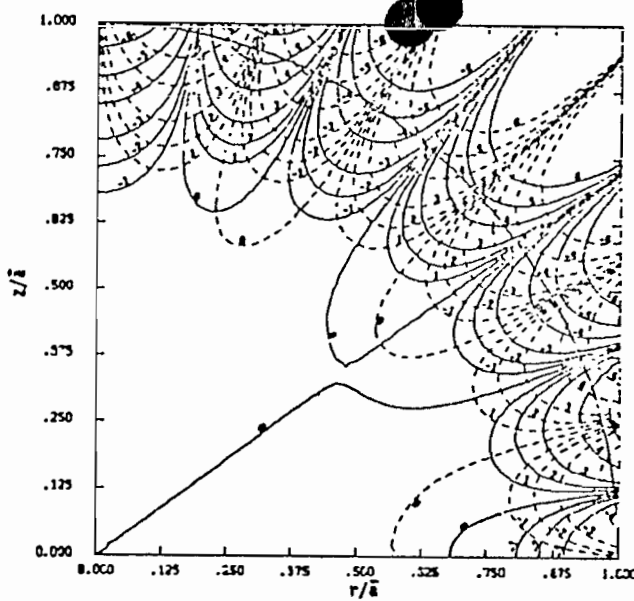
(a) $R = 0.5$ (b) $R = 0.6$ (c) $R = 0.7$ (d) $R = 0.8$

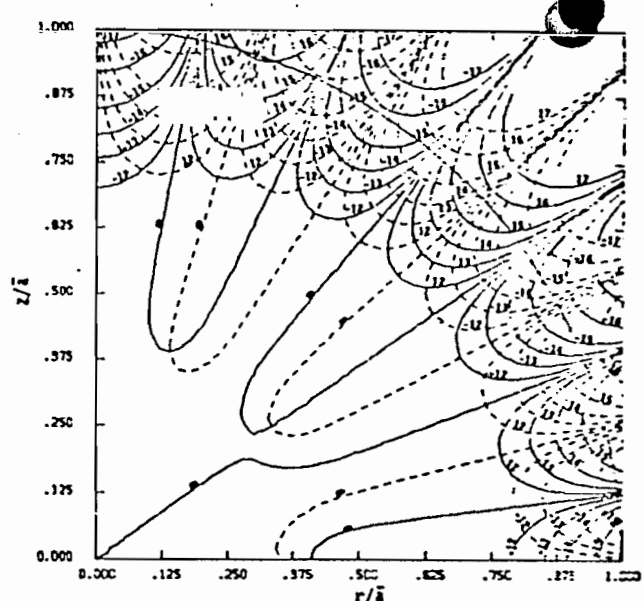
Figure 24. Contours of constant $(B_z - B_{z1})/B_{z1}$ (solid lines) and constant B_0/B_{z1} (dashed lines) for two pairs of loops using the surface-integral method; $R = 0.5, 0.6, 0.7,$ and 0.8 .

TO CONTOUR IDENTIFICATION

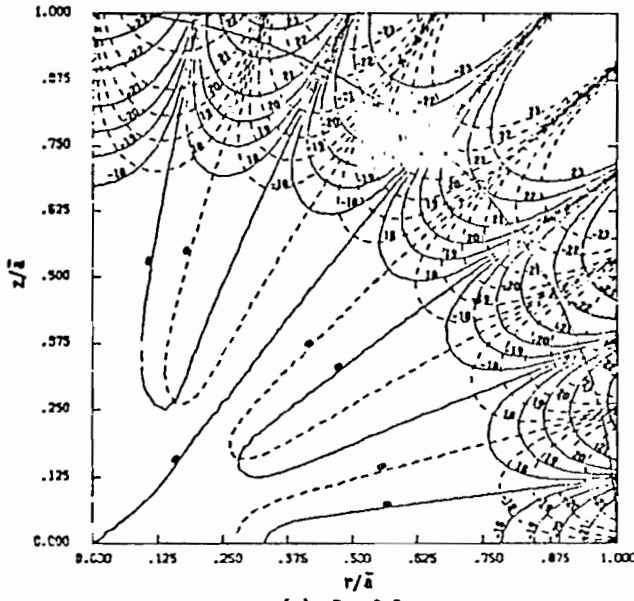
CONTOUR I.D.	CONTOUR VALUE
0	0
±1	±5x10 ⁻¹³
±2	±1x10 ⁻¹²
±3	±2x10 ⁻¹²
±4	±5x10 ⁻¹²
±5	±1x10 ⁻¹¹
±6	±2x10 ⁻¹¹
±7	±5x10 ⁻¹¹
±8	±1x10 ⁻¹⁰
±9	±2x10 ⁻¹⁰
±10	±5x10 ⁻¹⁰
±11	±1x10 ⁻⁹
±12	±2x10 ⁻⁹
±13	±5x10 ⁻⁹
±14	±1x10 ⁻⁸
±15	±2x10 ⁻⁸
±16	±5x10 ⁻⁸
±17	±1x10 ⁻⁷
±18	±2x10 ⁻⁷
±19	±5x10 ⁻⁷
±20	±1x10 ⁻⁶
±21	±2x10 ⁻⁶
±22	±5x10 ⁻⁶
±23	±1x10 ⁻⁵
±24	±2x10 ⁻⁵
±25	±5x10 ⁻⁵
±26	±1x10 ⁻⁴
±27	±2x10 ⁻⁴
±28	±5x10 ⁻⁴
±29	±1x10 ⁻³
±30	±2x10 ⁻³
±31	±5x10 ⁻³
±32	±1x10 ⁻²
±33	±2x10 ⁻²
±34	±5x10 ⁻²
±35	±1x10 ⁻¹
±36	±2x10 ⁻¹
±37	±5x10 ⁻¹



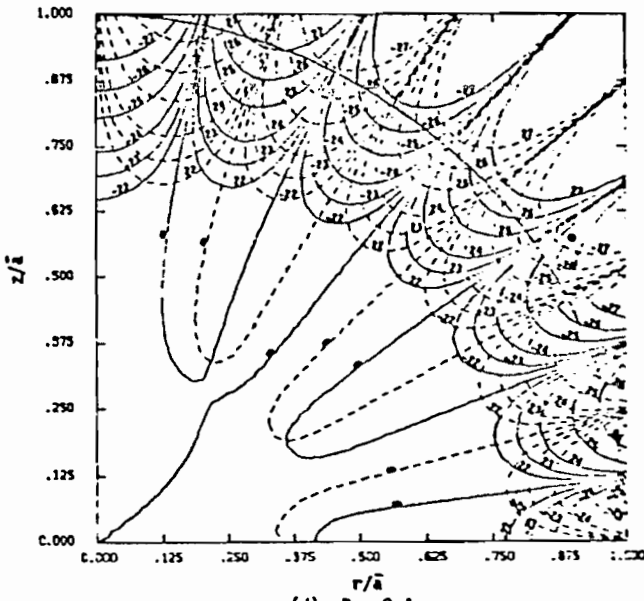
(a) R = 0.1



(b) R = 0.2



(c) R = 0.3



(d) R = 0.4

Figure 25. Contours of constant $(B_z - B_{z1})/B_{z1}$ (solid lines) and constant B_ρ/B_{z1} (dashed lines) for three pairs of loops using the surface-integral method; $R = 0.1, 0.2, 0.3,$ and 0.4 .

KEY TO CONTOUR IDENTIFICATION	
CONTOUR I.D.	CONTOUR VALUE
0	0
±1	±5×10 ⁻¹³
±2	±1×10 ⁻¹²
±3	±2×10 ⁻¹²
±4	±5×10 ⁻¹²
±5	±1×10 ⁻¹¹
±6	±2×10 ⁻¹¹
±7	±5×10 ⁻¹¹
±8	±1×10 ⁻¹⁰
±9	±2×10 ⁻¹⁰
±10	±5×10 ⁻¹⁰
±11	±1×10 ⁻⁹
±12	±2×10 ⁻⁹
±13	±5×10 ⁻⁹
±14	±1×10 ⁻⁸
±15	±2×10 ⁻⁸
±16	±5×10 ⁻⁸
±17	±1×10 ⁻⁷
±18	±2×10 ⁻⁷
±19	±5×10 ⁻⁷
±20	±1×10 ⁻⁶
±21	±2×10 ⁻⁶
±22	±5×10 ⁻⁶
±23	±1×10 ⁻⁵
±24	±2×10 ⁻⁵
±25	±5×10 ⁻⁵
±26	±1×10 ⁻⁴
±27	±2×10 ⁻⁴
±28	±5×10 ⁻⁴
±29	±1×10 ⁻³
±30	±2×10 ⁻³
±31	±5×10 ⁻³
±32	±1×10 ⁻²
±33	±2×10 ⁻²
±34	±5×10 ⁻²
±35	±1×10 ⁻¹
±36	±2×10 ⁻¹
±37	±5×10 ⁻¹

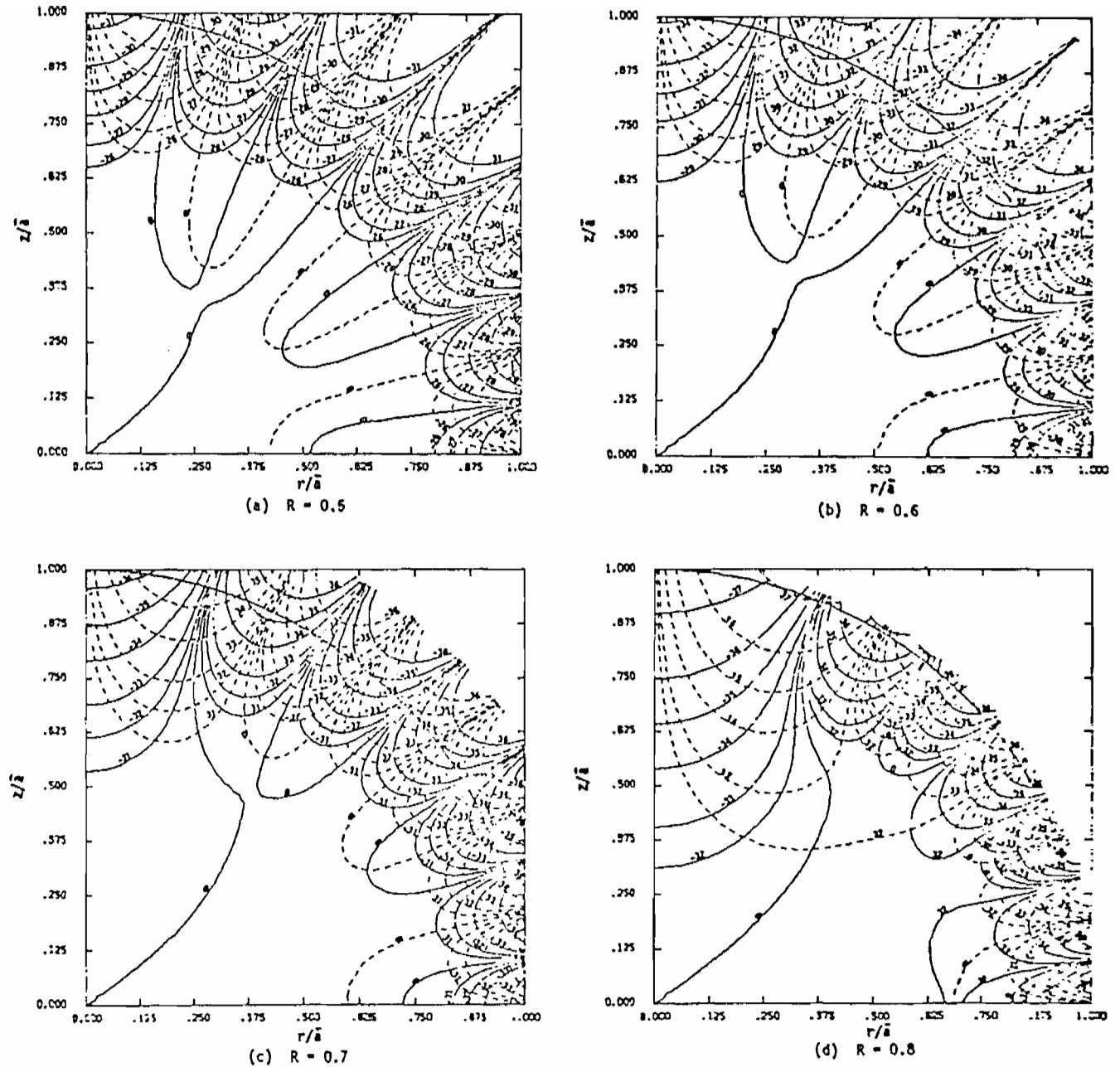


Figure 26. Contours of constant $(B_z - B_{z1})/B_{z1}$ (solid lines) and constant B_ρ/B_{z1} (dashed lines) for three pairs of loops using the surface-integral method; $R = 0.5, 0.6, 0.7,$ and 0.8 .

TABLE 5. OPTIMUM LOOP LOCATIONS FOR FIXED CURRENT RATIOS
(TWO PAIRS OF LOOPS), R = 0.1

I	Volume-Integral Method		Surface-Integral Method	
	α (Deg)	χ	α (Deg)	χ
1	69.70	2.43×10^{-6}	69.70	5.16×10^{-6}
1/2	30.60		30.60	
1	73.19	1.46×10^{-8}	73.19	3.67×10^{-8}
2/3	39.65		39.65	
1	74.42	5.38×10^{-8}	74.42	1.34×10^{-7}
3/4	41.70		41.70	
1	75.12	8.66×10^{-8}	75.12	2.17×10^{-7}
4/5	42.65		42.65	
1	75.58	1.06×10^{-7}	75.58	2.66×10^{-7}
5/6	43.20		43.20	
1	75.90	1.19×10^{-7}	75.90	2.99×10^{-7}
6/7	43.57		43.57	
1	76.14	1.29×10^{-7}	76.14	3.22×10^{-7}
7/8	43.83		43.83	
1	77.84	1.86×10^{-7}	77.84	4.66×10^{-7}
1	45.36		45.36	

TABLE 6. OPTIMUM LOOP LOCATIONS FOR FIXED CURRENT RATIOS
(TWO PAIRS OF LOOPS), $R = 0.2$

I	Volume-Integral Method		Surface-Integral Method	
	α (Deg)	χ	α (Deg)	χ
1	69.75	4.28×10^{-5}	69.77	9.37×10^{-5}
1/2	30.82		30.91	
1	73.19	1.22×10^{-6}	73.19	3.22×10^{-6}
2/3	39.65		39.65	
1	74.42	3.49×10^{-6}	74.42	8.76×10^{-6}
3/4	41.70		41.70	
1	75.12	5.56×10^{-6}	75.12	1.39×10^{-5}
4/5	42.65		42.65	
1	75.58	6.81×10^{-6}	75.58	1.70×10^{-5}
5/6	43.21		43.21	
1	75.90	7.65×10^{-6}	75.90	1.91×10^{-5}
6/7	43.57		43.57	
1	76.14	8.25×10^{-6}	76.14	2.06×10^{-5}
7/8	43.83		43.83	
1	77.84	1.19×10^{-5}	77.83	2.98×10^{-5}
1	45.36		45.37	

TABLE 7. OPTIMUM LOOP LOCATIONS FOR FIXED CURRENT RATIOS
(TWO PAIRS OF LOOPS), R = 0.3

I	Volume-Integral Method		Surface-Integral Method	
	α (Deg)	χ	α (Deg)	χ
1	69.91	2.82×10^{-4}	69.97	6.48×10^{-4}
1/2	31.64		31.98	
1	73.19	2.32×10^{-5}	73.19	6.42×10^{-5}
2/3	39.65		39.65	
1	74.42	4.20×10^{-5}	74.42	1.07×10^{-4}
3/4	41.70		41.70	
1	75.12	6.43×10^{-5}	75.12	1.61×10^{-4}
4/5	42.66		42.66	
1	75.57	7.81×10^{-5}	75.57	1.96×10^{-4}
5/6	43.22		43.22	
1	75.90	8.74×10^{-5}	75.90	2.19×10^{-4}
6/7	43.58		43.59	
1	76.14	9.41×10^{-5}	76.14	2.35×10^{-4}
7/8	43.85		43.85	
1	77.82	1.36×10^{-4}	77.81	3.38×10^{-4}
1	45.39		45.41	

TABLE 8. OPTIMUM LOOP LOCATIONS FOR FIXED CURRENT RATIOS
(TWO PAIRS OF LOOPS), $R = 0.4$

<u>I</u>	<u>Volume-Integral Method</u>		<u>Surface-Integral Method</u>	
	<u>α (Deg)</u>	<u>χ</u>	<u>α (Deg)</u>	<u>χ</u>
1	70.16	1.24×10^{-3}	70.27	2.94×10^{-3}
1/2	33.03		33.58	
1	73.19	2.17×10^{-4}	73.19	6.10×10^{-4}
2/3	39.67		39.69	
1	74.42	2.70×10^{-4}	74.42	7.07×10^{-4}
3/4	41.71		41.72	
1	75.11	3.76×10^{-4}	75.11	9.55×10^{-4}
4/5	42.68		42.69	
1	75.56	4.47×10^{-4}	75.56	1.13×10^{-3}
5/6	43.24		43.26	
1	75.88	4.96×10^{-4}	75.88	1.25×10^{-3}
6/7	43.62		43.64	
1	76.12	5.32×10^{-4}	76.11	1.33×10^{-3}
7/8	43.89		43.91	
1	77.78	7.57×10^{-4}	77.76	1.89×10^{-3}
1	45.47		45.51	

TABLE 9. OPTIMUM LOOP LOCATIONS FOR FIXED CURRENT RATIOS
(TWO PAIRS OF LOOPS), $R = 0.5$

I	Volume-Integral Method		Surface-Integral Method	
	α (Deg)	χ	α (Deg)	χ
1	70.46	4.21×10^{-3}	70.64	1.01×10^{-2}
1/2	34.57		35.30	
1	73.20	1.28×10^{-3}	73.22	3.64×10^{-3}
2/3	39.76		39.85	
1	74.41	1.28×10^{-3}	74.40	3.49×10^{-3}
3/4	41.75		41.78	
1	75.09	1.56×10^{-3}	75.08	4.07×10^{-3}
4/5	42.73		42.76	
1	75.54	1.79×10^{-3}	75.51	4.56×10^{-3}
5/6	43.31		43.35	
1	75.85	1.95×10^{-3}	75.82	4.93×10^{-3}
6/7	43.69		43.74	
1	76.08	2.07×10^{-3}	76.05	5.22×10^{-3}
7/8	43.97		44.02	
1	77.69	2.86×10^{-3}	77.62	7.11×10^{-3}
1	45.62		45.71	

TABLE 10. OPTIMUM LOOP LOCATIONS FOR FIXED CURRENT RATIOS
(TWO PAIRS OF LOOPS), R = 0.6

I	Volume-Integral Method		Surface-Integral Method	
	α (Deg)	χ	α (Deg)	χ
1	70.84	1.21×10^{-2}	71.20	2.94×10^{-2}
1/2	36.24		37.33	
1	73.26	5.61×10^{-3}	73.36	1.58×10^{-2}
2/3	40.10		40.49	
1	74.40	5.10×10^{-3}	74.42	1.43×10^{-2}
3/4	41.91		42.12	
1	75.06	5.49×10^{-3}	75.04	1.49×10^{-2}
4/5	42.87		43.03	
1	75.48	5.91×10^{-3}	75.44	1.56×10^{-2}
5/6	43.46		43.60	
1	75.78	6.25×10^{-3}	75.73	1.63×10^{-2}
6/7	43.85		43.99	
1	76.00	6.52×10^{-3}	75.94	1.68×10^{-2}
7/8	44.14		44.27	
1	77.51	8.50×10^{-3}	77.36	2.12×10^{-2}
1	45.87		46.04	

TABLE 11. OPTIMUM LOOP LOCATIONS FOR FIXED CURRENT RATIOS
(TWO PAIRS OF LOOPS), R = 0.7

I	Volume-Integral Method		Surface-Integral Method	
	α (Deg)	χ	α (Deg)	χ
1	71.45	3.11×10^{-2}	72.20	7.74×10^{-2}
1/2	38.34		40.21	
1	73.48	1.96×10^{-2}	73.87	5.47×10^{-2}
2/3	41.09		42.28	
1	74.48	1.77×10^{-2}	74.71	5.02×10^{-2}
3/4	42.55		43.44	
1	75.07	1.77×10^{-2}	75.20	4.95×10^{-2}
4/5	43.39		44.14	
1	75.45	1.81×10^{-2}	75.53	4.98×10^{-2}
5/6	43.93		44.60	
1	75.71	1.84×10^{-2}	75.76	5.03×10^{-2}
6/7	44.30		44.93	
1	75.91	1.88×10^{-2}	75.93	5.08×10^{-2}
7/8	44.57		45.17	
1	77.25	2.21×10^{-2}	77.11	5.65×10^{-2}
1	46.31		46.79	

TABLE 12. OPTIMUM LOOP LOCATIONS FOR FIXED CURRENT RATIOS
(TWO PAIRS OF LOOPS), $R = 0.8$

<u>I</u>	<u>Volume-Integral Method</u>		<u>Surface-Integral Method</u>	
	<u>α (Deg)</u>	<u>χ</u>	<u>α (Deg)</u>	<u>χ</u>
1	72.49	7.56×10^{-2}	74.01	1.92×10^{-1}
1/2	41.44		45.09	
1	74.12	5.84×10^{-2}	75.20	1.60×10^{-1}
2/3	43.34		46.36	
1	74.92	5.44×10^{-2}	75.79	1.52×10^{-1}
3/4	44.38		47.08	
1	75.38	5.32×10^{-2}	76.13	1.50×10^{-1}
4/5	45.01		47.53	
1	75.69	5.30×10^{-2}	76.36	1.49×10^{-1}
5/6	45.43		47.83	
1	75.91	5.30×10^{-2}	76.52	1.48×10^{-1}
6/7	45.72		48.05	
1	76.07	5.31×10^{-2}	76.64	1.48×10^{-1}
7/8	45.95		48.21	
1	77.15	5.59×10^{-2}	77.46	1.51×10^{-1}
1	47.44		49.37	

4. SENSITIVITY ANALYSIS

The extreme sensitivity of χ to changes in the parameters (near a minimum) has already been pointed out in Sections II-4 and III-1 of this report. In this section, the sensitivity is quantified. The sensitivity is needed to determine the fabrication tolerances required to achieve a given field uniformity. The field uniformity achievable using the type of simulator discussed in this report may well be determined by the minimum achievable engineering tolerances.

To quantify the change in χ from its minimum value χ_m due to small changes in the parameters, one can use the first few terms of a Taylor expansion about the minimum point in parameter space. Since the first derivatives are zero at the minimum, the first two non-zero terms in the expansion of χ/χ_m are

$$\chi/\chi_m \cong 1 + \sum_{i,j} (2-\delta_{ij}) C_{ij} \delta p_i \delta p_j \quad (31)$$

where

$$C_{ij} = \frac{1}{2\chi_m} \frac{\partial^2 \chi}{\partial p_i \partial p_j} \quad \text{and } \delta_{ij} \text{ is the Kronecker delta.}$$

Using Equation 49 (found in the Appendix and evaluated in the Newton-Raphson code), the values of C_{ij} were calculated with the formula

$$C_{ij} = \frac{1}{4\chi_m^2} \frac{\partial^2 \chi^2}{\partial p_i \partial p_j} \quad (32)$$

To simplify application of Equation 31, the coefficients involving the angles (α_i) have been transformed from radians to degrees. Hence, in Equation 31, a δp_i should be in degrees if it is an

angle coordinate. Since I_2 and I_3 can be correctly considered as dimensionless ratios to the current I_1 , δp_i is dimensionless if it is a current coordinate. The coefficients C_{ij} are given in Tables 13 through 15 for all the optimized parameter values given in Tables 1, 2, and 3. The index of the parameters corresponds to their order in Tables 2 and 3. That is, $\alpha_1 > \alpha_2 > \alpha_3$ and $I_1 > I_2 > I_3$ ($I_1 = 1$, a constant; hence, partial derivatives with respect to I_1 are zero and are not shown in the tables). To clearly identify the C_{ij} , they are listed in the tables with subscripts α_i or I_i . For instance,

$$C_{\alpha_1 I_2} = \frac{1}{4\chi_m^2} \frac{\partial^2 \chi^2}{\partial \alpha_1 \partial I_2}$$

The tables clearly demonstrate the extreme sensitivity of χ to parameter variations for small values of R . For instance, if $R = 0.1$ and there are two pairs, using the volume-integral method one finds $C_{\alpha_1 \alpha_1} = 3.057 \times 10^9$. This coefficient implies that χ is approximately doubled if α_1 is changed from its optimum value by 1.8×10^{-5} degrees while holding the other parameters constant. Such tolerances cannot be attained; hence, it is not sensible to attempt to attain such a small χ ($\sim 3 \times 10^{-9}$) with this type of device. The corresponding coefficient for $R = 0.8$ is 6.077×10^{-2} . This coefficient implies that a variation of about four degrees in α_1 will about double χ ($\chi_m = 0.053$). A four-degree tolerance is probably attainable. The design of a simulator using these techniques must balance attainable tolerances against test volume size and expected field uniformity.

TABLE 13. VALUES OF C_{ij} FOR ONE PAIR OF LOOPS

$$C_{\alpha_1 \alpha_1} = \frac{1}{4\chi_m^2} \frac{\partial^2 \chi^2}{\partial \alpha_1^2} \text{ (Deg}^{-2}\text{)}$$

<u>R</u>	<u>Volume-Integral Method</u>	<u>Surface-Integral Method</u>
0.1	4.432×10^1	2.692×10^1
0.2	2.766×10^0	1.679×10^0
0.3	5.431×10^{-1}	3.290×10^{-1}
0.4	1.691×10^{-1}	1.018×10^{-1}
0.5	6.688×10^{-2}	3.983×10^{-2}
0.6	3.023×10^{-2}	1.771×10^{-2}
0.7	1.460×10^{-2}	8.415×10^{-3}
0.8	7.119×10^{-3}	4.100×10^{-3}

TABLE 14. VALUES OF C_{ij} FOR TWO PAIRS OF LOOPS

a. Volume-Integral Method

R	$C_{\alpha_1\alpha_1}$	$C_{\alpha_1\alpha_2}$	$C_{\alpha_2\alpha_2}$	$C_{\alpha_1I_2}$	$C_{\alpha_2I_2}$	$C_{I_2I_2}$
0.1	3.057×10^9	1.062×10^8	3.912×10^6	-4.934×10^{10}	-1.720×10^9	7.964×10^{11}
0.2	7.475×10^5	2.508×10^4	1.712×10^3	-1.203×10^7	-4.274×10^5	1.942×10^8
0.3	5.799×10^3	1.652×10^2	3.873×10^1	-9.216×10^4	-3.541×10^3	1.490×10^6
0.4	1.870×10^2	2.872×10^0	3.462×10^0	-2.872×10^3	-1.326×10^2	4.657×10^4
0.5	1.334×10^1	-1.349×10^{-1}	5.776×10^{-1}	-1.905×10^2	-1.187×10^1	3.109×10^3
0.6	1.598×10^0	-7.874×10^{-2}	1.381×10^{-1}	-1.996×10^1	-1.816×10^0	3.298×10^2
0.7	2.760×10^{-1}	-2.682×10^{-2}	4.105×10^{-2}	-2.768×10^0	-3.782×10^{-1}	4.689×10^1
0.8	6.077×10^{-2}	-8.621×10^{-3}	1.348×10^{-2}	-4.434×10^{-1}	-9.006×10^{-2}	7.922×10^0

b. Surface-Integral Method

R	$C_{\alpha_1\alpha_1}$	$C_{\alpha_1\alpha_2}$	$C_{\alpha_2\alpha_2}$	$C_{\alpha_1I_2}$	$C_{\alpha_2I_2}$	$C_{I_2I_2}$
0.1	1.037×10^9	3.597×10^7	1.372×10^6	-1.674×10^{10}	-5.838×10^8	2.702×10^{11}
0.2	2.541×10^5	8.255×10^3	7.542×10^2	-4.080×10^6	-1.458×10^5	6.589×10^7
0.3	1.986×10^3	4.612×10^1	1.999×10^1	-3.123×10^4	-1.231×10^3	5.050×10^5
0.4	6.531×10^1	-1.118×10^{-2}	1.882×10^0	-9.702×10^2	-4.772×10^1	1.575×10^4
0.5	4.849×10^0	-2.073×10^{-1}	3.209×10^{-1}	-6.391×10^1	-4.401×10^0	1.048×10^3
0.6	6.203×10^{-1}	-6.263×10^{-2}	7.733×10^{-2}	-6.600×10^0	-6.717×10^{-1}	1.105×10^2
0.7	1.170×10^{-1}	-1.871×10^{-2}	2.274×10^{-2}	-8.922×10^{-1}	-1.326×10^{-1}	1.570×10^1
0.8	2.830×10^{-2}	-5.744×10^{-3}	7.241×10^{-3}	-1.369×10^{-1}	-2.821×10^{-2}	2.719×10^0

NOTE: $C_{\alpha_i\alpha_j}$ in Deg⁻²; $C_{\alpha_iI_2}$ in Deg⁻¹; and $C_{I_2I_2}$ dimensionless.

TABLE 15. VALUES OF C_{ij} FOR THREE PAIRS OF LOOPS

a. Volume-Integral Method

R	$C_{a_1 a_1}$	$C_{a_1 a_2}$	$C_{a_1 a_3}$	$C_{a_2 a_2}$	$C_{a_2 a_3}$	$C_{a_3 a_3}$	$C_{a_1 l_2}$	$C_{a_1 l_3}$	$C_{a_2 l_2}$	$C_{a_2 l_3}$	$C_{a_3 l_2}$	$C_{a_3 l_3}$	$C_{l_2 l_2}$	$C_{l_2 l_3}$	$C_{l_3 l_3}$
0.1	$1.651 \cdot 10^{17}$	$1.429 \cdot 10^{17}$	$1.551 \cdot 10^{16}$	$1.238 \cdot 10^{17}$	$-4.382 \cdot 10^{16}$	$1.551 \cdot 10^{16}$	$-2.027 \cdot 10^{18}$	$8.558 \cdot 10^{17}$	$-1.754 \cdot 10^{18}$	$-2.413 \cdot 10^{18}$	$6.212 \cdot 10^{17}$	$8.558 \cdot 10^{17}$	$2.488 \cdot 10^{19}$	$3.427 \cdot 10^{19}$	$4.722 \cdot 10^{19}$
0.2	$1.577 \cdot 10^{11}$	$1.358 \cdot 10^{11}$	$1.478 \cdot 10^{10}$	$1.178 \cdot 10^{11}$	$-4.166 \cdot 10^{10}$	$1.478 \cdot 10^{10}$	$-1.935 \cdot 10^{12}$	$8.135 \cdot 10^{11}$	$-1.667 \cdot 10^{12}$	$-2.302 \cdot 10^{12}$	$5.921 \cdot 10^{11}$	$8.135 \cdot 10^{11}$	$2.373 \cdot 10^{13}$	$3.256 \cdot 10^{13}$	$4.496 \cdot 10^{13}$
0.3	$4.802 \cdot 10^7$	$4.066 \cdot 10^7$	$4.466 \cdot 10^6$	$3.585 \cdot 10^7$	$-1.255 \cdot 10^7$	$4.466 \cdot 10^6$	$-5.847 \cdot 10^8$	$2.438 \cdot 10^8$	$-4.979 \cdot 10^8$	$-6.978 \cdot 10^8$	$1.782 \cdot 10^8$	$2.438 \cdot 10^8$	$7.127 \cdot 10^9$	$9.673 \cdot 10^9$	$1.359 \cdot 10^{10}$
0.4	$1.570 \cdot 10^5$	$1.265 \cdot 10^5$	$1.433 \cdot 10^4$	$1.161 \cdot 10^5$	$-3.971 \cdot 10^4$	$1.433 \cdot 10^4$	$-1.077 \cdot 10^6$	$7.513 \cdot 10^5$	$-1.543 \cdot 10^6$	$-2.241 \cdot 10^6$	$5.655 \cdot 10^5$	$7.513 \cdot 10^5$	$2.254 \cdot 10^7$	$2.950 \cdot 10^7$	$4.339 \cdot 10^7$
0.5	$1.935 \cdot 10^3$	$1.392 \cdot 10^3$	$1.722 \cdot 10^2$	$1.403 \cdot 10^3$	$-4.591 \cdot 10^2$	$1.722 \cdot 10^2$	$-2.216 \cdot 10^4$	$8.458 \cdot 10^3$	$-1.691 \cdot 10^4$	$-2.646 \cdot 10^4$	$6.548 \cdot 10^3$	$8.458 \cdot 10^3$	$2.587 \cdot 10^5$	$3.154 \cdot 10^5$	$5.065 \cdot 10^5$
0.6	$5.715 \cdot 10^1$	$3.262 \cdot 10^1$	$5.154 \cdot 10^0$	$4.005 \cdot 10^1$	$-1.233 \cdot 10^1$	$5.145 \cdot 10^0$	$-5.988 \cdot 10^2$	$2.030 \cdot 10^2$	$-4.613 \cdot 10^2$	$-7.141 \cdot 10^2$	$1.732 \cdot 10^2$	$2.030 \cdot 10^2$	$6.700 \cdot 10^3$	$7.023 \cdot 10^3$	$1.346 \cdot 10^4$
0.7	$3.233 \cdot 10^0$	$1.151 \cdot 10^0$	$3.454 \cdot 10^{-1}$	$2.155 \cdot 10^0$	$-6.310 \cdot 10^{-1}$	$3.366 \cdot 10^{-1}$	$-2.838 \cdot 10^1$	$7.698 \cdot 10^0$	$-1.552 \cdot 10^1$	$-3.371 \cdot 10^1$	$8.180 \cdot 10^0$	$7.698 \cdot 10^0$	$3.049 \cdot 10^2$	$2.344 \cdot 10^2$	$6.267 \cdot 10^2$
0.8	$3.051 \cdot 10^{-1}$	$3.410 \cdot 10^{-2}$	$5.206 \cdot 10^{-2}$	$1.919 \cdot 10^{-1}$	$-5.608 \cdot 10^{-2}$	$4.320 \cdot 10^{-2}$	$-1.935 \cdot 10^0$	$3.331 \cdot 10^{-1}$	$-7.851 \cdot 10^{-1}$	$-2.288 \cdot 10^0$	$5.022 \cdot 10^{-1}$	$3.331 \cdot 10^{-1}$	$2.103 \cdot 10^1$	$7.667 \cdot 10^0$	$4.240 \cdot 10^1$

b. Surface-Integral Method

0.1	$3.834 \cdot 10^{16}$	$3.362 \cdot 10^{15}$	$3.649 \cdot 10^{15}$	$2.912 \cdot 10^{16}$	$-1.031 \cdot 10^{16}$	$3.649 \cdot 10^{15}$	$-4.768 \cdot 10^{17}$	$2.013 \cdot 10^{17}$	$-4.127 \cdot 10^{17}$	$-5.688 \cdot 10^{17}$	$1.461 \cdot 10^{17}$	$2.013 \cdot 10^{17}$	$5.853 \cdot 10^{18}$	$8.061 \cdot 10^{18}$	$1.111 \cdot 10^{19}$
0.2	$3.720 \cdot 10^{10}$	$3.190 \cdot 10^{10}$	$3.478 \cdot 10^9$	$2.772 \cdot 10^{10}$	$-9.791 \cdot 10^9$	$3.478 \cdot 10^9$	$-4.560 \cdot 10^{11}$	$1.912 \cdot 10^{11}$	$-3.918 \cdot 10^{11}$	$-5.415 \cdot 10^{11}$	$1.394 \cdot 10^{11}$	$1.912 \cdot 10^{11}$	$5.592 \cdot 10^{12}$	$7.649 \cdot 10^{12}$	$1.053 \cdot 10^{13}$
0.3	$1.145 \cdot 10^7$	$9.518 \cdot 10^6$	$1.055 \cdot 10^6$	$8.463 \cdot 10^6$	$-2.948 \cdot 10^5$	$1.055 \cdot 10^6$	$-1.389 \cdot 10^8$	$5.718 \cdot 10^7$	$-1.166 \cdot 10^8$	$-1.646 \cdot 10^8$	$4.213 \cdot 10^7$	$5.718 \cdot 10^7$	$1.669 \cdot 10^9$	$2.262 \cdot 10^9$	$3.205 \cdot 10^9$
0.4	$3.854 \cdot 10^4$	$2.925 \cdot 10^4$	$3.435 \cdot 10^3$	$2.765 \cdot 10^4$	$-9.323 \cdot 10^3$	$3.435 \cdot 10^3$	$-4.552 \cdot 10^5$	$1.772 \cdot 10^5$	$-3.579 \cdot 10^5$	$-5.318 \cdot 10^5$	$1.353 \cdot 10^5$	$1.772 \cdot 10^5$	$5.424 \cdot 10^6$	$6.824 \cdot 10^6$	$1.022 \cdot 10^7$
0.5	$5.040 \cdot 10^2$	$3.108 \cdot 10^2$	$4.344 \cdot 10^1$	$3.416 \cdot 10^2$	$-1.089 \cdot 10^2$	$4.344 \cdot 10^1$	$-5.586 \cdot 10^3$	$1.931 \cdot 10^3$	$-3.849 \cdot 10^3$	$-6.342 \cdot 10^3$	$1.608 \cdot 10^3$	$1.931 \cdot 10^3$	$6.429 \cdot 10^4$	$7.038 \cdot 10^4$	$1.215 \cdot 10^5$
0.6	$1.653 \cdot 10^1$	$6.545 \cdot 10^0$	$1.512 \cdot 10^0$	$1.030 \cdot 10^1$	$-3.100 \cdot 10^0$	$1.504 \cdot 10^0$	$-1.600 \cdot 10^2$	$4.433 \cdot 10^1$	$-8.824 \cdot 10^1$	$-1.732 \cdot 10^2$	$4.481 \cdot 10^1$	$4.433 \cdot 10^1$	$1.766 \cdot 10^3$	$1.454 \cdot 10^3$	$3.284 \cdot 10^3$
0.7	$1.691 \cdot 10^0$	$1.433 \cdot 10^{-1}$	$1.356 \cdot 10^{-1}$	$6.228 \cdot 10^{-1}$	$-1.873 \cdot 10^{-1}$	$1.269 \cdot 10^{-1}$	$-8.122 \cdot 10^0$	$1.516 \cdot 10^0$	$-3.229 \cdot 10^0$	$-8.245 \cdot 10^0$	$2.289 \cdot 10^0$	$1.516 \cdot 10^0$	$8.847 \cdot 10^1$	$3.948 \cdot 10^1$	$1.563 \cdot 10^2$
0.8	$1.248 \cdot 10^{-1}$	$-1.184 \cdot 10^{-2}$	$2.897 \cdot 10^{-2}$	$6.670 \cdot 10^{-2}$	$-2.149 \cdot 10^{-2}$	$1.986 \cdot 10^{-2}$	$-5.865 \cdot 10^{-1}$	$5.115 \cdot 10^{-2}$	$-1.497 \cdot 10^{-1}$	$-5.538 \cdot 10^{-1}$	$1.746 \cdot 10^{-1}$	$5.115 \cdot 10^{-2}$	$7.042 \cdot 10^0$	$1.704 \cdot 10^{-1}$	$1.094 \cdot 10^1$

5. DRIVING IMPEDANCE CONSIDERATIONS

In the low-frequency approximation, the driving-point impedance is an inductance. To calculate the driving-point inductance, the self-inductance of each loop and the mutual inductances between the loops must be known. For the single-pair geometry connected in series,

$$L = 2aN^2 \left[(L_1/a) + (M_{12}/a) \right] \quad (33)$$

where

N = number of turns in each loop

a = radius of the sphere containing the loops (meters)

L_1/a = self-inductance of each loop (calculated as if it had only one turn) divided by a

M_{12}/a = mutual inductance of the loops (calculated as if they had only one turn) divided by a

The quantity M_{12}/a was calculated for each of the one-pair optimized geometries using the formula given by Smythe [Ref. 2, p. 313, Equation 8.06(3)]. These values are given in Table 16. The self-inductance, however, is dependent on the wire diameter and the permeability of the loop material. The self-inductance of a loop is given by Smythe (Ref. 2, p. 318) as

$$L_{11} = b \left[\mu \left(\ln \frac{8b}{a'} - 2 \right) + \frac{\mu'}{4} \right] \quad (34)$$

where

$b = a \sin \alpha$ = the radius of the loop (meters)

$\mu = \mu_o$ = the permittivity of the material the loop is embedded in (H/m)

a' = the radius of the wire the loop is made of (meters)

μ' = the permittivity of the material of the wire loop

TABLE 16. SELF AND MUTUAL INDUCTANCE -- ONE-PAIR CASE

<u>R</u>	<u>α (Deg)</u>	<u>$L/a - f(a', \mu')$ $(= 3 \mu_0 \sin \alpha_0)$ (H/m)</u>	<u>M_{12}/a (H/m)</u>
Volume-Integral Method Parameters:			
0.1	63.44	3.372×10^{-6}	4.419×10^{-7}
0.2	63.45	3.372×10^{-6}	4.424×10^{-7}
0.3	63.51	3.374×10^{-6}	4.443×10^{-7}
0.4	63.67	3.379×10^{-6}	4.495×10^{-7}
0.5	64.01	3.389×10^{-6}	4.606×10^{-7}
0.6	64.63	3.406×10^{-6}	4.815×10^{-7}
0.7	65.65	3.435×10^{-6}	5.181×10^{-7}
0.8	67.28	3.477×10^{-6}	5.814×10^{-7}
Surface-Integral Method Parameters:			
0.1	63.44	3.372×10^{-6}	4.420×10^{-7}
0.2	63.46	3.373×10^{-6}	4.427×10^{-7}
0.3	63.56	3.376×10^{-6}	4.458×10^{-7}
0.4	63.82	3.383×10^{-6}	4.544×10^{-7}
0.5	64.39	3.399×10^{-6}	4.732×10^{-7}
0.6	65.42	3.428×10^{-6}	5.095×10^{-7}
0.7	67.17	3.474×10^{-6}	5.768×10^{-7}
0.8	70.02	3.543×10^{-6}	7.054×10^{-7}

This formula can be written

$$L_{11}/a = \sin\alpha \left\{ \mu_0 \left[(X - 2) + \ln \left(\frac{8a \sin\alpha}{a' e^X} \right) \right] + \frac{\mu'}{4} \right\} \quad (35)$$

for any value of X (X is a dummy). The value of X is arbitrarily chosen as X = 5; then Equation 35 can be written

$$L_{11}/a = 3\mu_0 \sin\alpha + f(a', \mu') \quad (36)$$

where f is given by

$$f(a', \mu') = \sin\alpha \left[\mu_0 \ln \left(\frac{8a \sin\alpha}{a' e^5} \right) + \frac{\mu'}{4} \right] \quad (37)$$

Suppose $\mu' = \mu_0$ and $f(a', \mu')$ is set to zero. Then, it is easy to show that

$$\frac{a \sin\alpha}{a'} = \frac{e^{4.75}}{8} \approx 14.448$$

Or, the radius of the wire is

$$a' = \frac{a \sin\alpha}{14.448}$$

If $a = 1$ m and $\alpha = 64^\circ$, $a' = 6.2$ cm = 2.4 in. (a reasonable value)*. Hence, $3\mu_0 \sin\alpha$ yields a "reasonable" estimate of L_{11}/a ; for the correct value, one need merely add $f(a', \mu')$ evaluated with the proposed parameters a , a' , α , and μ' . The value of f may be positive or negative depending on the parameters. The values of $3\mu_0 \sin\alpha$ are tabulated in Table 16 for the various optimized one-pair geometries.

For the two-pair geometry, assuming series connection, the inductance can be written

*Such a fat wire is considered reasonable for low self inductance and dimensional stability under impulse loading during use.

$$L = 2a \left[N_1^2(L_1/a) + N_2^2(L_2/a) + N_1 N_2(M_{12}/a) + 2N_1 N_2(M_{13}/a) + N_1^2(M_{14}/a) + N_2^2(M_{23}/a) \right] \quad (38)$$

In Equation 38, the subscripts refer to the current-loop labels shown in Figure 27. Also, the symmetry of the M_{ij} has been used to simplify the expression, and the geometrical symmetry conditions $L_1 = L_4$, $L_2 = L_3$, $N_1 = N_4$, $N_2 = N_3$, and $M_{13} = M_{24}$ have been assumed. If the loops of each symmetrical half are connected in series, but the two halves are connected in parallel, then the inductance is one-fourth that given by Equation 38. The values of $3\mu_0 \sin\alpha$ are tabulated for each optimized two-pair geometry in Tables 17 and 18. In the same tables the values of (M_{12}/a) , (M_{13}/a) , (M_{14}/a) , and (M_{23}/a) are given. Again, the formula given by Smythe (Ref. 2, p. 313) was used.

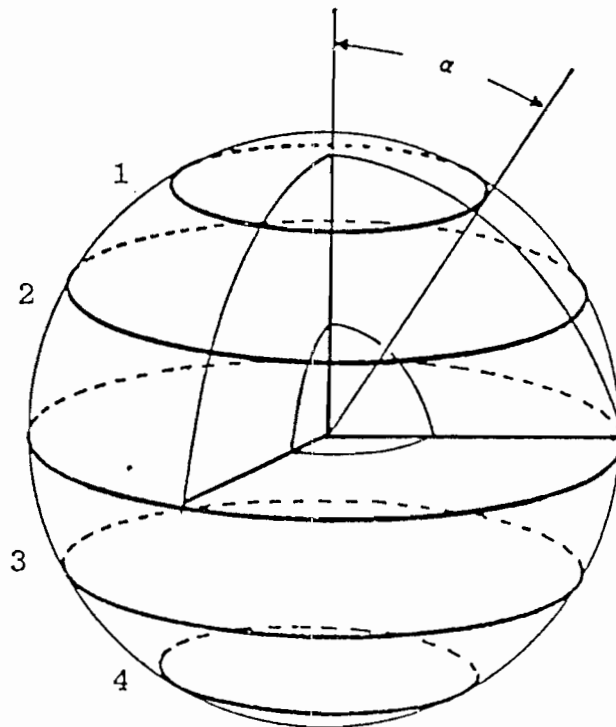


Figure 27. Current-loop labels for two-pair geometry.

TABLE 17. SELF AND MUTUAL INDUCTANCE--TWO PAIRS,
VOLUME-INTEGRAL-METHOD PARAMETERS

R	α (Deg)	$\frac{L/a - f(a', \mu')}{(= 3 \mu_0 \sin \alpha)} \text{ (H/m)}$	$M_{12}/a \text{ (H/m)}$	$M_{13}/a \text{ (H/m)}$	$M_{14}/a \text{ (H/m)}$	$M_{23}/a \text{ (H/m)}$
0.1	40.09 73.43	2.428×10^{-6} 3.613×10^{-6}	5.870×10^{-7}	2.265×10^{-7}	6.215×10^{-8}	8.986×10^{-7}
0.2	40.10 73.44	2.429×10^{-6} 3.613×10^{-6}	5.873×10^{-7}	2.268×10^{-7}	6.225×10^{-8}	8.991×10^{-7}
0.3	40.17 73.47	2.432×10^{-6} 3.614×10^{-6}	5.890×10^{-7}	2.278×10^{-7}	6.268×10^{-8}	9.015×10^{-7}
0.4	40.36 73.57	2.441×10^{-6} 3.616×10^{-6}	5.935×10^{-7}	2.307×10^{-7}	6.387×10^{-8}	9.079×10^{-7}
0.5	40.76 73.78	2.461×10^{-6} 3.620×10^{-6}	6.035×10^{-7}	2.371×10^{-7}	6.654×10^{-8}	9.215×10^{-7}
0.6	41.54 74.16	2.500×10^{-6} 3.627×10^{-6}	6.238×10^{-7}	2.498×10^{-7}	7.199×10^{-8}	9.468×10^{-7}
0.7	42.98 74.78	2.570×10^{-6} 3.638×10^{-6}	6.629×10^{-7}	2.738×10^{-7}	8.287×10^{-8}	9.903×10^{-7}
0.8	45.54 75.77	2.691×10^{-6} 3.654×10^{-6}	7.380×10^{-7}	3.196×10^{-7}	1.054×10^{-7}	1.064×10^{-6}

TABLE 18. SELF AND MUTUAL INDUCTANCE--TWO PAIRS,
SURFACE-INTEGRAL-METHOD PARAMETERS

R	α (Deg)	$\frac{L/a - f(a', \mu')}{(= 3 \mu_0 \sin \alpha)} \text{ (H/m)}$	$M_{12}/a \text{ (H/m)}$	$M_{13}/a \text{ (H/m)}$	$M_{14}/a \text{ (H/m)}$	$M_{23}/a \text{ (H/m)}$
0.1	40.09 73.43	2.428×10^{-6} 3.613×10^{-6}	5.870×10^{-7}	2.265×10^{-7}	6.215×10^{-8}	8.986×10^{-7}
0.2	40.11 73.44	2.429×10^{-6} 3.614×10^{-6}	5.875×10^{-7}	2.268×10^{-7}	6.228×10^{-8}	8.993×10^{-7}
0.3	40.20 73.49	2.433×10^{-6} 3.614×10^{-6}	5.896×10^{-7}	2.282×10^{-7}	6.284×10^{-8}	9.023×10^{-7}
0.4	40.43 73.61	2.445×10^{-6} 3.617×10^{-6}	5.954×10^{-7}	2.320×10^{-7}	6.439×10^{-8}	9.106×10^{-7}
0.5	40.97 73.88	2.472×10^{-6} 3.622×10^{-6}	6.090×10^{-7}	2.405×10^{-7}	6.797×10^{-8}	9.282×10^{-7}
0.6	42.05 74.37	2.525×10^{-6} 3.630×10^{-6}	6.375×10^{-7}	2.580×10^{-7}	7.567×10^{-8}	9.614×10^{-7}
0.7	44.14 75.21	2.625×10^{-6} 3.645×10^{-6}	6.970×10^{-7}	2.937×10^{-7}	9.257×10^{-8}	1.021×10^{-6}
0.8	48.22 76.65	2.811×10^{-6} 3.668×10^{-6}	8.253×10^{-7}	3.719×10^{-7}	1.340×10^{-7}	1.135×10^{-6}

6. CURRENT REQUIRED TO ACHIEVE PEAK FIELD

Equation 5 yields the uniform part of the field; i.e.,

$$B_{z1} = \frac{\mu}{a} \sum_{\ell=1}^L I_{\ell} \sin^2 \alpha_{\ell} \quad (5)$$

For one pair of loops ($L = 1$), let $\alpha = 63.43^{\circ}$ (Helmholtz value) and the desired $B_{z1} = 5 \times 10^{-3}$ teslas, then

$$\frac{I}{a} = \frac{B_{z1}}{\mu \sin^2 \alpha} = 4.97 \times 10^3 \text{ A/m} \quad (39)$$

Hence, the required current is about 5,000 A for a current-loop geometry 1 m in radius. The required current increases linearly with the radius of the simulator.

For a series-connected simulator with multi-turn current loops, one can write

$$B_{z1} = \frac{\mu I_w}{a} \sum_{\ell=1}^L N_{\ell} \sin^2 \alpha_{\ell} \quad (40)$$

where I_w is the current through each turn or wire of the series circuit. Hence, the current requirement can be written

$$I_w = \frac{a B_{z1}}{\mu \sum_{\ell=1}^L N_{\ell} \sin^2 \alpha_{\ell}} \quad (41)$$

Note that, again, the required current increases linearly with a ; also, the required current is inversely proportional to the number of turns. However, the inductance increases with the number of turns squared, motivating the designer to minimize the number of turns.

7. FIGURE OF MERIT AND EFFICIENCY

Chen and Baum (Ref. 4) define two figures of merit for magnetic-field simulators. The first is a dimensionless measure of the magnitude of the magnetic field in the working volume divided by the required driving current. In scalar form, it is given by

$$\xi_{\ell} = aR/\ell_c \quad (42)$$

where

$$\ell_c = \frac{I}{H_{z1}} = \frac{a}{\sum_{\ell=1}^L (I_{\ell}/I) \sin^2 \alpha_{\ell}}$$

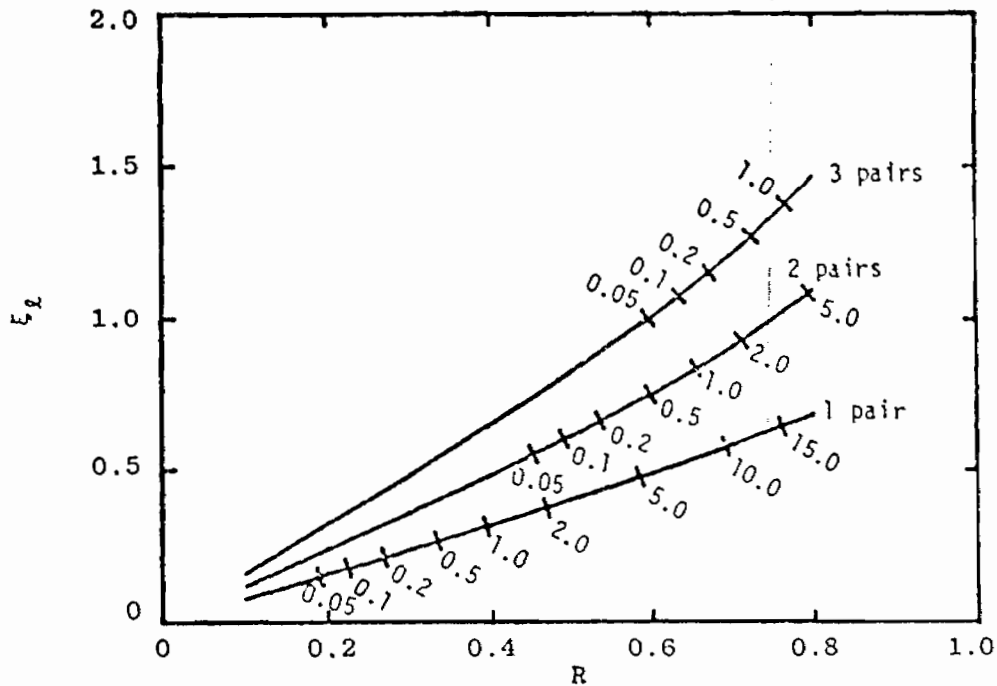
Hence

$$\xi_{\ell} = aRH_{z1}/I = R \sum_{\ell=1}^L (I_{\ell}/I) \sin^2 \alpha_{\ell} \quad (43)$$

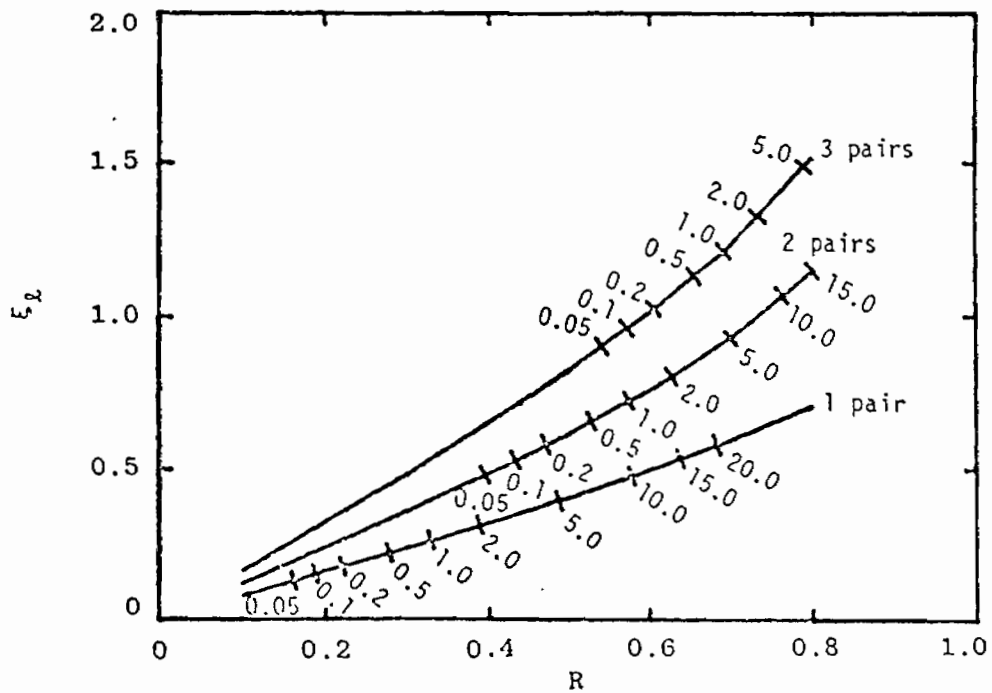
Assuming an ideal simulator where (I_{ℓ}/I) have the optimum values given in Section III-1, ξ_{ℓ} were calculated as a function of R . The results are shown graphically in Figure 28 for 1, 2, and 3 pairs of loops for both the volume- and surface-integral methods. Ticks on the curves indicate χ values expressed as a percent.

Note that the figure of merit ξ_{ℓ} is proportional to the number of turns in a given configuration. That is, if the number of turns is increased from 1 to N , then $\xi_{\ell} = aRH_{z1}/I$ is increased by the factor N . Hence it is not surprising that ξ_{ℓ} for 3 pairs is greater than ξ_{ℓ} for 2 pairs, which in turn is greater than ξ_{ℓ}

4. Chen, Leih-Wei, and Carl E. Baum, Performance Parameters Associated with the FINES-Type Small EMP Simulators, Sensor and Simulation Note 238, Air Force Weapons Laboratory, Kirtland AFB, NM, 16 January 1978.



(a) Volume-Integral Method



(b) Surface-Integral Method

Figure 28. Figure of merit ξ_x vs. R for 1-, 2-, and 3-pair configurations for both volume-integral and surface-integral methods without the turns factor (see text). Ticks indicate values of χ expressed as a percent of the central field.

for 1 pair (for any R), simply because of the number of current loops in the three cases. To compensate for this effect, a turns factor was included. Equation 43 was modified to include the turns factor N_L to become

$$\xi_{\ell} = RN_L \sum_{\ell=1}^L (I_{\ell}/I) \sin^2 \alpha_{\ell} \quad (44)$$

where

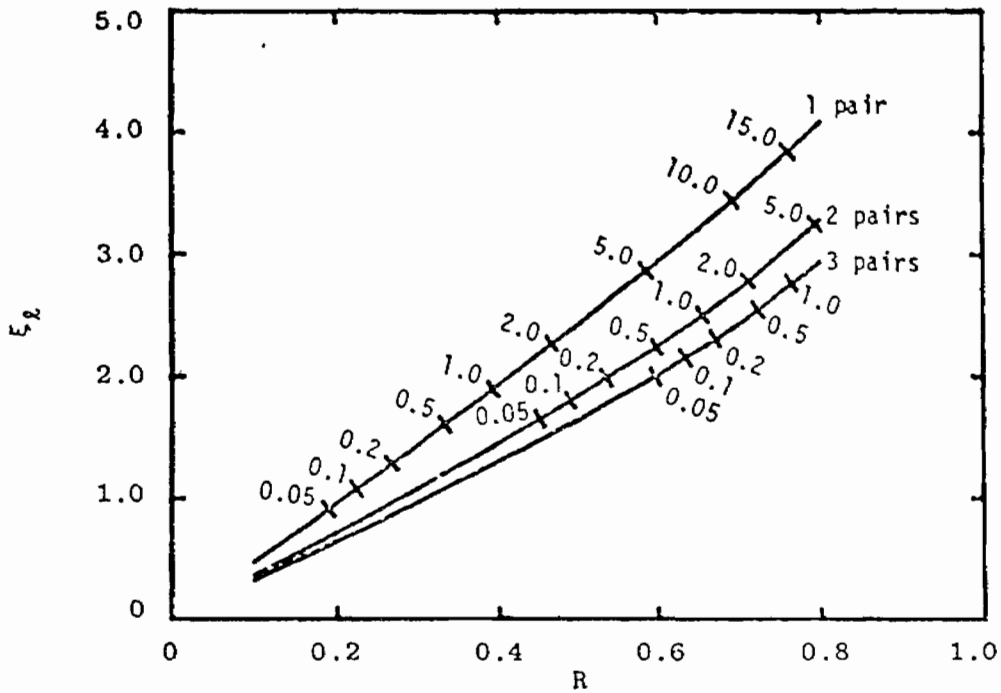
$$N_1 = 6$$

$$N_2 = 3$$

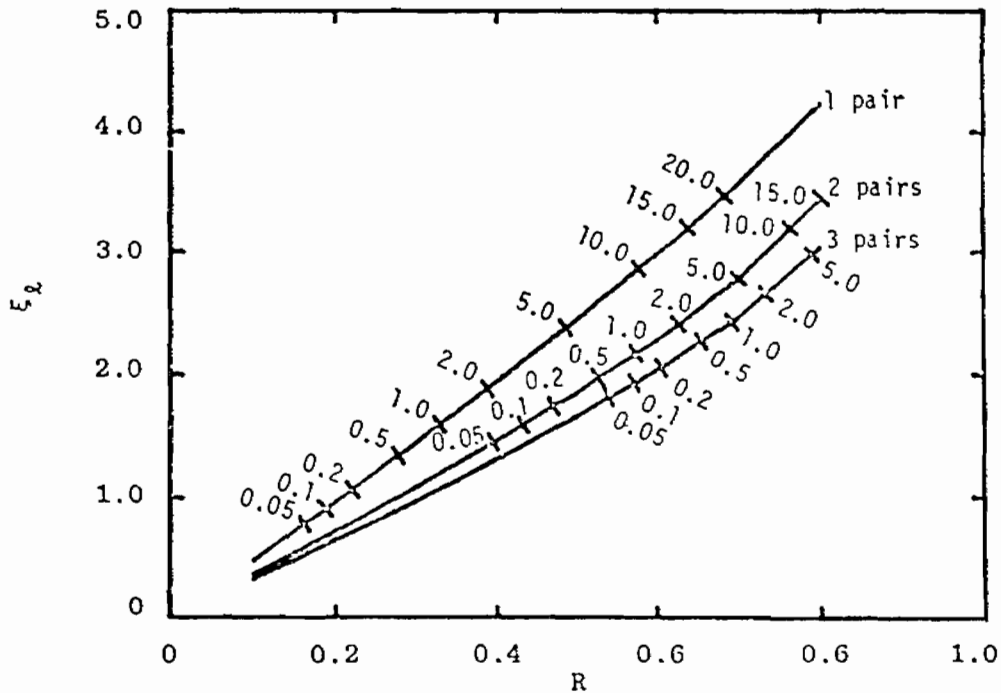
$$N_3 = 2$$

Thus, all three ideal simulators are assumed to have 6 turn-pairs since $L \cdot N_L = 6$. The results of evaluating Equation 44 are shown in Figure 29. Now, for a given R, the order of the values of ξ_{ℓ} are reversed. This is explained by noting that the effectiveness of the additional loops in the 3-pair and 2-pair configurations in producing a magnetic-field magnitude is less than that of the larger loops carrying a proportionately larger current. This apparent detrimental effect of the additional loops is more than offset by the increased field homogeneity. Note that, for a given χ value, ξ_{ℓ} (Eq. 44) is largest for the 3-pair configuration and smallest for the 1-pair configuration. The fact that this occurs at different R values is of little consequence since the effect of the size of the working volume has been included in the definition of ξ_{ℓ} .

The second figure of merit defined by Chen and Baum is the energy efficiency; it is the ratio of magnetic-field energy in the



(a) Volume-Integral Method



(b) Surface-Integral Method

Figure 29. Figure of merit ξ_ℓ vs. R for 1-, 2-, and 3-pair configurations for both volume-integral and surface-integral methods including the turns factor (see text). Ticks indicate values of χ expressed as a percent of the central field.

test volume divided by the total stored magnetic-field energy.

It can be written (Ref. 4, p. 15)

$$\xi_h = \frac{\frac{1}{2} \mu_o H_{z1}^2 V_w}{\frac{1}{2} L H_{z1}^2 \ell_c^2} = \frac{\mu_o V_w}{L \ell_c^2} \quad (45)$$

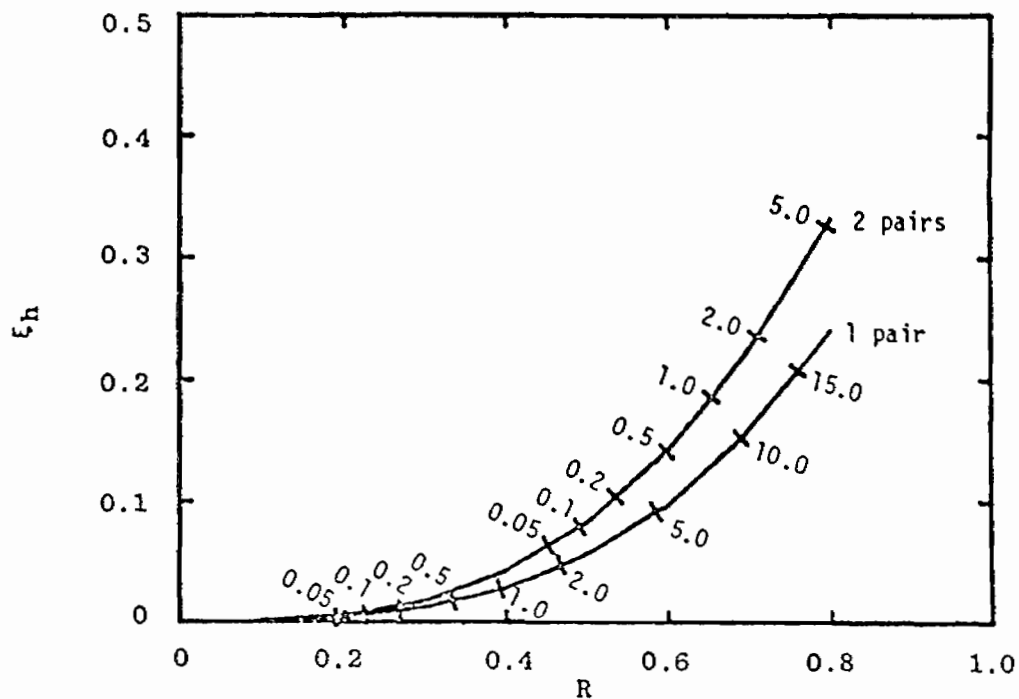
where

$$V_w = \frac{4}{3} \pi \bar{a}^3 = \text{working volume}$$

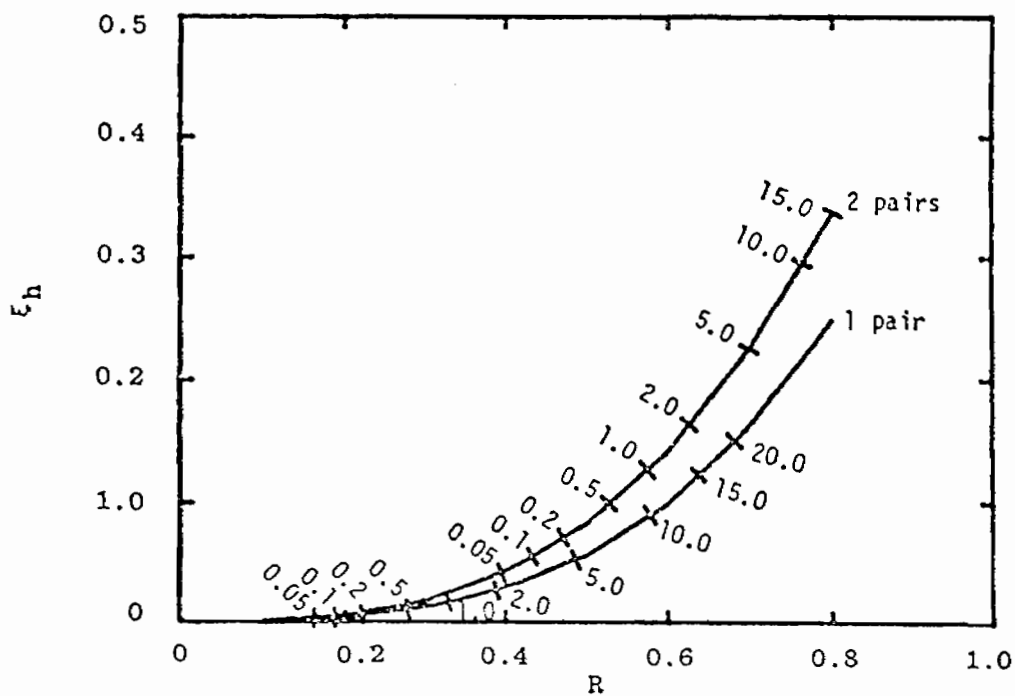
Substituting ℓ_c from below Equation 42 and letting $R = \bar{a}/a$, one obtains

$$\xi_h = \frac{\mu_o 4\pi R^3 \left[\sum_{\ell=1}^L (I_\ell/I) \sin^2 \alpha_\ell \right]^2}{3(L/a)} \quad (46)$$

Equation 46 was evaluated for 1 pair of loops with (L/a) given by Equation 33 ($N = 1$) and $I_1/I = 1$; the inductances of Table 16 were used. For the 2-pair configuration (L/a) was obtained from Equation 38 with $N_2 = 1$ and $N_1 = I_2/I$ (a hypothetical turns ratio that yields the optimized current in loops 1 and 4, Figure 27, with the simulator series connected); the inductances of Tables 17 and 18 were used. Optimum (Table 2) current ratios were used. (The parameter ξ_h was not calculated for the 3-pair configuration since the large number of required mutual inductances have not been calculated.) The results are shown in Figure 30. For the same value of error (χ), the 2-pair configuration is far superior to the 1-pair configuration as measured by the efficiency parameter ξ_h .



(a) Volume-Integral Method



(b) Surface-Integral Method

Figure 30. Efficiency parameter ξ_h vs. R for 1- and 2-pair configurations for both volume-integral and surface-integral methods. Ticks indicate values of χ expressed as a percent of the central field.

APPENDIX

DERIVATIVES FOR NEWTON-RAPHSON METHOD

For either Equation 18 or 22

$$\chi^2 = \frac{u}{v} \quad (47)$$

$$\frac{\partial \chi^2}{\partial p_i} = \frac{1}{v^2} \left(v \frac{\partial u}{\partial p_i} - u \frac{\partial v}{\partial p_i} \right) \quad (48)$$

$$\begin{aligned} \frac{\partial^2 \chi^2}{\partial p_j \partial p_i} = & \frac{1}{v^2} \left(v \frac{\partial^2 u}{\partial p_j \partial p_i} - u \frac{\partial^2 v}{\partial p_j \partial p_i} + \frac{\partial v}{\partial p_j} \frac{\partial u}{\partial p_i} - \frac{\partial u}{\partial p_j} \frac{\partial v}{\partial p_i} \right) \\ & - \frac{2}{v^3} \left(v \frac{\partial u}{\partial p_i} - u \frac{\partial v}{\partial p_i} \right) \frac{\partial v}{\partial p_j} \end{aligned} \quad (49)$$

Let

$$u = \sum_{n=3(2)\infty} D_n \left[\sum_{\ell=1}^L U_\ell^{(n)} \right]^2 \quad (50)$$

where

$$U_\ell^{(n)} = I_\ell R^n \sin \alpha_\ell P_n^1(\cos \alpha_\ell)$$

$$D_n = \begin{cases} \frac{3}{n(2n+1)} & , \text{ Volume-Integral Method} \\ \frac{2}{3} \frac{2n+1}{n(n+1)} & , \text{ Surface-Integral Method} \end{cases}$$

$$R = \bar{a}/a$$

$$\frac{\partial u}{\partial I_j} = \sum_{n=3(2)\infty} 2D_n U_{Ij}^{(n)} \sum_{\ell=1}^L U_\ell^{(n)} \quad (51)$$

$$\frac{\partial u}{\partial \alpha_j} = \sum_{n=3(2)\infty} 2D_n U_{\alpha_j}^{(n)} \sum_{\ell=1}^L U_{\ell}^{(n)} \quad (52)$$

where

$$U_{I_j}^{(n)} = \frac{\partial U_j^{(n)}}{\partial I_j} = R^n \sin \alpha_j P_n^1(\cos \alpha_j)$$

$$U_{\alpha_j}^{(n)} = \frac{\partial U_j^{(n)}}{\partial \alpha_j} = I_j R^n \frac{d}{d\alpha_j} \left[\sin \alpha_j P_n^1(\cos \alpha_j) \right]$$

$$\frac{\partial^2 u}{\partial I_k \partial I_j} = \sum_{n=3(2)\infty} 2D_n U_{I_j}^{(n)} U_{I_k}^{(n)} \quad (53)$$

$$\frac{\partial^2 u}{\partial \alpha_k \partial I_j} = \sum_{n=3(2)\infty} 2D_n \left[U_{I_j}^{(n)} U_{\alpha_k}^{(n)} + \delta_{kj} U_{\alpha I_j}^{(n)} \sum_{\ell=1}^L U_{\ell}^{(n)} \right] \quad (54)$$

where

$$U_{\alpha I_j}^{(n)} = \frac{\partial U_{I_j}^{(n)}}{\partial \alpha_j} = R^n \frac{d}{d\alpha_j} \left[\sin \alpha_j P_n^1(\cos \alpha_j) \right]$$

$$\frac{\partial^2 u}{\partial \alpha_k \partial \alpha_j} = \sum_{n=3(2)\infty} 2D_n \left[U_{\alpha_j}^{(n)} U_{\alpha_k}^{(n)} + \delta_{kj} U_{\alpha \alpha_j}^{(n)} \sum_{\ell=1}^L U_{\ell}^{(n)} \right] \quad (55)$$

where

$$U_{\alpha \alpha_j}^{(n)} = \frac{\partial U_{\alpha_j}^{(n)}}{\partial \alpha_j} = I_j R^n \frac{d^2}{d\alpha_j^2} \left[\sin \alpha_j P_n^1(\cos \alpha_j) \right]$$

and

$$\delta_{kj} = \begin{cases} 1, & \text{if } k = j \\ 0, & \text{if } k \neq j \end{cases}$$

the Kronecker delta.

Let

$$v = \left[\sum_{\ell=1}^L V_{\ell} \right]^2 \quad (56)$$

where

$$V_{\ell} = I_{\ell} R \sin^2 \alpha_{\ell}$$

$$\frac{\partial v}{\partial I_j} = 2V_{Ij} \sum_{\ell=1}^L V_{\ell} \quad (57)$$

$$\frac{\partial v}{\partial \alpha_j} = 2V_{\alpha j} \sum_{\ell=1}^L V_{\ell} \quad (58)$$

where

$$V_{Ij} = \frac{\partial V_j}{\partial I_j} = R \sin^2 \alpha_j$$

$$V_{\alpha j} = \frac{\partial V_j}{\partial \alpha_j} = I_j R 2 \sin \alpha_j \cos \alpha_j = I_j R \sin 2\alpha_j$$

$$\frac{\partial^2 v}{\partial I_k \partial I_j} = 2V_{Ij} V_{Ik} \quad (59)$$

$$\frac{\partial^2 v}{\partial \alpha_k \partial I_j} = 2 \left[V_{Ij} V_{\alpha k} + \delta_{kj} V_{\alpha Ij} \sum_{\ell=1}^L V_{\ell} \right] \quad (60)$$

where

$$V_{\alpha Ij} = \frac{\partial V_{Ij}}{\partial \alpha_j} = R \sin 2\alpha_j$$

$$\frac{\partial^2 v}{\partial \alpha_k \partial \alpha_j} = 2 \left[V_{\alpha j} V_{\alpha k} + \delta_{kj} V_{\alpha \alpha j} \sum_{\ell=1}^L V_{\ell} \right] \quad (61)$$

where

$$V_{\alpha\alpha_j} = \frac{\partial V_{\alpha_j}}{\partial \alpha_j} = 2I_j R \cos 2\alpha_j$$

Using formulas from Reference 3, p. 334, the following quantities can be obtained:

$$\frac{d}{d\alpha} \left[\sin \alpha P_n^1(\cos \alpha) \right] = (n+1) \left[\cos \alpha P_n^1(\cos \alpha) - P_{n-1}^1(\cos \alpha) \right] \quad (62)$$

$$\frac{d^2}{d\alpha^2} \left[\sin \alpha P_n^1(\cos \alpha) \right] = \frac{n+1}{\sin \alpha} \left\{ \left[(n+1) \cos^2 \alpha - 1 \right] P_n^1(\cos \alpha) - 2n \cos \alpha P_{n-1}^1(\cos \alpha) + n P_{n-2}^1(\cos \alpha) \right\} \quad (63)$$

These are required for evaluation of Equations 52, 54 and 55.